Spectral Tailoring for Boron Neutron Capture Therapy

The research described in this thesis was performed within a cooperation of the Institute for Energy of the Joint Research Centre (JRC) of the European Commission, P.O. Box 2, 1755 ZG, Petten, The Netherlands and the Section Physics of Nuclear Reactors (PNR), of the Department of Radiation, Radionuclides & Reactors (R^3) of the Faculty of Applied Sciences of the Delft University of Technology, Mekelweg 15, 2629 JB, Delft, The Netherlands.

Spectral Tailoring for Boron Neutron Capture Therapy

Proefschrift

ter verkrijging van de graad van doctor
aan de Technische Universiteit Delft,
op gezag van de Rector Magnificus prof. dr. ir. J.T. Fokkema,
voorzitter van het College voor Promoties,
in het openbaar te verdedigen
op dinsdag 26 juni 2007 om 15:00 uur

door:
Victor Alexander NIEVAART
natuurkundig ingenieur,
geboren te Apeldoorn

Dit proefschrift is goedgekeurd door de promotoren:
Prof.[em] dr. ir. H. van Dam
Prof. dr. ir. T.H.J.J. van der Hagen
Toegevoegd promotor:
Dr. ir. J.L. Kloosterman

Samenstelling promotiecommissie:

Rector Magnificus, voorzitter	
Prof.[em] dr. ir. H. van Dam	Technische Universiteit Delft
Prof. dr. ir. T.H.J.J. van der Hagen	Technische Universiteit Delft
Dr. ir. J.L. Kloosterman	Technische Universiteit Delft
Prof. dr. med. W. Sauerwein	University Hospital Essen
Prof. dr. ir. M. Hendriks-de Jong	Erasmus Medisch Centrum Rotterdam
Prof. dr. H.T. Wolterbeek	Technische Universiteit Delft
Dr. R.L. Moss	Joint Research Centre Petten

ISBN 978-1-58603-762-8

Keywords: Boron Neutron Capture Therapy, Optimal Source Neutrons, Adjoint Monte Carlo

Published and distributed by IOS Press under the imprint Delft University Press

Publisher
IOS Press
Nieuwe Hemweg 6b
1013 BG Amsterdam
The Netherlands
tel: +31-20-688 3355
fax: +31-20-687 0019
email: info@iospress.nl
www.iospress.nl
www.dupress.nl

PRINTED IN THE NETHERLANDS

This thesis consists of two parts. The first part provides a complete overview of the research performed and the second part consists of a collection of key papers:

I. V.A. Nievaart, R.L. Moss, J.L. Kloosterman, T.H.J.J. van der Hagen and H. van Dam, "A parameter study to determine the optimal source neutron energy in Boron Neutron Capture Therapy of brain tumours," Phys.Med.Biol. 49, 4277-4292 (2004).

II. V.A. Nievaart, D. Légràdy, R.L. Moss, J.L. Kloosterman, T.H.J.J. van der Hagen and H. van Dam, "Application of adjoint Monte Carlo to accelerate simulations of mono-directional beams in treatment planning for Boron Neutron Capture Therapy," Med.Phys. 34 (4), 1321-1335 (2007).

III. V.A. Nievaart, R.L. Moss, J.L. Kloosterman, T.H.J.J. van der Hagen, H. van Dam, A. Wittig, M. Malago and W. Sauerwein, "Design of a Rotating Facility for Extracorporal Treatment of an Explanted Liver with Disseminated Metastases by Boron Neutron Capture Therapy with an Epithermal Neutron Beam," Rad.Res. 166, 81-88 (2006).

CONTENTS

Spectral Tailoring for Boron Neutron Capture Therapy

Since the first clinical trials on Boron Neutron Capture Therapy in the 1950s, BNCT research has been mainly focussed on the treatment of (deep-seated) brain tumours, in particular, glioblastoma multiforme. Promising work to treat other cancers at other locations and even other diseases are in progress. Therefore, the chemists, medical doctors, physicists and biologists involved in BNCT are not only continuing to investigate and improve the (brain) clinical results, but are also investigating the new applications in BNCT. The work presented in this thesis is in the field of physics and deals, from three different viewpoints, with obtaining the optimal source neutron energy to optimise BNCT. The optimal source neutron energy is defined such as to obtain as many as possible (n,α)-absorptions due to ^{10}B in the tumours and as low as possible total neutron dose in the healthy tissues and organs at risk.

Firstly, the relation between the optimal source neutron energy and the radiation biology of brain BNCT was investigated. The biological weighting factors of the four major BNCT dose components, the skin and cranium thickness, the tolerance dose in skin and brain, the ^{10}B concentration and the number of beam gammas per source neutron were varied in a theoretical study. The parameter value ranges are bounded by unexpected and/or unrealistic values. It was investigated as to what is the optimal source neutron energy for four tumours at different depths, in each of the 136 million configurations for all combinations of parameter values. By far, the modality of the optimal source neutron energies is between 1 keV and 10 keV. However, depending on where the tolerance dose is reached first, in the skin or brain, low values for ^{10}B and fast neutron related parameters in this limiting tissue result in lower or higher than modal source neutron energies.

Secondly, adjoint Monte Carlo (MC) techniques are developed to find more quickly the optimal source neutrons' location, direction and energy. The adjoint MC is very suitable for this task because the adjoint particles fly mainly towards regions that from the statistics point of view are the best directions to irradiate from. Until now it was impossible to gather acceptable statistics of adjoint MC particles which traverse the adjoint detector perpendicularly, rendering the adjoint method inapplicable for mono-directional beams. The BNCT beam available in Petten can be regarded as mono-directional. This problem is solved with the use of next event estimators or with the application of a Legendre expansion technique. In the first case, adjoint particles are transported deterministically through a beam shaped channel to a point detector far away from the geometric model. The particles will traverse the disk shaped entrance of this tube (the beam exit in the actual geometry) perpendicularly. This method is slow when many events are involved that are not contributing to the point detector, e.g. neutrons in a scattering medium. In a second approach, adjoint particles that traverse an adjoint shaped detector plane are used to estimate the Legendre coefficients for expansion of the angular adjoint function. This provides an estimate of the adjoint function for the direction normal to the detector plane. In a realistic head phantom with 10 organs at risk and 10 tumours, the two adjoint techniques are 1.8 to 3.3 times faster than the forward MC calculations when 1020

different orientations of a gamma beam with a diameter larger than 5 cm are simulated. In case of a neutron beam, only the adjoint technique based on Legendre expansion is faster, 6.6 up to 20 times, than forward MC. In general, in case of small diameter beams adjoint MC calculations are only preferable for a large number of beams and a small number of regions of interest. For larger beam sizes, fewer beams and/or many regions of interest makes the adjoint favourable over the forward calculations. As well as being able to obtain the optimal locations to irradiate from, the optimal source neutron energy at every location around the head can also be obtained with adjoint MC. Compared with the Petten beam spectrum, it is found that only thermal and low-energy epithermal source neutrons can give significant improvements to the ratio of the thermal neutron flux in tumours to organs at risk.

Thirdly, the optimal source neutron energies are determined in order to obtain a homogeneous thermal neutron fluence in a prescribed volume. Ideally, when the homogeneity, defined as the ratio of minimum to maximum thermal neutron flux, is unity, the same thermal neutron related dose can be given in every part of this volume. When using the Petten beam with its current neutron spectrum for the extracorporeal BNCT treatment of liver cancer, the best homogeneity obtained is 0.68 in a volume of 2.4 litres. This volume is spheroidal shaped and rotating. The rotation is simulated in MCNP by averaging the particle tracks in tori shaped tally volumes. With a combination of source neutrons of 30% around 0.1 eV and 70% around 10 keV, a homogeneity of 0.95 can be reached in a cuboid model. This result was obtained after calculating the detector response functions for thermal neutrons in different volume shapes (i.e. cuboid, cylinder and sphere) as a function of source neutron energy. By applying linear programming, the detector response functions of the source neutron energies were combined such that the homogeneity in each volume shape is optimised.

The outcome of the three parts of this thesis shows that 3 neutron energy regimes should be prescribed in BNCT. As well as the 10 keV epithermal source neutrons, low epithermal source neutrons of around 1 eV and thermal source neutrons with energies of 0.1 eV must be used.

Petten, May 2007,
V.A. Nievaart

Spectrum Optimalisatie voor Boron Neutron Capture Therapy

Al vanaf de eerste klinische studies naar Boron Neutron Capture Therapy[1] (BNCT) in de jaren 50 ligt de nadruk van het BNCT onderzoek voornamelijk op de behandeling van diep gesitueerde hersentumoren en wel in het bijzonder de glioblastoma multiforme. Pas de laatste decennia zijn veelbelovende ontwikkelingen gaande om andere vormen en locaties van kanker en zelfs niet kankerzijnde ziektes te gaan behandelen. Dit betekent dat de bij BNCT betrokken chemici, artsen, fysici en biologen niet alleen proberen de hersenresultaten te verbeteren maar ook onderzoek te doen naar de nieuwe BNCT toepassingen. Dit proefschrift heeft een fysische grondslag en behandelt vanuit 3 invalshoeken het verkrijgen van de optimale bronneutronenenergie om zodoende BNCT te verbeteren. De optimale bronneutronen worden gekenmerkt door een energie die zoveel mogelijk (n,α)-absorpties tengevolge van ^{10}B in de tumor genereert en tegelijkertijd een zo laag mogelijke dosis geeft in de gezonde weefsels en stralingsgevoelige organen.

De eerste invalshoek van dit proefschrift is de relatie tussen de optimale bronneutronenenergie en de radiobiologie van BNCT toegepast voor hersenen. Hiervoor zijn in deze theoretische studie de biologische weegfactoren van de vier belangrijkste BNCT dosiscomponenten, de huid- en schedeldiktes, de tolerantiedosis in huid en hersenen, de ^{10}B concentratie en het aantal brongamma's per bronneutron in de bundel gevarieerd. Voor al deze parameters zijn intervallen gekozen die zijn begrensd door onrealistische en/of niet meer te verwachten waarden. Onderzocht is wat de optimale bronneutronenenergie is voor tumoren op 4 verschillende dieptes in elk van de 136 miljoen configuraties tengevolge van alle mogelijke combinaties van parameterwaarden. Voor veruit de meeste configuraties blijken bronneutronen met een energie tussen de 1 keV en 10 keV optimaal te zijn. Alleen voor lage waarden van de ^{10}B en snelle neutronen dosis gerelateerde parameters zijn er soms afwijkende (lagere of hogere) optimale bronneutronenenergieën. Dit geldt voor deze parameters in het weefsel (huid of hersenen) waar de tolerantiedosis als eerste wordt bereikt.

Ten tweede zijn er adjoint Monte Carlo (MC) technieken ontwikkeld om sneller de optimale locatie, richting en energie van de bronneutronen te vinden. Adjoint MC is zeer geschikt omdat de adjoint deeltjes zich voornamelijk bewegen naar die plekken die statistisch gezien het gunstigste zijn om vanuit te bestralen. Tot nu toe was het onmogelijk om genoeg adjoint MC deeltjes te verzamelen die loodrecht door het detectievlak gaan. Het verkrijgen van een goede statistiek voor de adjoint in geval van een eenrichtingsbundel was dus onmogelijk. De BNCT bundel in Petten (NL) kan worden beschouwd als een eenrichtingsbundel. Het probleem is opgelost met het gebruik van 'volgende-gebeurtenis-schatters' en door toepassing van een 'Legendre-ontwikkelings' techniek. In het eerste geval worden adjointdeeltjes

[1] In het Nederlands is BNCT vertaald als Borium Neutronenvangst Therapie.

deterministisch door een kanaal getransporteerd, die is gevormd zoals de bundel, naar een punt ver weg van de ingang. Zodoende zullen de adjointdeeltjes deze ingang (de bundelopening in werkelijkheid) loodrecht passeren. Deze methode is nadelig als veel deeltjes moeten worden gevolgd die het detectiepunt niet kunnen bereiken zoals het geval is bij neutronen in een verstrooiend medium. Bij de tweede methode worden de adjointdeeltjes die een adjointdetectorvlak passeren gebruikt voor het schatten van de Legendre coëfficiënten om zodoende de hoekafhankelijke adjointfunctie te kunnen ontwikkelen. Dit resulteert in een schatting voor de adjointfunctie in de richting loodrecht op het adjoint detectievlak. In een realistisch scenario, een hoofdfantoom met 10 tumoren in de hersenen en 10 stralingsgevoelige organen, zijn de twee adjoint technieken 1,8 tot 3,3 keer sneller dan normale voorwaartse MC berekeningen als 1020 verschillende posities van een gammabundel met een diameter groter dan 5 cm moeten worden gesimuleerd. In het geval van een neutronenbundel is alleen de Legendre techniek sneller dan normale voorwaartse MC berekeningen en wel 6,6 tot 20 keer. Voor kleine bundeldiameters kan worden geconcludeerd dat adjoint MC berekeningen voordelig zijn als er relatief veel bundelposities en weinig tumoren en/of stralingsgevoelige organen in het spel zijn. Voor grotere bundeldiameters is de adjoint methode al aantrekkelijk voor minder bundelposities en/of meer gebieden waarin de dosis berekend moet worden. Buiten de optimale bundelposities kan de adjoint techniek ook worden gebruikt om de optimale bronneutronenenergie overal rondom het hoofd te bepalen. In vergelijking met het spectrum van de Pettenbundel blijkt dat toepassing van de ene keer alleen thermische en de andere keer alleen laagepithermische bronneutronen significante verbeteringen geven in de verhouding tussen het thermische neutronenfluentietempo in de tumoren en stralingsgevoelige organen.

Ten derde is de optimale bronneutronenenergie onderzocht om een homogeen thermische neutronenfluentie te verkrijgen in een bepaald volume. Deze homogeniteit is gedefinieerd als de verhouding tussen de minimale en de maximale thermische neutronenfluentietempi in een volume. Idealiter heeft deze verhouding een waarde 1 wat betekent dat de thermische neutronen gerelateerde dosis overal in het volume hetzelfde kan zijn. In geval van behandeling van leverkanker met BNCT in Petten, waarbij de lever buiten het lichaam wordt gebracht, is de homogeniteit 0,68. Deze waarde wordt bereikt in een roterende sferoïde met een volume van 2,4 liter en gebruikmakend van het bestaande spectrum van de Pettenbundel. Met de MCNP code kan rotatie worden gesimuleerd door de geregistreerde padlengtes van de deeltjes in een torus te middelen over het torusvolume. Een mix van 30% 0,1 eV bronneutronen en 70% 10 keV bronneutronen resulteert in een homogeniteit van 0.95 in een kubusvormig model. Dit resultaat is verkregen door als functie van de bronneutronenenergie de detectorresponsiefuncties te berekenen voor thermische neutronen in verschillende modellen (te weten: kubus-, cilinder- en bolvormig). Met behulp van lineair programmeren zijn de detectorresponsiefuncties zo gecombineerd dat de homogeniteit in elke volumevorm is geoptimaliseerd.

De uitkomst van deze drie delen van het promotieonderzoek is dat 3 bronneutronenenergieregimes beschikbaar zouden moeten zijn in BNCT. Buiten de

10 keV epithermische bronneutronen moeten ook laagepithermische bronneutronen van rond de 1 eV en thermische bronneutronen met energieën van 0,1 eV beschikbaar zijn.

Petten, Mei 2007,
V.A. Nievaart

PUBLICATIONS

FIRST AUTHOR:

V.A. Nievaart, R.L. Moss, J.L. Kloosterman and T.H.J.J. van der Hagen, "Calculating the tumour-specific optimal source neutron energy for Boron Neutron Capture Therapy with particle production and adjoint Monte Carlo techniques," PHYSOR 2002, Seoul Korea, October 7-10, (2002).

V.A. Nievaart, J.L. Kloosterman, T.H.J.J. van der Hagen, R.L. Moss, "Forward and adjoint Monte Carlo calculations for investigating the use of an adjustable filter in BNCT," In: W. Sauerwein, R. Moss, A. Wittig, editors Research and Development Neutron Capture Therapy. Bologna: Monduzzi Editore, 1065-72 (2002).

V.A. Nievaart , "Maximising the α-production in brain tumours under different equivalent dose configurations in BNCT," ISNCT/YMNM3 meeting, Pisa Italy, Nov 27 - Dec 2, (2003).

V.A. Nievaart, R.L. Moss, J.L. Kloosterman, T.H.J.J. van der Hagen and H. van Dam, "A parameter study to determine the optimal source neutron energy in Boron Neutron Capture Therapy of brain tumours," Phys.Med.Biol. 49, 4277-4292 (2004).

V.A. Nievaart, R.L. Moss, J.L. Kloosterman, T.H.J.J. van der Hagen, H. van Dam, "Feasibility study for the extra-corporal treatment of liver cancer by BNCT at the HFR Petten," ISNCT-11, October 11-15, Boston, Conference proceeding, USA (2004).

V. Nievaart, A. Wittig, R. Moss, J. Rassow, W. Sauerwein, "Optimisation of treatment planning for multi-beam Boron Neutron Capture Therapy (BNCT) using epithermal neutron beams in patients with multiple metastases to the brain from malignant melanoma," Strahlentherpie und Onkologie, Abstractband zum DEGRO-Kongress, Sondernr.1, May (2006).

V.A. Nievaart, R.L. Moss, J.L. Kloosterman, T.H.J.J. van der Hagen, H. van Dam, A. Wittig, M. Malago, W. Sauerwein, "Design of a rotating facility for extra-corporal treatment of an explanted liver with disseminated metastases by BNCT with an epithermal neutron beam at the HFR in Petten", Radiation Research 166, 81-88 (2006).

V.Nievaart, R Moss, A Wittig, and W Sauerwein, "Extra-corporal treatment of Liver Metastases by BNCT at the HFR Petten", Journal of Physics: Conference Series of the Institute of Physics 41, 369-374 (2006).

Sander Nievaart, Ray Moss, Wolfgang Sauerwein, Massimo Malago, Jan Leen Kloosterman, Tim van der Hagen and Hugo van Dam, "An optimum source neutron spectrum and holder shape for extra-corporal treatment of liver cancer by BNCT,"

12th International Congress on Neutron Capture Therapy Kagawa International Conference Hall, Sunport Takamatsu, Japan, Oct 9-13 (2006).

Sander Nievaart, Ray Moss, Wolfgang Sauerwein and Andrea Wittig, "Use of linear programming to obtain an optimum, multi-beam treatment plan in BNCT," 12th International Congress on Neutron Capture Therapy Kagawa International Conference Hall, Sunport Takamatsu, Japan, Oct 9-13 (2006).

V.A. Nievaart, D. Légràdy, R.L. Moss, J.L. Kloosterman, T.H.J.J. van der Hagen and H. van Dam, "Application of adjoint Monte Carlo to accelerate simulations of mono-directional beams in treatment planning for Boron Neutron Capture Therapy," Med.Phys. 34 (4), 1321-1335 (2007).

V.A. Nievaart , G.G. Daquino and R.L. Moss, "Monte Carlo based treatment planning systems for Boron Neutron Capture Therapy in Petten The Netherlands," submitted to Journal of Physics: Conference Series of the Institute of Physics (2007).

CO-AUTHOR:

Mudde, RF , Deutz, L, Nievaart, VA , & Maanen, HRE van, "LDA-measurements of the turbulence in and around a venture," In W Rodi & M Mulas (Eds.), Proceeding of Ercoftac internationa symposium of engineering turbulence modelling and measurements, Ercoftac, Sardinia, Italy, pp. 80-91 (2005).

W. Sauerwein, M. Malago, R. Moss, S. Altieri, G. Hampel, A. Wittig, V. Nievaart, L. Collette, P. Mauri, R. Huiskamp, J. Michel, G. Daquino, G. Gerken, N. Bornfeld, C.E. Broelsch, "Bor-Neutroneneinfangtherapie (BNCT) zur Behandlung diffuser, nicht resektabler Lebermetastasen," Strahlentherpie und Onkologie, Abstractband zum DEGRO-Kongress, Sondernr.1, May (2006).

A. Wittig, L. Collette, J. Heimans, P. Paquis, K. Haseslsberger, V. Barsegian, C. Loquai, G. Kaiser, R. Moss, J. Rassow, F. Stecher-Rasmussen, R. Huiskamp, V. Nievaart, S. Bührmann, P. Bet, B. Hahn, K. Hideghéty, H. Arlinghaus, W. Sauerwein, "A strategy to introduce Boron Neutron Capture Therapy (BNCT), a novel radiotherapy modality, into clinical practice," The clinical trials of the EORTC BNCT Group; Strahlentherpie und Onkologie, Abstractband zum DEGRO-Kongress, Sondernr.1, May (2006).

G.Gambarini, G.G.Daquino, R.L.Moss, M.Carrara, V.A.Nievaart, E.Vanossi, "Gel dosimetry in the BNCT facility for extra-corporal treatment of corporal of liver cancer at the HFR Petten," 10th Symposium on Neutron Dosimetry. Progress in dosimetry of neutrons and light nuclei Uppsala (SV), 12-16 June (2006).

A. Roca, G.G. Daquino, R.L. Moss, S. Nievaart, R. Schmidt F. Stecher-Rasmussen, "Determination of the neutron capture sensitivity of ionisation chambers based on

neutron capture reaction rates," 12th International Congress on Neutron Capture Therapy Kagawa International Conference Hall, Sunport Takamatsu, Japan, Oct 9-13 (2006).

Ray Moss, Sander Nievaart, Lucien Pott, Andrea Wittig, Wolfgang Sauerwein, "Design and testing of a rotating, cooled device for extra-corporal treatment of liver cancer by BNCT in the epithermal neutron beam at the HFR Petten," 12th International Congress on Neutron Capture Therapy Kagawa International Conference Hall, Sunport Takamatsu, Japan, Oct 9-13 (2006).

G.G.Daquino, G.Gambarini, S.Nievaart, M.Carrara, E.Vanossi, "Use of Gel dosimetry to characterize the dose distribution in the spheroidal holder for liver treatment at the HFR Petten," 12th International Congress on Neutron Capture Therapy Kagawa International Conference Hall, Sunport Takamatsu, Japan, Oct 9-13 (2006).

P. van Lent, A. Sloetjes, A. Blom, G. Krijger, G. Koning, S. Nievaart, W. van den Berg and R. Moss, "Selective elimination of synovial macrophages by boron neutron capture therapy prevents onset of murine experimental arthritis," Journal of Controlled Release, Volume 116, Issue 2, 28, pp e106-e107 (2006).

Peter van Lent, Gerard Krijger, Wouter Hofkens, Sander Nievaart, Annet Sloetjes, Gerben Koning, Ray Moss, Wim van den Berg, "Selective Elimination of Synovial Macrophages by Boron Neutron Capture Therapy prevents onset of Joint Inflammation and Cartilage Destruction during Experimental Arthritis," submitted to Annals of Rheumatic diseases (2007).

Andrea Wittig, Massimo Malago, Laurence Collette, René Huiskamp, Sandra Bührmann, Victor Nievaart, Gernot M. Kaiser, Karl-Heinz Jöckel, Kurt Werner Schmid, Uta Ortmann, Wolfgang A. Sauerwein, "Uptake of two 10B-compounds in liver metastases of colorectal adenocarcinoma for extracorporeal irradiation with BNCT (EORTC trial 11001)," in preparation.

M.M. Fretz, G.C. Krijger, U.D. Woroniecka, V.A. Nievaart, W. Jiskoot, R. Moss, G.A. Koning and G. Storm, "Targeted liposomes for boron neutron capture therapy (BNCT): importance of target receptor density," in preparation.

A. Roca, S. Nievaart, R.L. Moss, F. Stecher-Rasmussen, "Validating a MCNPX model of Mg(Ar) and TE(TE) ionisation chambers exposed to 60Co gamma-rays," in preparation.

Chapter 1

Introduction

1. General introduction

Boron Neutron Capture Therapy (BNCT) is a form of radiotherapy using neutrons for treating various types of cancer and some other non-malignant diseases. The basics of BNCT will be discussed in the next section followed by two sections describing theory that is important for the three successive chapters. To put the research presented in this thesis in context, a brief description of the history and present status of BNCT is given. This thesis is based on three articles in the field of BNCT published in journals covering the combined field of physics and medicine. Chapters 2, 3 and 4 are written as extended summaries of the articles with some novelties added. The full articles are printed in part II of this thesis. The motives for performing this research are explained in Section 1.2 which ends with the description of the scope of this thesis.

1.1 The basics of BNCT

The basic concept of BNCT is that cancer or other 'bad' cells are loaded with the isotope boron-10 (^{10}B) after which the site containing these cells is irradiated with neutrons. ^{10}B and the neutrons are non-toxic. After ^{10}B has captured a neutron, a nuclear reaction takes place and releases two heavy particles, being an alpha particle (^{4}He) and lithium ion (^{7}Li). This so-called (n,α) absorption reaction is illustrated in Figure 1.1. According to the energies, the alphas and ^{7}Li nuclei can be regarded as short ranged particles since they travel less than 10 μm in tissue. This range is similar to the size of a human cell and implies that the heavy particles have a high probability to kill or damage the cancer cell.

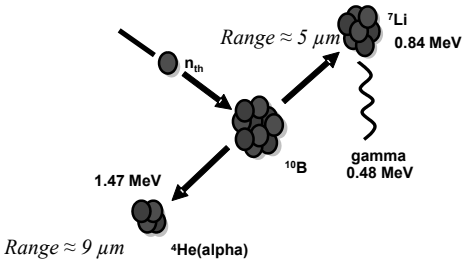

Figure 1.1. Reaction of ^{10}B with low energy neutrons which produce two highly energetic particles. In 96% of these reactions, a gamma ray is also produced.

The cell is killed when the alpha or Li particle causes a double-strand break of the DNA. This occurs when a heavy particle travels through the cell nucleus. The probability of this event together with the probability of having a neutron reacting with a ^{10}B in the first place requires that for successful BNCT the cell is loaded with around 10^{9} of ^{10}B atoms [1,2].

In the field of BNCT, often the energy spectrum of the neutrons is classified in 3 parts: Thermal neutrons below 0.5 eV, epithermal neutrons between 0.5 eV and 10 keV and fast neutrons above 10 keV and below 20 MeV. It is for thermal neutrons,

indicated with n_{th} in Figure 1.1, that the probability to react with ^{10}B is high. For thermal neutrons, this probability, known as the microscopic nuclear absorption cross section[1] (σ_a) of ^{10}B is proportional with $1/v$, where v is the velocity of the incoming neutron. For example, the absorption cross section of ^{10}B for 0.025 eV neutrons is 3837 barn and only 6 barn for 10 keV neutrons. However, the neutrons slow down due to interactions with tissue. This means that the starting neutron energy, coming from the source, has to be epithermal or fast in order to become thermal in a deep seated tumour after slowing down.
BNCT is a disease targeted therapy as the neutrons will only kill the cells which are labelled with ^{10}B. Unfortunately, with the presently available ^{10}B administrating compounds, also healthy cells will contain some ^{10}B. Besides this, human tissue contains certain isotopes that react with neutrons as well. These reactions result in a dose given to the healthy tissue which should not exceed a certain limit, called the tolerance dose. These extra dose components will be further explained in the two following sections.
Although the concept of BNCT might look quite simple and despite the fact that it is seven decades after its first proposal, BNCT is still under investigation. So far, as a maximum achievement, only phase I/II[2] clinical trials are performed with only a relatively low number (a few hundred) of patients involved. After all these years, researchers of various disciplines are still challenged by the two key issues of BNCT: Finding a non-toxic ^{10}B administrating compound, which brings the isotope into the 'bad' cells only or at least significantly more than in the healthy tissue and designing a treatment beam which is developed to deliver the optimal neutrons at the right location while minimizing the dose to healthy tissue. This latter issue about finding the BNCT source neutrons with the optimal energy and direction is studied in this thesis. The research took place at the BNCT facility of the Institute for Energy, Joint Research Centre (JRC) of the European Commission in Petten, The Netherlands. The centre's main target is to lead and participate in so-called scientific networks. For the optimisation of the *neutronics* as performed in this work, the JRC worked together with the section Physics of Nuclear Reactors (PNR) of the Delft University of Technology in The Netherlands.

1.1.1 The four major BNCT dose components in tissue

Human tissue consists mainly of hydrogen, oxygen, carbon and nitrogen. By far, most reactions of neutrons are with H and N. Together with the presence of boron in

[1] The microscopic cross section is a measure for the probability of a nuclear reaction for the nucleus and is expressed in *barn* which is $10^{-24}cm^2$ [3].
[2] Most often clinical studies consist of four separate stages. They start from studying the effects of the treatment on healthy tissues (phase I), after which the focus is shifting towards treating the disease (phase II) and come to a scheme to treat the disease optimally (phase III) and ends with registering the treatment (phase IV).

the tissue, the majority of the total physical dose[3] considered in BNCT is delivered by H, N and ^{10}B. Because H has two types of reactions giving a physical dose, the total physical dose in BNCT consists of four components. These two H-related physical doses are described in the last two rows of Table 1.1. Rows 1 and 2 of this table describe the physical doses due to the isotopes ^{10}B and ^{14}N, respectively. In the remaining text the 'physical dose' is often shortened by writing 'dose'. As indicated in Table 1.1 in light and dark grey, the first three dose components are related to 'thermal' neutron reactions while the fourth dose component is due to reactions with 'fast' neutrons.

Table 1.1. Overview of the four major dose components in BNCT.

	Physical dose name	Dose* symbol	Reaction type	Scheme	Remarks
Thermal	Boron dose	D_B	n,α		Biological effects in tumour and normal tissue are related to ^{10}B micro-distribution
Thermal	Thermal neutron dose	D_p	n,p	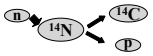	Induced proton 620 keV
Thermal	Induced gamma-ray dose	D_γ	n,γ	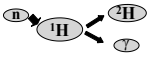	Induced γ-rays 2.2 MeV
Fast	Fast neutron dose	D_n	n,n	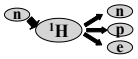	Energy of recoiling proton is on average half the neutron energy

* According to IAEA Techdoc 1223 [4].

In a block-shaped model of H_2O, see Figure 1.2, in which realistic amounts of N and ^{10}B are added, is the behaviour of the four dose components as a function of source neutron energy and depth in the model illustrated (see Figures 1.3 to 1.7). Light water with a few mass percent of nitrogen makes a good material to simulate average human tissue. As drawn in Figure 1.2, a spherical tumour (ø 4 cm) is positioned at 4 cm depth and contains 30 ppm of ^{10}B which is uniformly distributed. The assumption of having a three times higher ^{10}B-concentration in the tumour than in the healthy surroundings is a realistic 'average' [5,6]. The D_B (see definition Table 1.1) as a function of source neutron energy and depth in the phantom is shown in Figure 1.3. The location of the tumour is at all energies clearly visible because of

[3] Physical dose is defined as the specific energy deposited around a certain point in a medium due to ionising radiation. It is written in unit Gray with symbol Gy. 1 Gy = 1 J/kg.

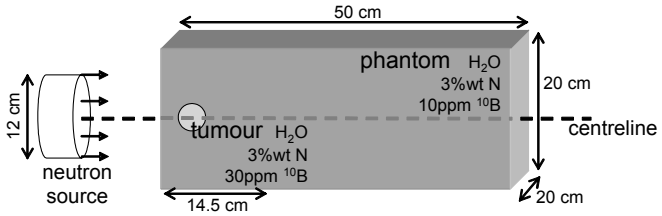

Figure 1.2. Set-up of the block shaped phantom with a tumour irradiated with neutrons.

the three times higher concentration of ^{10}B and consequently more (n,α)-reactions. This results in the horizontal darker grey band at the full width of the figure. For source neutron energies above 1 eV and below 3 keV, the D_B is significantly higher in the first 2 cm of the tumour. Between 10 keV and 100 keV the boron dose is more uniformly distributed in the whole tumour and is still in high contrast to the healthy surroundings. This is desired. Figures 1.4 and 1.5 show the D_p and D_γ respectively, which look quite similar due to the fact that they are related to thermal neutron reactions as well. At low source neutron energies there are many thermal reactions at shallow depths. For increasing source neutron energy the majority of the thermal reactions occurs somewhat deeper until, above 1 keV, the thermal reactions are

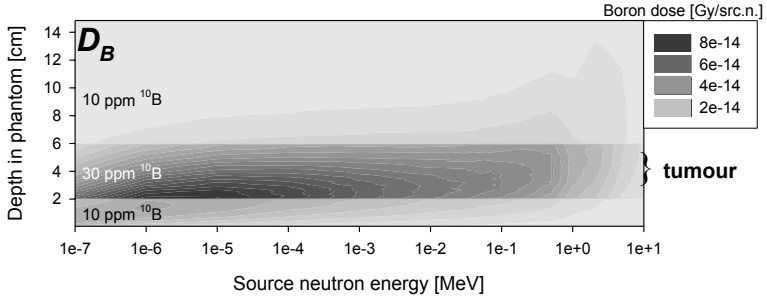

Figure 1.3. Physical boron dose per source neutron as a function of source neutron energy and depth in the light water model with tumour at the centreline.

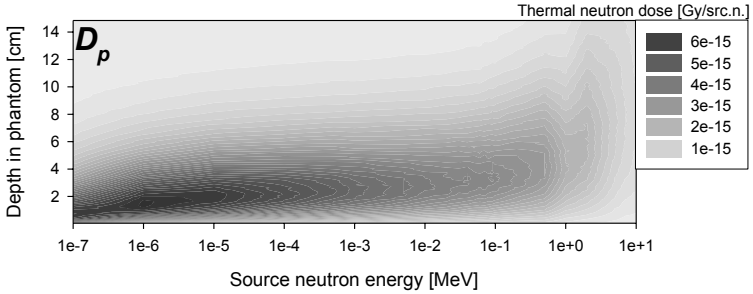

Figure 1.4. As in Figure 1.3 but for the physical thermal neutron dose per source neutron.

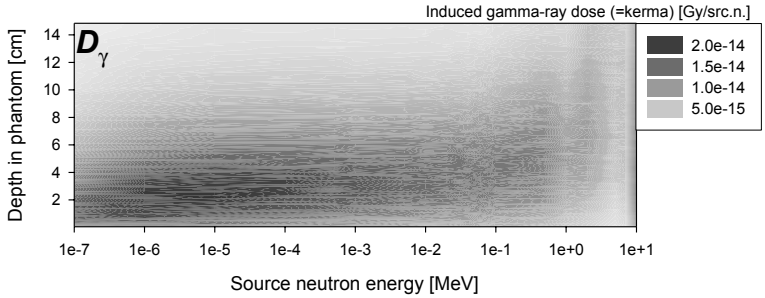

Figure 1.5. As in Figure 1.3 but for the physical gamma dose per source neutron (actually kerma).

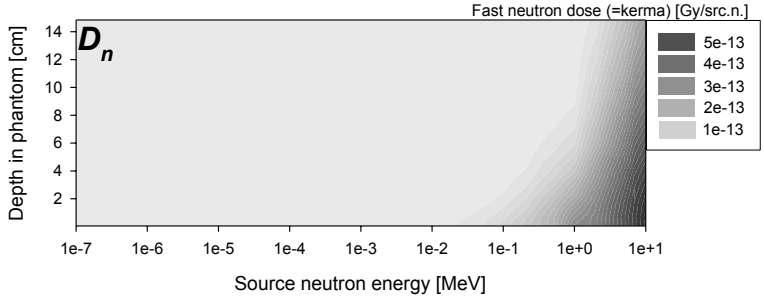

Figure 1.6. As in Figure 1.3 but for the physical fast neutron dose per source neutron (actually kerma).

'smeared out' stretching deeper into the phantom. The stripes and 'folding' behaviour around 1 MeV is due to resonances in the oxygen neutron cross section data. The typical 'thermal-reaction' look is also visible in Figure 1.3 but affected by the presence of the tumour. Figure 1.6 shows the D_n which is completely different from the described thermal dose figures. According to this figure, only for source neutrons above 30 keV, there is a physical fast neutron dose which increases rapidly with neutron energy. It is not visible in Figure 1.6 that D_n is already significant for source neutrons between 1 keV and 30 keV. This dose contribution can not be neglected, compared with the thermal dose components but is only significant superficially at the first 5 to 10 mm of the phantom.

The D_B and D_p presented here are determined by calculating with the Monte Carlo (MC)[4] code MCNP4C2 from Los Alamos Laboratories [7], the alpha and proton productions, due to the ^{10}B and N respectively. Since these alphas and protons deposit their energy locally, the physical doses result from multiplying the calculated particle production densities with the released energy. The D_γ and D_n are

[4] Monte Carlo method: Weights of simulated particles are followed when travelling through the geometry. These weights can change due to interactions with the materials. These interactions occur probabilistically and are based on the nuclear cross section data of the materials.

calculated by multiplying the photon and neutron fluxes in MCNP with energy dependent tables of kerma[5] factors for water taken from ICRU46 [8]. Therefore, the D_γ and D_n are kermas rather then physical doses. Nevertheless, kerma and physical dose are equal in case of a charged particle equilibrium[6] which is supposed here. Furthermore, a background dose exists due to gamma rays in the BNCT neutron beam. Figure 1.7 depicts the D_γ from these 'beam' gammas which will be further indicated as $D_{b\gamma}$. For mono-directional source gammas having 24 discrete energies, chosen at logarithmically equal intervals between 1 keV and 20 MeV, the plot indicates a very slowly decreasing dose as a function of depth that is hardly visible. Note that the scale is logarithmic. A typical ratio of source neutrons to source gammas is 20 which is the case at the BNCT facility in Petten.

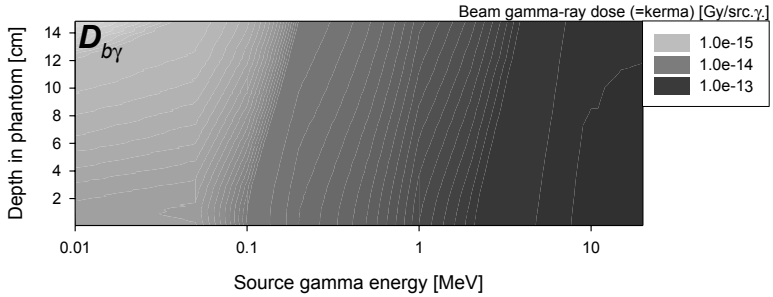

Figure 1.7. Physical gamma dose per source gamma due to (unwanted) gammas already present in the beam as a function of source gamma energy and depth in the light water model.

1.1.2 Biologically weighted doses and ^{10}B compounds

The secondary particles in BNCT, i.e. the alpha particles, protons, recoiling protons and electrons accompanying the D_B, D_p, D_n and D_γ as presented in Table 1.1, deposit their energy differently in the tissue. For example, the energy deposition along the short track of an alpha particle is very dense in comparison with that of an electron of which the track is longer. As a result, the human cells respond biologically differently when irradiated with 1 MeV alpha particles or 1 MeV gammas. This makes that the sum of the different particle energy depositions per unit of mass, the physical doses, has no biological meaning.

Many BNCT investigations aim to establish that the biological effects of D_B, D_p and D_n can be translated into gamma dose equivalents. In this way the four dose components in BNCT can be added and the (total) dose given to the patient at each point in tissue can be described. The reason to translate the doses into gamma dose

---

[5] Kerma is defined as the Kinetic Energy Released per unit Mass and consists of the energy that is transferred after the first collision.

[6] There is charged particle equilibrium when for every charged particle leaving a certain volume in an irradiated medium, another charged particle of the same type, having the same energy and direction, enters the volume.

equivalents comes from the fact that a lot of experience in conventional radiotherapy (using mainly gammas) is gathered in the last century. The translation is performed by multiplying each physical dose component by a biologically weighted factor also known as the Relative Biological Effectiveness (RBE) factor. After addition, the total dose is called the 'total biologically weighted dose'[7] having the symbol D_w [4]. Currently, however, after many years of research, the values of these factors are still under discussion. As will be seen in Chapter 2, the RBE factor to 'translate' the D_B is replaced by a Compound related Biologically Effectiveness (CBE) factor. This factor embodies the 'normal' boron dose related RBE but is corrected for the applied boron compound [5,9]. Up to now, only two boron compounds are approved to be given to patients in clinical BNCT trials. The first drug is Borocaptate Sodium (BSH) and the second Borono-phenylalanine (BPA) of which the chemical structures are shown in Figure 1.8 [10-13]. Due to their respective natures, the distribution of the ^{10}B over the cells and the positioning in the cells, with respect to the cell nucleus, are different. This is taken into account by the CBE factor.

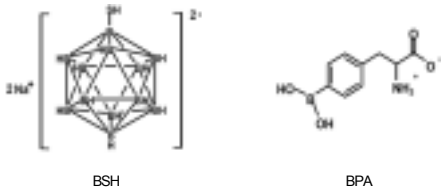

Figure 1.8. Chemical structures of BSH and BPA

1.1.3 Brief history of BNCT

(This section is partly a brief outline taken from section 1.3.2 by Philipp [14]).

The existence of neutrons was proven by Chadwick [15] twelve years after Rutherford had already postulated the existence of these particles in 1920 [16]. In 1936, after ^{7}Li and alpha particles were detected when ^{10}B reacts with thermal neutrons [17], Locher [18] suggested to apply this phenomenon in radiation therapy. In the early 1940s, Kruger and Zahl et al. [19-22] made some first promising radiobiological experiments in cell-cultures and mice, proving that BNCT worked as suggested. In 1941, it was Zahl et al. [22] who first proposed the use of epithermal neutrons instead of thermal neutrons, whenever humans would be treated in clinical trials. This remark of Zahl et al. about the usage of thermal and/or epithermal neutrons will be shown to play a very important role throughout this thesis.

It was not until 1950s that the first clinical trial on BNCT was started in the United States using thermal source neutrons [23]. At Brookhaven National Laboratory (BNL) and the Massachusetts Institute of Technology (MIT), 10 patients suffering from glioblastoma multiforme (a malignant type of brain tumour), were irradiated after a ^{10}B-enriched borax solution was intravenously given. The overall result, including a further 18 patients treated at MIT in a second protocol in which the skin, cranium and dura were removed, was unsatisfactory and consequently BNCT was

[7] In Paper I the biological weighted dose, as defined for BNCT according to IAEA-TECDOC-1223, is assumed to be similar to the equivalent dose throughout the whole manuscript.

halted in the US in 1961. It was concluded that thermal neutrons do not penetrate deep enough and the boron compounds used were not very tumour selective [24]. From 1968, in Japan, clinical trials continued with the open-craniotomy procedure, where several intracerebral malignancies were treated. The Japanese professor Hatanaka who had been already involved in a clinical trial in the US, can be regarded as the catalyst of BNCT at that time. Together with other researchers, the Japanese investigated new boron compounds and treated more than 120 patients of whom some survived for a long term [25,26]. This outcome encouraged BNL and MIT to start new BNCT trials in the US in 1994 and 1996, respectively. From then onwards the focus was merely on the use of epithermal neutron beams which are able to penetrate skin and cranium and make removal of these unnecessary. In 1997, a European trial at the High Flux Reactor (HFR) in Petten (the Netherlands) started under the medical supervision of the university hospitals in Amsterdam (NL) and Essen (D), involving glioma patients [27-29]. In 1999 and 2000 respectively, similar clinical trials were started in Finland and Sweden [30,31]. All the trials mentioned so far were performed at nuclear reactors of which the 'medical' reactor at BNL in the US closed in 2000 and the Studsvik reactor in Sweden halted in 2005. In Italy (Pavia), in 2001, a very promising BNCT experiment was initiated by irradiating an explanted liver suffering from (inoperable) diffuse metastases. In 2003, a phase I/II clinical trial on skin melanoma started at a reactor in Argentina. In the same year, in Petten, a new protocol was approved and a phase I/II clinical trial started for patients suffering from melanoma metastases in the brain. This trial is performed in cooperation with the MIT. Reactor based clinical trials are also under investigation in Czech Republic, South-Korea, Taiwan and Russia. Accelerator-based BNCT is being investigated in Birmingham (UK), Italy, Argentina, Russia and in the US.

1.1.4 Present status of BNCT

The overall opinion of BNCT researchers and its critics is that *the* major improvement in BNCT is to be expected from new boron compounds that bring more ^{10}B in the tumour cells. In this respect, the application of liposomes is studied [32,33] which can be seen as bags (ø 50-200nm) carrying a medicine. The liposomes can be programmed to connect only to 'bad' cells after which the medicine is transferred. The Petten BNCT group, in cooperation with the Delft University of Technology and the Universities of Utrecht and Nijmegen, are investigating the treatment of ovarian-carcinoma [34,35] and rheumatoid arthritis (after earlier studies [36,37]) using liposomes filled with BPA [38]. Other ongoing medical and biological studies concern the possibility of mixing the presently registered boron-carriers BSH and BPA [39,40] and the visualisation of the ^{10}B-uptake in cells by special microscopy (e.g. EELS [41]).

After many investigations, a major challenge in BNCT is still the translation of the several dose components into biological equivalents as discussed in section 1.1.2. It is impossible to compare the results among BNCT centres because different weighting factors have been applied or a different concept of dose-description is followed. In this respect, Riley and Binns [42,43] have started inter-comparison measurements using their own detectors and techniques at many BNCT facilities in order to standardize the used beams and enable the comparison of the results of the

treated patients. Promising and related to this issue is the development of a typical BNCT beam dependent radiobiological number which characterises the response of the cells when irradiating with this beam [44,45].
To predict the BNCT dose components as well as the neutron and gamma fluxes in patient treatment planning and experiments, MC based computer simulations are performed. The advantage of MC is the 3D-modelling capability and often the obtained precision in the results when compared with measurements whilst the disadvantage is the rather long calculation time. It is for the first reason (precision) that also physicists in conventional radiotherapy are interested and 'variance reduction' investigations to reduce the calculation time are in progress to overcome the MC disadvantage.
The last interesting trend in BNCT to be reported here concerns the disease targeted nature of BNCT which is most valuable when dealing with metastasised diseases. As already mentioned in Section 1.1.3, the treatment of an explanted liver full of metastases resulted in the survival of one of the patients for almost 4 years. This result encouraged many BNCT groups and also the group of Petten/Essen and Delft, to investigate the feasibility of such a project at the HFR in Petten.

1.2 Spectral tailoring for BNCT

As written in section 1.1.3, Zahl et al. was the first to propose the use of epithermal instead of thermal source neutrons. The use of epithermal source neutrons was extensively studied by Fairchild [46,47] at Brookhaven. Mainly epithermal neutrons in the range of 1 eV to 20 keV were shown to be useful for treating deep-seated brain tumours through the intact skull. The many succeeding publications discuss the characteristics of newly designed epithermal beams at the BNCT research centres [48-53]. The focus in these articles is on the application of filter and moderator materials, the shape of the beam assemblies and the quality of the resulting beam. Furthermore, these publications have in common that an existing neutron source is filtered and moderated such that it delivers neutrons in the energy range recommended by Fairchild. Actually, the spectral tailoring for BNCT consists of two parts:

1. *Defining the source neutron energies of the BNCT treatment beam in order to obtain the most ^{10}B absorption reactions in the tumour. In addition, the location, direction and dimensions of the BNCT treatment beam need to be optimised for every individual tumour size and location.*
2. *Developing and constructing the filter with the appropriate materials and obtain the from 1. resulting energies starting with an available source.*

The first part became the main issue of this PhD-research as will be further explained in Section 1.2.2.
As an example, the neutron filter in Petten has been designed and installed to let pass through only epithermal neutrons, whilst at the same time it has to reduce the unwanted photons, coming from the HFR reactor core. The design and used filter materials together with its main 'treatment' characteristics are given in Figure 1.9.

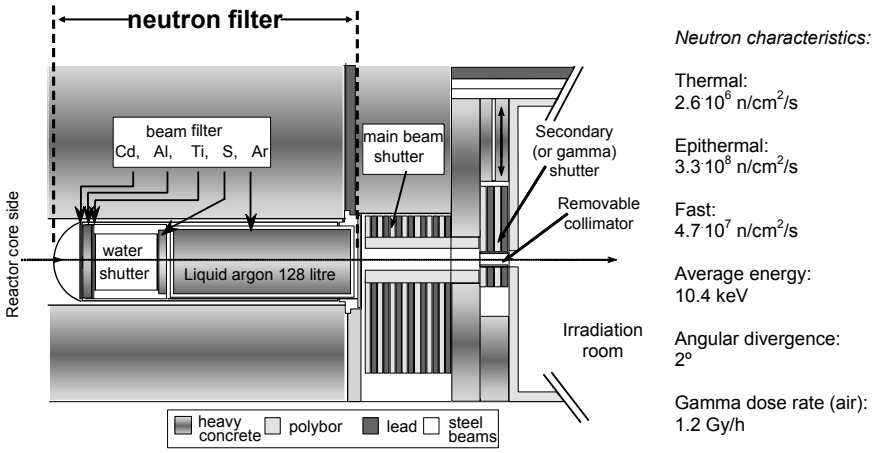

Figure 1.9. The current neutron filter for BNCT at the High Flux Reactor in Petten.

1.2.1 Search for the optimal source neutron energy for BNCT

To the knowledge of the author, there are four publications (Yanch et al. [54,55], Bisceglie et al. [56] and Bleuel et al. [57]) that deal with the tailoring of the source neutrons as described in the last section. These more fundamental investigations are mainly initiated by the development of accelerator-based neutron sources which have the ability to obtain narrow neutron energy spectra that can be varied. The publications have in common that mono-energetic and mono-directional neutrons are simulated using MC and describe the doses and fluxes realised in a phantom. Succinctly, in all these investigations the focus is on deep-seated brain tumours whilst the doses are calculated with a fixed set of CBE/RBE factors. In all these investigations, the simulated neutrons and gammas start from the source after which the resulting effects are calculated in the tumour and healthy tissues.
The publications of Yanch et al. describe the dosimetric properties as a function of discrete neutron energies, beam size, collimation and different phantom shapes. It is reported that only the geometric differences show an influence on the contribution of the individual dose components to the tumour dose. The optimal source neutron energies to treat a tumour at 7 cm depth in tissue are in the range of 4.0 eV to 40.0 keV. Bisceglie et al. conclude that an optimal source neutron energy for BNCT is in the order of a few keV's for deep-seated tumours at 5 cm. Bleuel et al. conclude that neutrons between 2 keV to 20 keV are the most desirable in BNCT.

1.2.2 The scope of this thesis

The Petten BNCT group together with the PNR department in Delft initiated a study to optimise the neutronics component of BNCT. In this respect, an investigation started to search for the optimal source neutron energies and continue the work already performed and described in Section 1.2.1. When taking into account some related challenges (see Section 1.1.4) the BNCT-physicists and medical physicists in conventional radiotherapy are currently facing, this thesis deals with the following issues:

- The influence of the dose weighting factors, and other dose related issues such as the tolerance doses in the tissues and the ^{10}B concentrations, on the optimal source neutron energy in BNCT. This issue is discussed in Chapter 2 that is based on *Paper I*.
- The development and application of adjoint MC calculation techniques. In adjoint MC the simulated particles travel 'backwards' which means from the tumour to the source which is the exit of the treatment beam. In realistic scenarios, this approach should be able to provide much faster the information on the optimal origin, direction and energy of the source particles compared with 'normal' MC. Chapter 3 and *Paper II* discuss the outcomes in all details.
- The analysis of having the optimal source neutrons not only for deep seated tumours, but also for mid-range and shallow positioned tumours. This is relevant when applying BNCT to cancer metastases which are spread throughout the brain or other organ, such as the liver. Chapter 4 describes a set-up to obtain a homogeneous (to a certain degree) thermal neutron field in a volume that contains a liver, given an epithermal neutron beam. This subject is published in *Paper III*. Chapter 4 describes also a method to obtain with adjoint-like techniques the optimal shape of the liver container and source neutron energy spectrum whenever this spectrum is free to choose.

From the knowledge obtained by studying these issues we may conclude that a 'variable' or set of different neutron filter(s) in BNCT would give, in every specific case, an optimal treatment from the neutrons point of view. This is essential knowledge, for designing a 'new' filter at the HFR in Petten or elsewhere.

It is often stated that the future of BNCT as a serious treatment relies on the availability of new boron carriers. However, this thesis shows that a better understanding of the BNCT *neutronics* gives a considerable improvement as well.

Chapter 2

Optimal neutrons and dosimetry

2. Optimal source neutrons with regard to dosimetry in BNCT

In this chapter, the optimal source neutron energy in BNCT for brain tumours is investigated as a function of several biological and physical parameters. When investigating the optimal source neutron energy for BNCT one is looking for those source neutrons which cause maximum damage to the cancer cells and ideally none, but practically only a tolerable damage to the healthy cells. For the case concerning irradiation of the human head, different types of cells (tissues) with different tolerance doses are involved. Therefore, in principle, the best source neutrons are not simply the neutrons producing the highest ^{10}B absorption rate in the tumours but the source neutrons giving the most ^{10}B absorption-reactions in the tumour before reaching the tolerance dose in one of the healthy tissues. This requires insight into the 'dosimetry' that is based on results coming from radiobiology.

2.1 Background on BNCT dosimetry and radiobiology

The values of the tolerance doses that are currently being used in conventional radiotherapy have been mainly determined empirically by observing the levels of early and late side effects which develop in patients who underwent radiotherapy. The vast amount of data that has been collected during the time since the introduction of radiotherapy stems from treating patients with different fractionation schemes and doses of gamma rays and megavoltage X-rays [58]. The value of the tolerance dose strongly depends on the number of fractions into which the total dose delivered to the patient was divided. Mathematical methods have been developed that allow adjusting the value of the tolerance dose depending on the number of fractions [59]. Another factor which has a profound impact on the level of the tolerance dose is the quality of radiation used for treating the patient. It is well known that the biological effect per unit dose is higher for high LET[8] radiation as compared to low LET radiation [60]. This is due to the differences in the density of ionisation events inside a cell. While the cellular DNA repair mechanisms can cope with DNA damage that is evenly distributed inside a cell nucleus, multiple damaged sites produced by high LET radiation pose a more serious problem. Hence, at the same level of dose, high LET radiation is more effective in killing cells than low LET radiation. The need for comparing the doses of radiations of different qualities that induced the same level of biological damage triggered the introduction of the relative biological effectiveness – RBE (defined in Chapter 1). RBE values can be determined experimentally in *in vivo* and *in vitro* experiments.

---

[8] In radiobiology LET stands for Linear Energy Transfer and is defined as the energy lost by charged particles due to interactions per unit of distance.

The problem with the RBE values is that their level depends on the cell system used for the experiment and the analysed endpoint [61]. Hence, when a new radiotherapy modality is developed, during which high LET radiation will be applied, it is not possible to simply recalculate the tolerance doses for irradiated organs on the basis of RBE values that were determined under laboratory conditions. Hence, no validated methods exist with the help of which the tolerance doses for high LET radiation could be calculated based on the clinical experience with low LET radiation. For ethical reasons it is not possible to determine the tolerance dose by exposing patients to various doses of high LET radiation as was done with X-rays and photons during the early days of radiotherapy [58]. This problem is especially pertinent to such complex radiotherapy modalities as BNCT, where the organs at risk are exposed to a mixed beam of both high and low LET radiations. Despite numerous radiobiological investigations it is not clear whether the effects of both radiation qualities are additive or synergistic [62,63]. In order to circumvent the radiobiological and medical issues described above, the optimal source neutron energy can be determined for a range of *RBE* values. This approach, extended by varying other parameters, such as the ^{10}B concentration, is applied in this chapter. Such an approach is at least a strong indication, as to whether there is a significant influence of the biological and clinical values on the optimal source neutron energy in BNCT and if so, what are these influencing parameters.

2.2 A parameter study for BNCT of the brain

The biological and physical parameters that are varied enclose the *RBE* factors, the ^{10}B concentration, the intensity of the gammas present in the beam and the thickness of skin and cranium. Another parameter that is chosen to vary is the tolerance dose set in skin and brain. All parameter value ranges are discussed in the next section. After setting ranges for these parameters, for every configuration, the optimal source neutron energy is calculated. The optimal source neutron energy allows most of the neutrons to react with ^{10}B present at certain tumour positions under the constraint of not exceeding a pre-set dose limit in healthy tissue.

2.2.1 Set-up and chosen parameter ranges

A cubic phantom is irradiated with neutrons from a 120 mm diameter disc shaped source with 22 discrete neutron energies, logarithmically chosen between 0.1 eV and 1 MeV. The calculations are carried out with the Monte Carlo code MCNP4C2 [7]. The MCNP geometry is shown in Figure 2.1. The neutrons are mono-directional. They first hit a layer of skin, then a layer of cranium before reaching the brain in which the tumours are located at four separate depths. All tissue compositions and densities are as defined in the ICRU46 report [8]. Small MCNP tallies (volume 78.5 mm^3) are located along the beam centre line, at every millimetre, in order to calculate the dose as a function of depth in the phantom. As will be seen in the next section, the dose is also averaged over the whole volume (1.366 litres) of the brain which is represented by the drawn hemisphere in Figure 2.1.

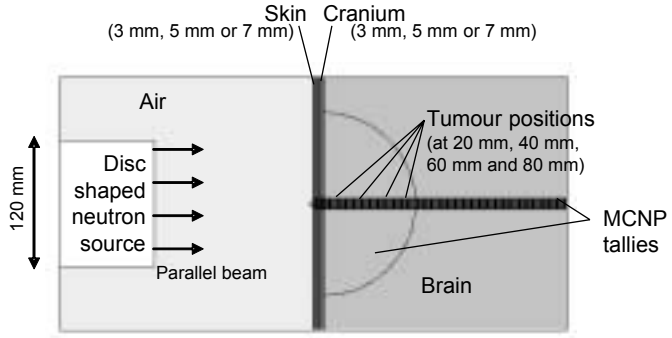

Figure 2.1. Cross section of the MCNP geometry.

The biologically weighted dose[9] D_w in every tally i in the phantom is determined, as follows:

$$D_w = \left(C_B \cdot CBE_B \cdot D_B\right)_i + RBE_p \cdot \left(D_p\right)_i + \left(RBE_n \cdot D_n\right)_i + RBE_\gamma \cdot \left(D_\gamma + \lambda_{b\gamma} \cdot D_{b\gamma}\right)_i \qquad (2.1)$$

The CBE_B in this equation is the compound adjusted *RBE* as explained in Section 1.1.2 and the C_B is the concentration of ^{10}B. The D's represent the absorbed doses for the thermal neutrons (p), the fast neutrons (n) and induced gammas (γ). The absorbed dose[10] for the beam gammas ($b\gamma$) is given per source gamma and therefore has to be corrected with the term $\lambda_{b\gamma}$ which is defined as the ratio of source gammas to source neutrons. The ranges of these parameters are shown in Table 2.1. The ranges are mainly based on the BPA [64] and BSH [65] related treatment protocols used in Petten and on a boron uptake study [66]. Since these protocols are based on current literature, it is of no surprise that these ranges practically include all values used in BNCT literature (see Nigg [67]).

During the MCNP calculation, 10 ppm of ^{10}B is assumed in all tissues. The influence and implications of the boron concentration in the tissues is discussed in section 3.1 of Paper I. After the MCNP calculations, a post-processing program calculates all the different configurations. When combining all parameters in categories III and IV in Table 2.1, there are almost 25 million possible configurations. By ignoring double occurrences, mostly zero values, and obviously deleting physically impossible combinations, the number of possible configurations could be reduced significantly and becomes 4,527,600.

[9] Notation here is according to IAEA-TECDOC-1223 [4]. In Paper I the used indices are different, e.g. D_w=H (see Footnote 1), D_B=D_{10B}, D_p=D_N and D_n=D_H.

[10] The absorbed dose is also known as the physical dose.

Table 2.1. All varied parameters in this study categorized with their values, ranges and/or step sizes.

I. Thickness of skin and cranium					
Skin–Cranium [mm]: 3-3, 5-5 and 7-7					
II. Tolerance dose ratios					
$\frac{\text{skin(point}^*\text{)}}{\text{brain(point}^*\text{)}} = \frac{1}{5}, \frac{1}{3}, 1, 3 \text{ or } 5$					
$\frac{\text{skin(point}^*\text{)}}{\text{brain(volume)}} = \frac{1}{5}, \frac{1}{3}, 1, 3 \text{ or } 5$					
III. Relative biological effectiveness factors and boron concentrations					
	C_B [ppm]	CBE_B [-]	RBE_p [-]	RBE_n [-]**	RBE_γ [-]
Skin	0-80 step 10	0-4 step 1	1-5 step 1	1-6 step 1	0.5-1 step 0.5
Cranium	0-20 step 10	0-2 step 1		1-6 step 1	
Brain	0-30 step 10	0-2 step 1		1-6 step 1	
IV. Beam gammas					
Source gamma energy [MeV]: 1, 5 and 10					
Number of source gammas on every source neutron ($\lambda_{b\gamma}$) [-]: 0, 1/20 and 1/10					

*) Point is defined as tally volume of 78.5 mm^3

**) The RBE_n cannot exceed its previous tissue value [68].

2.2.2 The influence of parameter biasing on the results

One of the major problems when interpreting the results of this study is the presence of some parameter values a reader regards as unrealistic. The problem is that the optimal source neutron energies resulting from the 'unwanted' parameter value(s) cannot be recognized. It is simply impossible to produce a graph that shows the outcome of every single configuration, as every parameter needs a dimension. A solution to this problem can only be obtained interactively: first record the outcomes of all 4,527,600 configurations into a data file and after the user has selected the parameter value ranges of interest, the results are collected, processed and presented. Furthermore, due to physical and other criteria by which the parameter values are selected, not every parameter value is equally represented in the total result. This can be regarded as biasing. For example (see Table 3 in Paper I) a RBE_n (=RBE_H) value in skin of 6 is present in 38% of all configurations. Again the outcomes of such a parameter value cannot be 'recognized' in the presented results. The interactive solution proposed above is necessary to accomplish this.

To re-cap, the main interest of this study is to investigate the role of each parameter and its value for all settings.

2.2.3 Results: the optimal source neutron energy

The percentage of parameter configurations resulting in a certain optimal source neutron energy when treating tumours between 20 mm and 80 mm from the skin, under the constraint that the allowed tolerance dose in skin is three times higher than in the volume of the brain is represented in Figure 2.2. This tolerance dose ratio is comparable with the ratio as described in the EORTC protocol on 'metastatic malignant melanoma in the brain' [64] that prescribes not to exceed a biologically weighted dose of 22 Gy in a point in the skin and 7 Gy averaged in the brain. In Figure 2.2, the skin and cranium thicknesses are 3 mm (further referred to as the '3 mm phantom').

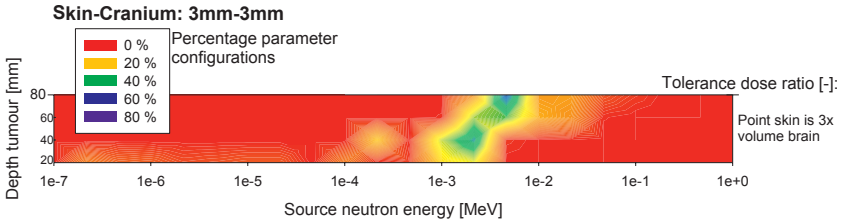

Figure 2.2. Percentage of parameter configurations resulting in a certain optimal source neutron energy as function of one tolerance dose ratio in the 3 mm phantom. The vertical axis displays the location of the tumour.

Note that Figure 2.2 is an interpolated contour plot over 22 x 4 grid points; 22 discrete energies on the horizontal axis times 4 depths of the tumour. It can be seen that for tumours at 20 mm depth, roughly 30% (yellow) of the configurations prescribe 1 keV source neutrons and another 40% result in 2 keV.
Although it is difficult to see in Figure 2.2, for the same depth, approximately 20% (orange) of the configurations result in 0.2 eV source neutrons. Overall, for all tumour depths the majority of the configurations prefer source neutron energies between 1 keV and 10 keV. For all ten tolerance dose ratios studied, for the 3 mm phantom, the percentage configurations with certain optimal source neutron energies are presented in Figure 2.3. The graph is an interpolation over 22 x 10 x 4 grid points (energies x tolerance ratios x tumour depths). The results for the 5 mm and 7 mm phantoms are shown in Figures 2.4 and 2.5, respectively. Some obvious trends noticeable in Figures 2.3 to 2.5 are mentioned here and are explained further in the next section.

- The differences between the Figures 2.3 to 2.5 show that there is an influence of the skin and cranium thicknesses on the optimal source neutron results.
- The tolerance dose ratios show an influence. For every phantom, whenever the tolerance dose in skin is below or equal to the tolerance dose in brain, the same 'image' is obtained. The other tolerance ratios can be further classified according to 'point' brain or 'volume' brain.
- Despite the skin and cranium thicknesses, the tumours at 40 mm and 60 mm depth result mostly in 2 keV and 4 keV source neutrons, whatever phantom, whilst the tumour at 80 mm 'needs' source neutrons with higher energies when the skin and cranium becomes thicker.

- For the tumour at 20 mm depth, the majority of the configurations prefer lower source neutron energies whenever the skin and cranium become thicker.

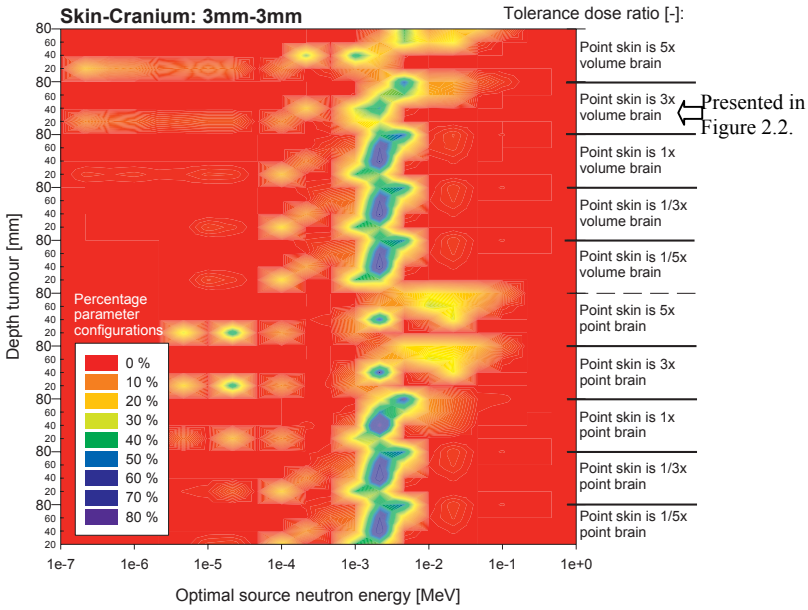

Figure 2.3. As in Figure 2.2 but for all the ten studied tolerance dose ratios (3 mm phantom).

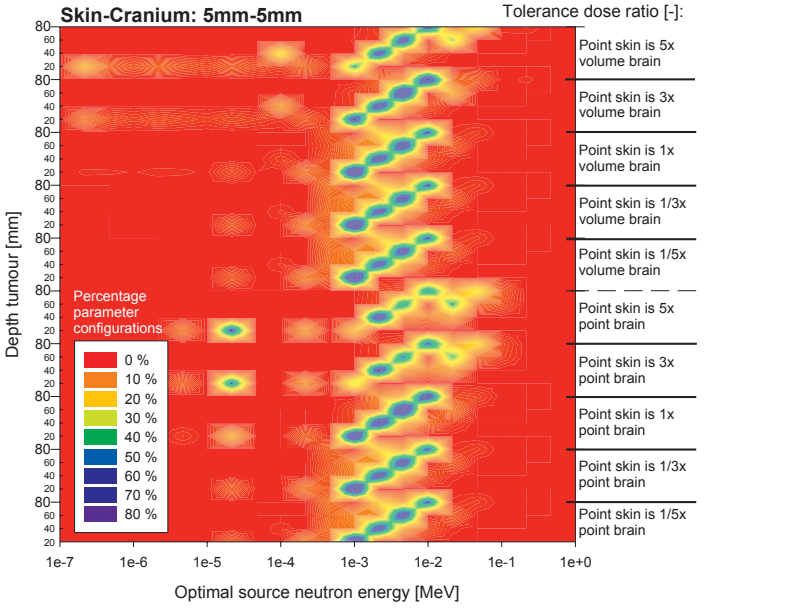

Figure 2.4. As in Figure 2.3, but for the 5 mm phantom.

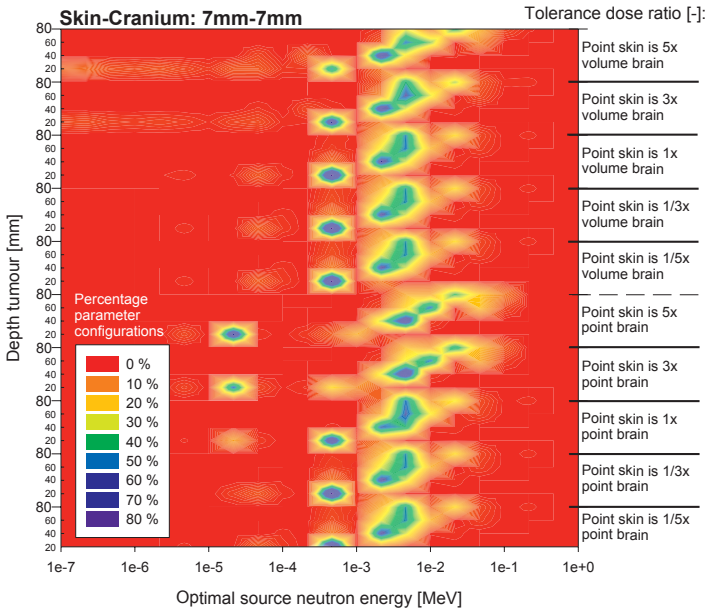

Figure 2.5. As in Figure 2.3, but for the 7 mm phantom.

2.2.4 Results: the influencing parameters

In the following, the influencing parameters are discussed in the order as presented in Table 2.1.

Category I: *Thickness of skin and cranium*

The thickness of the skin and cranium has a significant influence on the optimal source neutron energy results for the shallowest and deepest seated tumours. A transition can be seen when comparing the Figures 2.3 to 2.5.

In the case of the shallow seated tumour (at 20 mm depth), with increasing skin and cranium thickness, the majority of the optimal source neutron energies 'moves' from 2 keV and some 100 eV towards 1 keV and finally to 500 eV for the 7 mm phantom. The explanation for this transition is given with the help of Figure 2.6 which shows the ratios of the thermal neutron flux in the tumour located at 20 mm to the maximum flux in skin for the three studied thicknesses. The lowest curve represents the ratio of the flux in the tumour to the maximum in brain. The higher the value of the ratios, the more thermal neutrons are in the tumour than in skin or brain. This is preferable. At first sight, source neutrons greater than 100 keV are optimal but, regarding the fast neutron dose due to recoiling protons as shown in Figure 1.6 in Chapter 1, appear unusable. Furthermore, the brain-result in Figure 2.6 is slightly curved between 0.1 eV and 10 keV with a maximum around 100 eV. The skin curves become steeper with decreasing skin thickness. As a result, it seems that the skin curves prescribe 'higher' source neutron energies whilst the brain curve prescribes 'lower' energies. Consequently, there is more profit using source neutrons with higher energies with decreasing skin thickness. For the deepest seated tumour

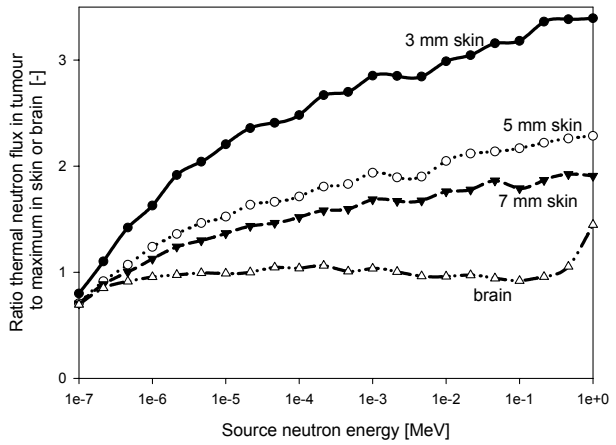

Figure 2.6. This graph belongs to the explanation given in the text for the relation between skin-cranium thicknesses and the optimal source neutron energy for shallow seated tumours.

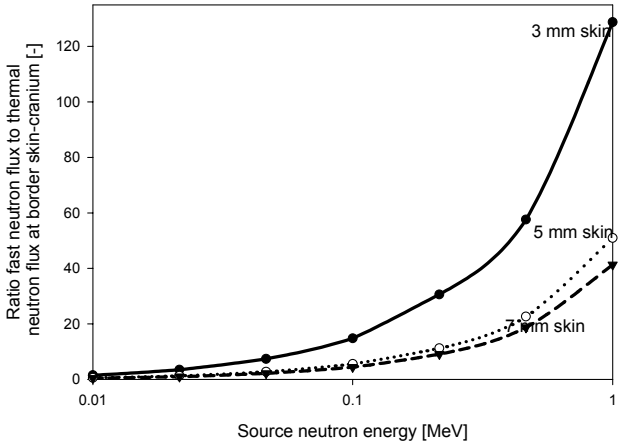

Figure 2.7. This graph belongs to the explanation given in the text for the relation between skin-cranium thicknesses and the optimal source neutron energy for deep seated tumours.

at 80 mm, a transition towards higher optimal source neutron energies is observed from 5 keV via 10 keV towards 20 keV (see Figures 2.3 to 2.5). The basic mechanisms causing this dependence on skin thickness is explained with Figure 2.7. Figure 2.7 shows the ratios of the fast neutron flux to the thermal neutron flux for the three skin thicknesses at the border between skin and cranium. The lower this

ratio the better and thus lower source neutron energies are preferable. The opposite effect is caused by that the number of thermal neutrons in the deepest seated tumour increases with increasing source neutron energy (see Figure 1.3 in Chapter 1). Although, the higher the energy of the source neutrons the better, the 3 mm skin curve is limited by a more quickly increasing fast neutron component in the skin than the other skin thicknesses. This explains the relation between the increasing energy of the optimal source neutrons and increasing skin thickness.

Category II: *Tolerance dose ratios*
An important outcome of this parameter study is that the optimal source neutron energy as a function of parameter variations shows clear dependence on the chosen tolerance dose in skin and brain (see Figures 2.3 to 2.5). Three groups, distinguished by having similar characteristics in the results, can be identified according to the tolerance ratios:
*Group 1, in which the tolerance dose in a point in the skin is lower than or equal to the tolerance dose in a point in the brain and also over the total volume of the brain. For this group the skin turns out to be the treatment limiting tissue.
*Group 2, which has a higher tolerance dose in a point in the skin than in a point in the brain. The brain turns out to be the treatment limiting tissue in the majority of the cases.
*Group 3, is the same as Group 2, except that the tolerance dose in brain is set over the whole volume of the brain, then both the skin as well as the brain can be the treatment limiting tissue.

Category III: *Relative biological effectiveness factors and boron concentrations*
According to Table 5 in Paper I, it is clear which parameters are of direct influence on the optimal source neutron energy; i.e. C_B, CBE_B and the RBE_n. For Group 1, by far, all dose limits are reached in skin at the interface with cranium. Furthermore, in the case of Group 2, the C_B and CBE_B for brain tissue and the RBE_n for all tissues are the influencing parameters. In recording the location of where the tolerance dose is exceeded, most positions are at the thermal neutron fluence peak between 20 mm and 40 mm. Finally, in the case of Group 3, a mixture of C_B and CBE_B for both skin and brain tissue and the RBE_n for all tissues, are the influencing parameters.

Category IV: *Beam gammas*
For all phantom dimensions, there is an influence notable for tumours at 20 mm and 40 mm for Groups 2 and 3. For the higher values of the gamma related parameters, the optimal source energies tend to lower energies.

2.2.5 Results: Improvements when using the optimal source neutrons

Following the above results concerning which source neutron energy ensures the maximum alpha production in the tumour, a logical follow-up question is: is it necessary to provide all these 22 source neutron energies? To investigate this, the number of alphas generated by the optimal neutrons is compared with the number of alphas as produced by each of the 22 source neutron energies as described in section 2.2.1. To clarify this, as an example, the alpha productions in the tumours obtained

with the optimal source neutron energies are compared with the alpha productions resulting from using only 10 keV source neutrons. This is done for all the 4,527,600 configurations. The improvements in alpha production when one could select in every configuration the optimal source neutron energy instead of only 10 keV source neutrons, is shown in Figure 2.8 for the 5 mm phantom. The percentage of alphas in the tumours that are produced *more* with the optimal source neutrons than with the 10 keV source neutrons, goes up to 400%. In other words: for a specific parameter setting (configuration) the optimal source neutron energy is 5 times better.

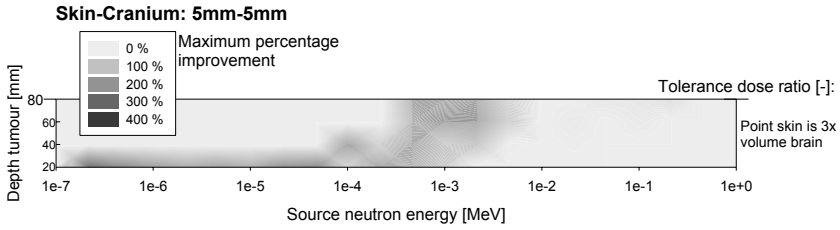

Figure 2.8. Maximum percentage improvement of the number of alphas produced with the optimal source neutron energy in comparison with the number of alphas produced with 10 keV source neutrons for one tolerance ratio (5 mm phantom).

All the percentages presented in Figure 2.8 are taken for the configurations where this improvement in alpha production is a maximum. As mentioned in Paper I, graphs like Figure 2.8 show a dependency with the tolerance ratio but then there is no significant difference concerning these graphs for the 3 mm and 7 mm phantoms. In Figure 2.8, for this particular '400% improvement' case, the use of 0.2 eV source neutrons for superficially located tumours becomes a reality when dealing with very low ^{10}B related parameter values in skin (see further Table 5 in Paper I). The same article predicts that besides using 10 keV source neutrons, the availability of source neutrons with energies in the order of tens of eV will cover all configurations and assure the best alpha production possible in BNCT. In how far this prediction is true was investigated after the publication of Paper I. The results are presented here.
All possible pair-configurations out of the above mentioned 22 source neutron energy results are investigated. For example, the outcomes of the maximum improvement when using the optimal source neutron energies instead of only 0.1 eV source neutrons is combined with the results of the 2 keV source neutrons. For every pair of source neutron energies the smallest improvement values are collected. It turns out that the availability of 500 eV and 10 keV source neutrons provide the smallest difference in alpha production compared with the optimal source neutrons. However, the 'maximum' improvement when these 500 eV and 10 keV source neutrons are available is still 50%, for a certain parameter setting. The outcome of an attempt to minimise the maximum improvement even further is shown Figure 2.9. When 3 beams with three different source neutron energies can be chosen out of the 22 studied source neutron energies, it turns out that the best set consists of 5 eV, 500 eV and again 10 keV. With this trio the maximum improvement of having all 22 source neutron energies available is only 28%.

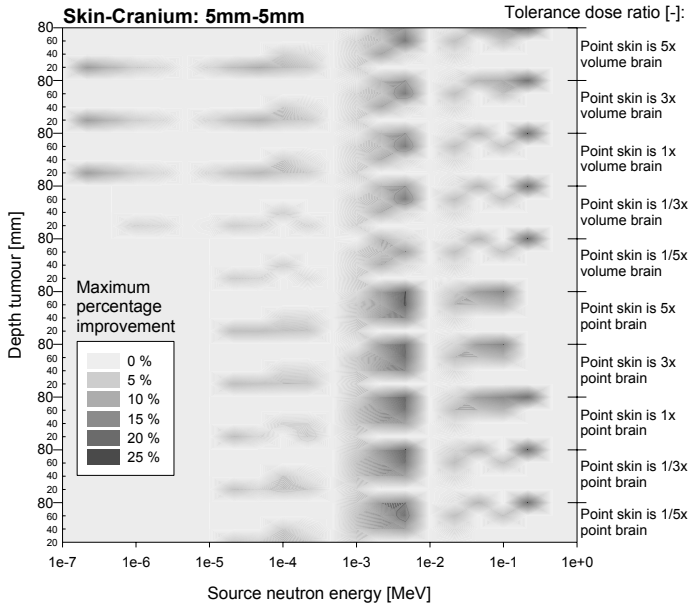

Figure 2.9. With the availability of source neutrons of 5 eV, 500 eV and 10 keV only a maximum improvement of 28% in alpha production would be achieved when using the optimal source neutron energy.

2.3 Conclusions

The optimal source neutron energy delivers a maximum of alphas in the tumour, while not exceeding tolerance dose constraints. It turns out that the definition of these tissue dependent tolerance doses greatly influence the source energy making a neutron 'optimal'. The results presented in Figures 2.3 to 2.5 indicate that according to the ratio of the tolerance dose set in skin to brain three groups can be distinguished. The thickness of skin and cranium affects also the choice of which source neutrons are better to use. The parameters of influence are the ^{10}B concentration (C_B), the boron related *CBE* and the *RBE* for fast neutrons. It turns out that the tissue in which the tolerance dose is reached first determines the parameters causing the major deviation in the source neutron energies. Future studies will involve the field size of the beam and the influence of the shape of the phantom. Also the possibility to process user-defined ranges of the parameter values on-line, by using an interactive program, is necessary to continue and control the discussed parameter biasing.

Another important conclusion from the alpha production improvement results (see Figure 2.9), is that the availability of 5 eV, 500 eV and 10 keV source neutrons would improve the treatment plans (in this study) enormously. In this studied brain case, the nuclear physicist and/or treatment planner in BNCT could deliver, no matter what the circumstances or parameter settings, most of the alphas at the tumour location.

Chapter 3

Adjoint techniques in BNCT

3. Application of adjoint Monte Carlo techniques in BNCT
In specific cases, adjoint Monte Carlo (MC) calculations can provide the optimum setting to the treatment planner giving shorter calculation times compared with 'normal' forward MC. However, the adjoint method in its standard form is not applicable when dealing with mono-directional treatment beams as in BNCT. In this chapter, techniques are developed to overcome this problem and the method is demonstrated in a specific example.

3.1 Background, theory and MCNP
In reactor physics, an equation can be defined that is adjoint to the neutron transport equation. With the proper adjoint source the solutions of this adjoint equation can be physically defined as a measure of the "importance" of a neutron in contributing to the response of the detector [69]. In the field of irradiating materials, e.g. phantoms and patients, it can simply provide at defined locations (points, areas, volumes) the expected detector contribution of source particles, as a function of energy, position and starting angle. These 'detectors' can be tumours or organs at risk (OAR), which together, will be further mentioned as regions of interest (ROI).
In MCNP [7] the adjoint equation is solved by tracing histories 'backward'; the normal MC method is reversed and the adjoint particle obtains after an event the energy and angle that a forward particle would normally have before this event. As stated in the manual, MCNP in forward (=normal or standard) mode is preferable when the detector volume or area is large. The adjoint mode is interesting when the detector volume or area is small but the source volume or area is large. Because the histories start in this small detector area and are traced 'backward', they will have a higher probability to contribute to the larger phase space region of the source[11]. In principle, regarding the statistics, the more particles contribute to the estimate under investigation, the smaller the variance becomes. A good description of adjoint MC is given in Wagner et al. [70] and Hoogenboom [71].
An important result, as derived in Bell and Glasstone [69], is the relation between the 'forward' flux and the adjoint function, ϕ and ϕ^+ respectively. The total detector response, depending on the detector response function Σ_d is the integral at the right hand side of

$$\int Q(r,\Omega,E)\phi^+(r,\Omega,E)dVd\Omega dE = \int \Sigma_d(r,\Omega,E)\phi(r,\Omega,E)dVd\Omega dE \qquad (3.1)$$

[11] In adjoint MC the forward source becomes the adjoint detector and forward detector becomes the adjoint source

in which r is the position, Ω the solid angle, E the energy and V the volume. This integral is taken over all phase-space variables and provides the same result as the integral of ϕ^+ multiplied with the source function Q. In other words: knowing the adjoint function and source function of a treatment beam enables to determine e.g. the total detector response of the flux, dose or reaction rate inside a certain area, as similarly obtained with a forward calculation.
As written in the manual, MCNP has an option called 'SCX' which enables to register at the detector the initial energy of the particle emitted by the source. Regardless of the mode in which MCNP is running (forward or adjoint), four possible outcomes can be gathered. These, sometimes confusing possibilities, are listed in Table 3.1.

Table 3.1. Overview MCNP modes.

MCNP mode / Particles start at source:	Obtained at detector:
Forward	**Total detector response**
Forward+SCX	**Expected contribution of forward source particles to the forward detector response (=numerically proportional to the adjoint function)**
Adjoint	**Adjoint function**
Adjoint+SCX	**Expected contribution of adjoint source particles to the adjoint detector response (=numerically proportional to the total detector response)**

Because MCNP normalizes every source description automatically, this means in BNCT that the results of the adjoint calculation are normalized to the tumour (adjoint source) instead of the neutron beam (forward source). A proper normalization is necessary as one is interested in 'per-particle-results' related to the real source. Although the re-normalization of the adjoint results can be derived analytically, the 'SCX' option provides an additional check. The normalization of adjoint results is discussed in the report by Wagner et al. [70] and also Difilippo [72].

3.2 General adjoint set-up for BNCT

In BNCT, to know the contribution of source neutrons to a reaction rate in the tumour, the adjoint source spectrum should be similar to the (n,α) capture cross section of ^{10}B. Most of the organs at risk, as defined in, for example, the melanoma metastasis of the brain protocol, are in deeper lying structures which will only suffer from the dose given by the thermal reactions. In theory, a well defined adjoint source energy spectrum should be similar to the (n,α), (n,p) and (n,γ) cross sections of ^{10}B, ^{14}N and ^{1}H, respectively, depending on the reaction rate of interest. These cross sections have in common that the probability to have a reaction at thermal neutron energies is orders of magnitude higher than for high energies. In practice, in

BNCT, calculating the thermal neutron flux will provide a good first estimate of how the thermal neutron related doses in the phantom will behave (see Chapter 1). In the following, the adjoint source spectrum as well as the forward detector response function are taken to be thermal and defined uniform up to 0.5 eV.
Most of the fast neutron dose is delivered at the outside in the first few centimetres of the tissue. Because the interaction of the beam-particles always starts in the skin, the fast neutron dose component can be regarded as uniform and needs only to be estimated at one location. Note that when dealing with the fast neutrons in the adjoint approach, it is difficult or maybe even impossible, as the skin will form a large adjoint source.
For all calculations presented in this chapter, a new 172 group neutron cross section library is made, according to the XMAS energy structure. All cross section tables, for nuclides present in human tissue used in BNCT, are based on JEF2.2 evaluations for 37ºC and with S(α,β) thermal treatment.

3.3 Adjoint treatment planning with a mono-directional beam
Nowadays, most investigations in treatment planning focus on decreasing the computational time to obtain the doses without making concessions on the accuracy [73-75]. When less time is needed for the dose calculations, simply more time is available for optimization of a treatment plan. There are mainly three algorithms used in treatment planning to calculate the dose which are the convolution/superposition method, the pencil beam method and the MC method. The first two mentioned methods are widely applied in treatment planning and can be characterized as being fast but less accurate compared with the MC method which is accurate but needs more calculation time. Acceleration of Monte Carlo calculations by variance reduction techniques is also of great interest and is investigated in a wide area of research. Especially in treatment planning, Monte Carlo provides more accurately calculated dose rates in the heterogeneous human tissues [76,77] than with the other methods. However, the current long calculation times prevent that the MC methods can be applied for every single beam configuration for every patient.
In comparison with the above mentioned investigations, far less articles have been published in the field of adjoint MC as used in treatment planning. The existing articles [72, 78-81] all deal with gammas and it is only in the work of Lilly [82] in which the adjoint method is related to BNCT. However, Lilly uses a discrete ordinate radiation transport code to optimize a neutron filter for BNCT.
Since BNCT is worldwide still in a clinical trial phase, relatively, not many patients are treated. As a consequence, little experience exists in positioning neutron beams and making treatment plans for various locations and positions of the cancer. In this chapter, we will show that the adjoint MC technique can be an improvement for BNCT and can help the treatment planner in selecting optimum beam settings.
In the published adjoint articles mentioned above, two approaches concerning the adjoint detectors can be distinguished:

1. The adjoint detectors are formed by segmentation of a sphere or cylinder surrounding the irradiated geometry. All adjoint particles are tallied in the angular and energy bins for each segment.

2. The adjoint detectors are shaped according to the beam exit of the treatment beam. Only adjoint particles resembling the characteristics of the treatment beam, e.g. energy and angle, are tallied in the appropriate bins.

If the interest is to know the delivered dose or reaction rate of a treatment beam to a certain ROI, the first approach would be ideal if the segments are very small and the bin structure very fine. Knowing this (almost) continuous adjoint function for the phase space coordinates around the geometry, the treatment beam could be positioned everywhere and directed freely. However, to obtain reasonable statistics the segments and binning have to be coarse, as such the response of a treatment beam cannot be obtained. Nevertheless, this is useful as a way to obtain a first impression of the directions that are interesting to irradiate from [78].
The second approach delivers, together with the appropriate source function Q (see equation 3.1), the same total detector response as a forward MC calculation. However, a major drawback of this approach is that only adjoint particles at the adjoint detector can contribute with flight directions and energies in the ranges of the treatment beam; e.g. a 2 degree angular divergence requires adjoint particles arriving at the detector within an angle of 2 degrees with the normal of the adjoint detector plane. The probability that adjoint MC particles arrive at the adjoint detector within certain (narrow) boundary conditions is small and it will take a long calculation time before good statistics are obtained. As a result, the adjoint MC approach seems inapplicable for performing BNCT with a mono-directional neutron beam. To overcome this, two techniques are developed which will be discussed in the next sections.

3.3.1 Adjoint Point Detector Technique (APDT)

Since the probability that particles will traverse a plane detector perpendicularly within a narrow solid angle is very small, one has to 'force' them. In MCNP this 'forcing' technique is called DXTRAN; at every event the contribution a particle will have to a certain specified region is calculated deterministically. DXTRAN can be used in forward and adjoint mode. This specified region can be defined as a point and by positioning this point far away from the geometry and surrounding it by a beam-shaped body, a situation as depicted in Figure 3.1 arises.

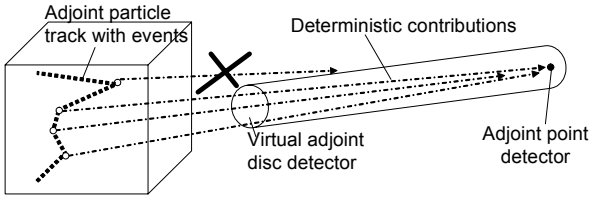

Figure 3.1. Adjoint Point Detector Technique (APDT).

For a disc shaped beam opening, the adjoint point detector is surrounded by a cylinder. As can be seen in Figure 3.1, all contributions to the adjoint point detector pass the entrance of the cylinder (almost) perpendicularly, while all others are "killed". This entrance behaves as a virtual disc shaped adjoint detector. The further

away the adjoint point detector is positioned the more perpendicular the contributions traverse the entrance. In order to prevent angular spreading in the example discussed in section 3.4, the distance from the centre of the irradiated phantom to the beam exit (=adjoint detector disc) is chosen to be 10^4 cm. This value depends on the size of the phantom and the size of the beam exit. The normalisation factor for this adjoint technique is provided in Appendix A. As there is a possibility for a score at the adjoint point detector for every event, the relative error decreases more quickly, as compared with the analogue MCNP. A disadvantage of the technique is when a lot of particle events are involved of which many will not contribute to the point detector because these contributions 'travel' through the region outside the beam-shaped body (see Figure 3.1) and a lot of CPU time is wasted. Many particle events are caused by e.g. highly scattering materials and large geometric dimensions.

3.3.2 Legendre EXpansion Technique (LEXT)

The second technique to determine the adjoint function for the direction perpendicular to the adjoint detector is by use of the Functional Expansion Technique (FET). Suppose that the angular adjoint function at a certain adjoint detector for a certain energy group looks like the 2D function *f(α,β)* plotted in Figure 3.2. When this function behaves well, it can be expressed by

$$f(\alpha,\beta)=\sum_{l=0}^{\infty}\sum_{m=0}^{\infty}d_l d_m \psi_l(\alpha)\psi_m(\beta) \qquad (3.2)$$

in which $d_{l,m}$ are coefficients and $\psi_{l,m}$ are orthonormal basis functions. It is in the work of Beers and Pine [83] that this so-called FET is applied in MC. They accomplished that all samples contribute to the estimates of the coefficients $d_{l,m}$. This can be proven, for example, for one dimension (d_l) by combining the definition

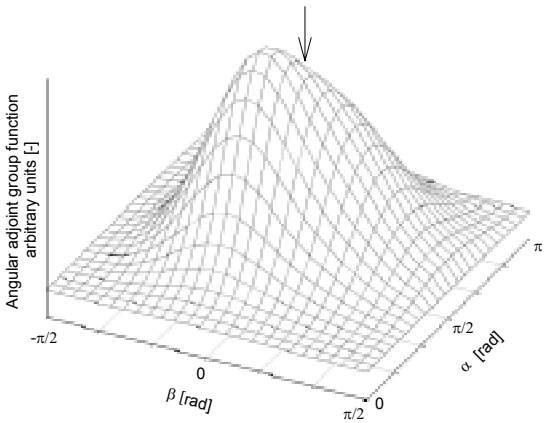

Figure 3.2. Example of an angular adjoint function in 2D at an adjoint detector for one energy group.

for the total detector response and the scalar product describing the coefficients (equation 8 and 9 in Paper II),

$$d_l = \int f(\alpha)\psi_l(\alpha)d\alpha \approx \frac{1}{N}\sum_{i=1}^{N} w_i\psi_l(\alpha) \qquad (3.3)$$

in which N is the number of samples and w is the statistical weight. For the two dimensions (α,β), both accompanying coefficients $d_{l,m}$ can be evaluated from N. The indices l and m have to be truncated by values of L and M such that the function f is still well approximated by the sums of the products of d and ψ. In any case, L and M should be high enough for a converged result but not too high because of the increasing relative error for every extra coefficient used. Note that there is a direct relation among the number of samples, number of used coefficients, the convergence of the result and its relative error. This relation should be investigated once for every geometric model and problem set-up (e.g. detector size, number of energy bins, material characteristics). This may be regarded as a disadvantage of the technique.
In this work it is chosen that the orthonormal basis functions are the Legendre polynomials: Legendre EXpansion Technique (LEXT). At this stage it is not well known how angular adjoint functions in different circumstances (e.g. other geometries and particle types) will look like. Therefore, investigating other base functions which describe the adjoint functions better in particular cases is expected to be subject of future studies. The Legendre polynomials are orthogonal at (-1,1) and have the best pointwise convergence properties near the centre of this interval [84,85]. As a consequence, since the interest is in the normal direction, α and β have to be chosen such that the normal falls in the centre of their ranges (see the arrow in Figure 3.2). The parameterisation in Figure 3.2 is as chosen and described in Paper II. Actually, α and β are the angles which describe the directions of the adjoint particles traversing the adjoint detector and can be defined in many ways as long as the normal directions fall at the centres of the intervals. Note that the adjoint particle can cross the adjoint detector from one side only. In this parameterisation the ranges of [-π/2, π/2] and [0, π] will be linearly scaled into the Legendre range of [-1,1]. Functions f with steep gradients and/or zero values demand extra coefficients to describe these characteristics properly. The use of too many coefficients should be prevented and can be accomplished by truncating the angles (see Section II.F of Paper II).
Before the Legendre technique is applied, all adjoint particles will be recorded in a so-called PTRAC file written by MCNP, on a sphere surrounding the geometry. With the recorded position and flight direction information it can be determined whether an adjoint particle traversed a certain area. In a post processing program these areas can be mathematically described with a shape resembling the neutron beam exit (=adjoint detector). The number, positions and orientations of these adjoint detectors are free to choose in the post-processing program and no new MCNP calculation has to be done. As described in Paper II the weight of every adjoint particle traversing an adjoint detector is recalculated directly with the LEXT to provide its weight if it was flying in the normal direction. After this ‘weight-

adaptation' the average and relative error are calculated like in a normal tally result of MCNP.

3.4 Example: Optimum characteristics in the irradiation of a human head

The APDT and LEXT are demonstrated by calculating the total detector responses of the fluxes due to thermal neutrons and gammas[12] in 10 randomly distributed tumours and 10 OAR (in total 20 adjoint sources) in a patient suffering from brain cancer. The MCNP geometry of the patient's head is shown in Figure 3.3, as created by the program Sabrina [86]. The OAR are defined as written in the protocol in Petten used to treat metastatic malignant melanoma in the brain [64]. CT-images of the head of a patient are translated, using Scan2MCNP [87], into a MCNP geometry consisting of 47520 voxels. Each voxel can be filled with either brain tissue, soft tissue, cranium or mixtures of these.

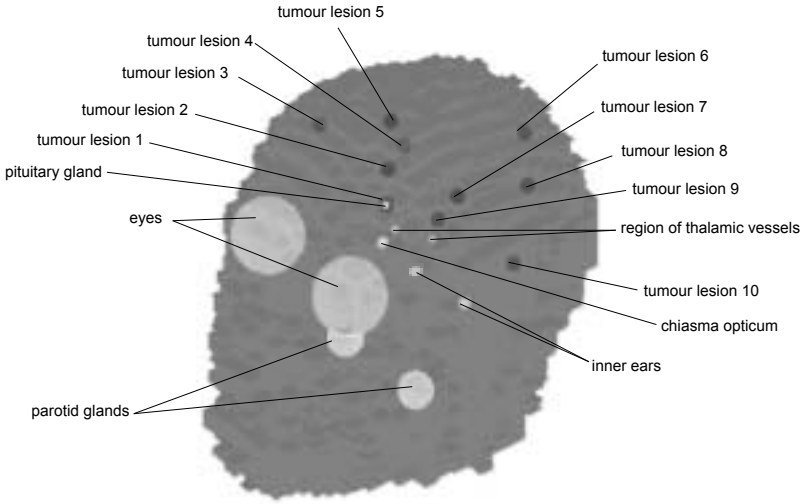

Figure 3.3. Phantom head with 10 OAR and 10 tumours which is used as an example throughout this section.

The model is surrounded by air. Figure 3.4a shows the head phantom surrounded by 60 centre points where all adjoint detector discs are positioned. These centre points are described in azimuthal and polar angles as shown for one adjoint detector disc in Figure 3.4b. At each of the 60 positions, 17 discs with different, systematically chosen orientations of their outer normals (pointing away from the phantom) are positioned. See Figure 3.4c.

[12] In the remaining text shortened as 'thermal neutron flux' and 'gamma flux'

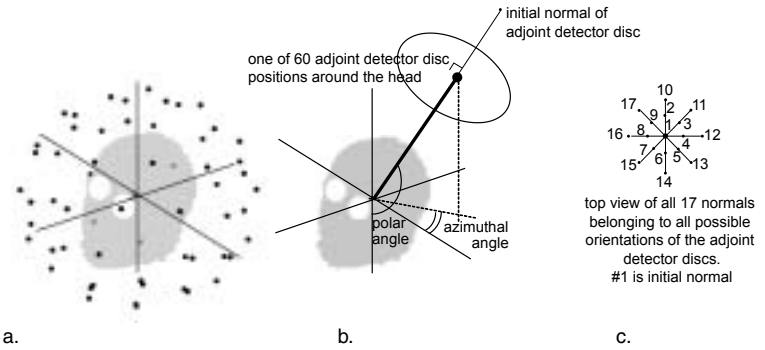

Figure 3.4. (a) MCNP head model surrounded by 60 adjoint detector disc centre points. (b) The adjoint detector centre points are described in polar and azimuthal angles. The initial disc normal points at the centre of the phantom. (c) At each of the 60 centre points, 17 adjoint detector discs with different orientations are defined.

This implies that in total 1020 beams around the head are modelled. These 1020 adjoint detector discs are also the virtual adjoint disc detectors in the APDT and the beam exits in the forward MC method. All calculations, for all 1020 beams, are performed for beam diameters of 5 cm, 10 cm and 15 cm. The source energy spectrum is taken from the BNCT treatment beam called HB11 as available in Petten. It consists of mainly 10 keV source neutrons and has a 2 degree divergence which can be regarded as mono-directional. The gamma source spectrum is taken uniform between the limits 0.01 MeV and 20.0 MeV.
In the next subsections the results will be discussed, starting with the calculation times of the forward MC and the two adjoint MC techniques. Thereafter, the results for this phantom head itself will be discussed by showing the optimum positions and orientations for the Petten neutron beam to irradiate from. The other feature coming out of the adjoint calculation, the optimum source neutron energies, is discussed last.

3.4.1 Calculation times of forward MC, APDT and LEXT

The calculation times of the forward MC, APDT and LEXT can be compared after setting the allowed relative error in the 20 ROI for the three methods to <5% (95% confidence interval). These relative errors are averaged values from the results of a certain number of beams. To save time, 255 out of the 1020 beams around the head are chosen and their relative errors in the tumours and OAR are averaged. Since the relative error of the results in Monte Carlo is 'scaled' with the square root of the number of tracked particles, it can be determined how many particles need to be run and consequently how much time it takes to get a certain relative error. All averaged relative errors are, before scaling, up to 15% in the 95% confidence interval. In case of the LEXT, the post-processing time is linear proportional with the MCNP time to obtain the PTRAC file. The resulting times for the three methods are summarized in Table 3.2. In the column containing the forward MC results, the absolute times are given in days. The calculation times of the adjoint techniques are normalised towards these forward MC times and written in bold face. It is clear from Table 3.2 that in the case of the head phantom example, the smallest beams (5 cm) are

calculated most quickly with forward MC for both neutrons and gammas. In the case of neutrons, the 10 cm and 15 cm beams are 6 and 20 times faster calculated with the LEXT respectively. The APDT lacks from the fact that the adjoint thermal neutrons scatter a lot due to the hydrogen in the tissues, for which each time, a contribution to the adjoint point detector is determined. In many cases the contribution cannot be made for the reason described at the end of section 3.3.1.

Table 3.2. The total calculation times for the three methods.

Diameter of adjoint detector/ beam exit [cm]	Time to calculate 1020 beams **Normalised to forward**		
NEUTRONS	FORWARD	APDT	LEXT
5	**1.00** *(=140 days*)*	**27.40**	**1.52**
10	**1.00** *(=113 days*)*	**18.42**	**0.15**
15	**1.00** *(=88 days*)*	**12.94**	**0.05**
GAMMAS			
5	**1.00** *(=53 days*)*	**1.57**	**1.47**
10	**1.00** *(=42 days*)*	**0.52**	**0.55**
15	**1.00** *(=27days*)*	**0.33**	**0.30**

**) Results gathered on a Pentium IV with a 3 GHz processor and 512 Mb of memory.*

For gammas, for the 10 cm and 15 cm beam exits, the calculation times for the APDT improve because gammas interact far less with the head phantom materials. The calculation times for these large beam exits are similar to the LEXT in case of 20 ROI. One can imagine that when less ROI and/or less gamma beams are involved, less APDT calculations are needed and the APDT becomes preferable to the LEXT. An overview of when forward MC calculations are faster than the two presented adjoint MC techniques, as a function of the number of ROI against the number of beams, is given in Figures 3.5 and 3.6, for neutrons and gammas respectively. Every figure contains 3 lines belonging to each beam exit diameter. Above the line of a certain beam diameter, the calculations are faster using forward MC, below the line by adjoint MC. Figures 3.5 and 3.6 are based on scaling the calculation times of the forward MC, APDT and LEXT head phantom results according to:

$$\textit{Forward MC} \propto \textit{number of beams}$$

$$\textit{APDT} \propto \textit{number of beams and number of ROI}$$

$$\textit{LEXT MCNP} \propto \textit{number of ROI}$$
$$\textit{LEXT Post Proc.} \propto \textit{number of beams and number of ROI}$$

The increase of MCNP calculation time due to the increasing complexity of the geometry when more ROI are involved is not taken into account. Due to this, in reality, the LEXT results will be somewhat better than presented because of the post processing time which does not depend on the complexity of the geometry.

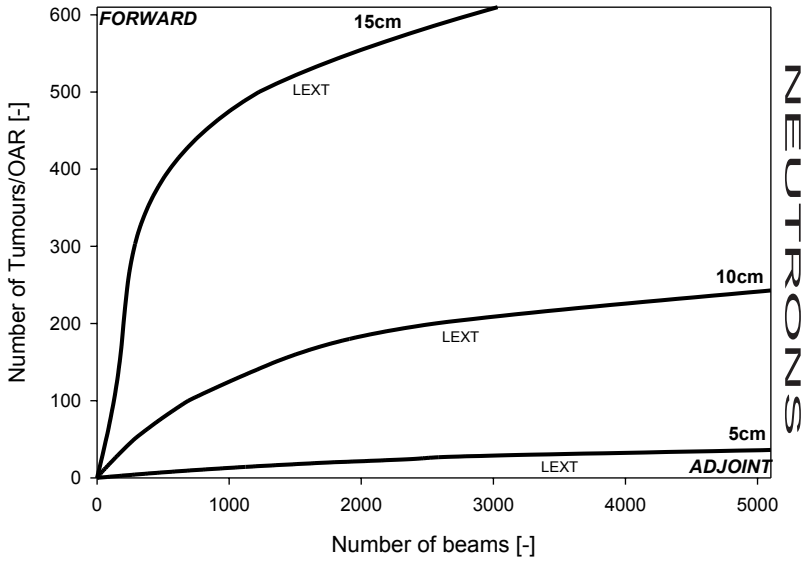

Figure 3.5. Number of neutron beams with different diameters vs. number of tumours/OAR for which adjoint or forward MC is preferable. For a given beam diameter, the region below the line is the area where adjoint MC is preferable.

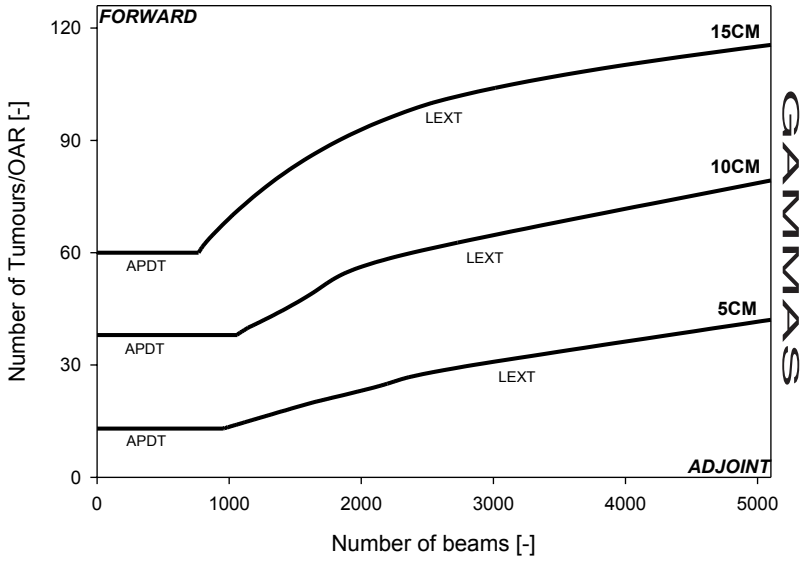

Figure 3.6. Like Figure 3.5 but for gamma beams with different diameters.

The exercise presented here can also be performed for a fixed beam diameter but as a function of ROI size/volume. The same kind of curves would be expected, as presented in Figures 3.5 and 3.6, although the largest beam diameters will represent the smallest ROI and vice versa.

3.4.2 Optimum irradiation locations and directions

The following results are obtained with the LEXT for the Petten neutron beam with a diameter of 15 cm. The differences between the LEXT outcomes and 255 controlling forward calculations are within the statistical uncertainties. From this point, the thermal neutron fluxes used are chosen to be the average fluxes over all tumours and the average over all OAR. Due to this averaging, the statistics improve and therefore an optimum treatment plan can be obtained more quickly. It is subject for further research to see if such an approach can hold in comparison with a treatment plan which is optimised taking into account every single tumour and OAR. Figure 3.7 shows the optimum orientation out of the 17 discrete orientations the Petten beam can have at each of the 60 positions around the phantom head as shown in Figure 3.4.

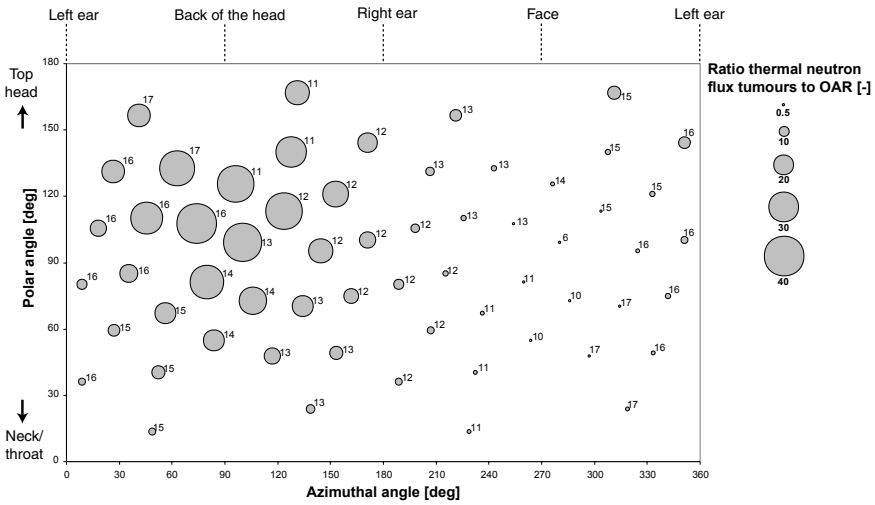

Figure 3.7. An example outcome for treatment planning with the 15 cm neutron beam in Petten: the maximum ratios of the thermal neutron fluxes in tumours to OAR at each of the 60 positions around the phantom head example.

This optimum is defined as to have the highest ratio of thermal neutron flux in the tumours to OAR. As a constraint, it is chosen that the thermal neutron flux in the tumours has to be >75% of the maximum attained thermal neutron flux in the tumours for that beam position. This constraint prevents the situation that the flux in the tumours is low but the flux in the OAR is close to zero which gives anyhow a high ratio. However, the time the patient needs to be irradiated becomes too long.
The optimum ratios around the head are also given in the grey histogram in Figure 3.8; the 60 beam positions are ordered with the azimuthal angle. The polar angles

and orientation numbers information is omitted. For instance at beam position 13 in Figure 3.8, around 40 times more thermal neutrons are delivered in the tumours then in the OAR. It is clear that the best locations to irradiate the tumours are from the back of the head. Therefore, with the LEXT, 20 times faster than with normal forward MC, the whole head has been 'scanned' by 1020 beams and the treatment planner can obtain the best positions and orientations for irradiation. It is nearly impossible to have 'missed' a good beam configuration. This is therefore a good starting point to combine the best beams and optimise the treatment plan.

3.4.3 Optimum source neutron energy group

The optimum source particle energy can also be obtained with the adjoint technique. This is simply the source particle energy giving the highest contribution of interest in the tumour and the lowest in the OAR. In terms of adjoint MC, this means that only a few (or ideally none) adjoint source particles originating from the OAR will reach the adjoint detector. This results in a large accompanying relative error. Of course one has to be confident that enough histories have been run in order to assure that the result has converged. It is expected that obtaining acceptable relative errors within various bins at several adjoint detectors around the phantom when using an isotropic adjoint source, is a good indicator that the MC run has converged. This problem of having large errors in some ROI will not occur rapidly in the results with the Petten beam, as many energy groups are involved by which the statistical uncertainty decreases after integration. In the case of single source neutron energy groups, it is for now impossible to draw conclusions on the absolute ratio values of the thermal neutron flux in the tumours to OAR. It is expected that MCNP variance reduction techniques are needed to overcome this problem of the large relative errors in the OAR. This is subject for further investigations. Another approach would be the use of deterministic codes.

For our phantom head example, irradiated with a 15 cm diameter neutron beam, the maximum ratios of the thermal neutron flux in the tumours to OAR are displayed in Figure 3.9. The grey levels indicate the maximum ratios out of 17 orientations, for 17 energy groups as a function of the 60 positions around the head. For this purpose, the 172 energy groups are condensed to 17 groups (the first 12 groups and 16 times 10 groups) in order to improve the statistics and be more realistic regarding obtaining a certain energy group; it is impossible to obtain neutrons in a very narrow energy range apart from having them in a great number. In Figure 3.9, the accompanying optimum orientation is not indicated. The maximum ratios have to meet two additional constraints concerning the thermal neutron flux in the tumours: (1) It has to be >75% of the highest possible thermal neutron flux at that position for a certain orientation and energy group. (2) The relative error has to be <5% in the 95% confidence interval. When these constraints are not met the ratio is displayed as zero. Constraint 1, in particular, truncates the results in Figure 3.9 by which no results are obtained for the lowest and highest energy groups; the values are shown in white. The order of the 60 beam positions in Figure 3.9 is similar to Figure 3.8 and it can be seen that the beams irradiating the back of the head prefer lower source neutron energies. The white histogram in Figure 3.8 shows the ratios obtained similar to those discussed earlier for the Petten beam results, but for the optimum

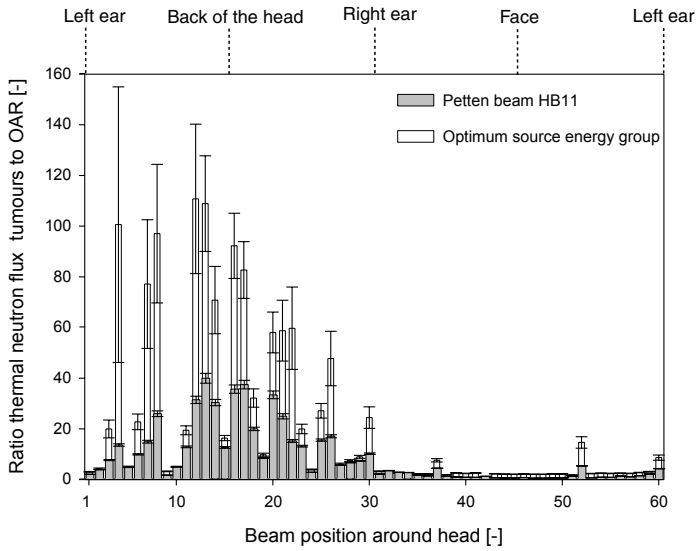

Figure 3.8. Maximum ratios thermal neutron flux in tumours to OAR of the Petten beam in 60 positions around the phantom head example.

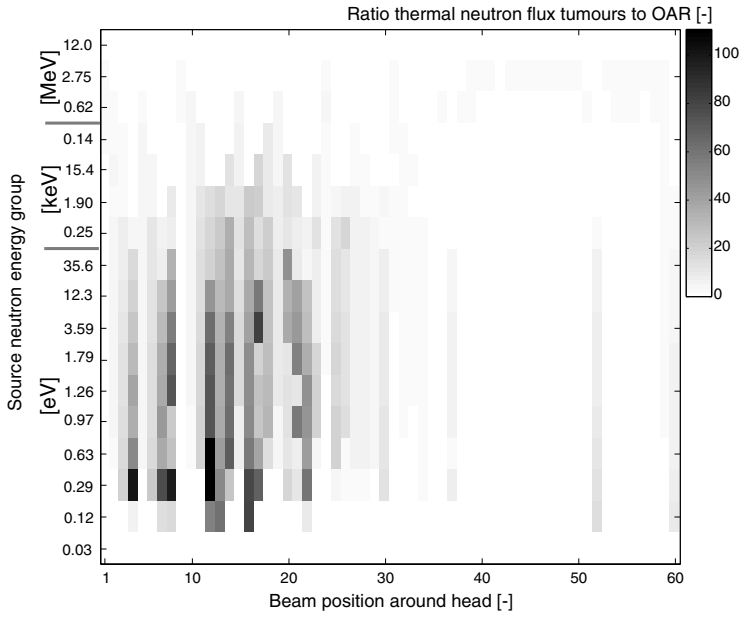

Figure 3.9. Maximum ratios of the thermal neutron flux in the tumours to OAR out of 17 orientations for 17 source neutron energy groups around the phantom head.

energy groups. Because of the high relative errors for the OAR, these ratio values are not trustworthy but nevertheless presented to indicate the kind of improvements that can be expected. In any case, less thermal neutrons in the OAR means that the tumours can be irradiated longer and more boron reactions can be realised.

3.5 Conclusions

Application of the adjoint MC for mono-directional neutron beams enables the optimum irradiation directions and positions for a BNCT treatment plan to be obtained more quickly. The next step would be investigating how to optimise the treatment plan by selecting the best beams out of all information provided by the adjoint. The adjoint also provides information on which source energies give high contributions to the tumours and small to the OAR. It needs investigating further how to deal with the accompanying large relative error in the OAR since this makes it difficult to judge the absolute improvements when using single energy groups. Nevertheless, the adjoint outcome suggests using low source neutron energies, in case of the head phantom example. This has to be further investigated with respect to the skin dose and the dose given to the deepest seated tumours.

Chapter 4

Thermal neutron field facility

4. Design of a homogeneous thermal neutron field facility for BNCT

The BNCT treatment of organs suffering from cancer which are irradiated extra-corporally becomes more and more interesting after the promising results obtained by researchers in Italy [88-90]. Furthermore, researchers in the field of drug development for BNCT desire a facility containing a homogeneous thermal neutron field for in-vitro studies. In this chapter, a measure for homogeneity is defined as the ratio of minimum thermal neutron flux to maximum thermal neutron flux in a volume. As explained in Chapter 1, the thermal neutron flux is a perfect indicator for the ^{10}B absorptions.

In section 4.1, the description of a facility especially designed for liver treatment by an epithermal neutron beam is given, while section 4.2 discusses the best design for a facility if a new neutron beam would be constructed.

4.1 Design of an irradiation facility for the extra-corporal treatment of liver cancer with an existing epithermal beam

In Pavia (Italy), two livers of patients suffering from haematogenous metastasis of colorectal cancer, were treated extra-corporally with BNCT. The first patient lived for almost 4 years (communication from A. Zonta, Pavia Italy) while the second patient died a month after the operation due to heart failure. The success of the first patient, which implies undeniable evidence that BNCT can be a promising treatment, encouraged us to investigate whether extra-corporal liver irradiations can be performed with the existing epithermal neutron beam at the High Flux Reactor in Petten (The Netherlands). The study has the aim to design a facility in which a homogeneous thermal neutron field can be obtained with epithermal source neutrons; the BNCT treatment beam in Petten itself cannot be tailored due to the ongoing clinical trials concerning BNCT of brain tumours {REF 5,6}. As the treatment will be extra-corporal, there is a limit which the patient may be anhepatic, which when corrected for the loss of transportation time, according to the liver surgeon, allows an irradiation time of at most 180 minutes. The study has the additional goal to obtain the same thermal neutron fluence of $4x10^{12}$ (+/- 20%) cm^{-2} as was applied in Pavia. Another requirement (according to the Pavia researchers) is that the liver should not exceed a total weighted dose (as defined in [4] of 15 Gy [89]. The weighting factors (explained in Chapter 1) for the different dose components are those as applied for BPA: RBE_B=1.3 or 3.8 (healthy or tumour tissue) ; RBE_p = 3.2 ; RBE_n=3.2 ; RBE_γ=1.0. An important issue that should be investigated thoroughly after a facility has been built is the dose limit for healthy liver. In this chapter, the focus is mainly on obtaining the homogeneous thermal neutron field. This means finding the parameters with the greatest influence, obtaining their optimum values and describing the choice of the materials. More details about the project to treat extra-corporal livers in Petten are given in Paper III.

4.1.1 Design parameters and selected materials

The BNCT neutron beam at Petten has an epithermal neutron flux of 3.3×10^8 $cm^{-2}s^{-1}$ with an average energy of 10 keV [29]. The skin, cranium and brain tissues are used to thermalise the neutrons by the elastic scattering properties of the prevailing hydrogen to E<0.5eV. This thermalisation effect is indicated in Figure 4.1: The epithermal neutron flux decreases while the thermal neutron flux increases when the neutrons travel into a cube or sphere of H_2O which has similar properties to human tissue. The thermal neutron flux has a maximum at around 2.5 cm depth, the so-called thermal maximum. The thermal neutron flux in the sphere (with diameter of 25.0 cm) is higher than in the cube (sides of 20.0 cm) at deeper positions; the thermal flux is distributed over a larger area.

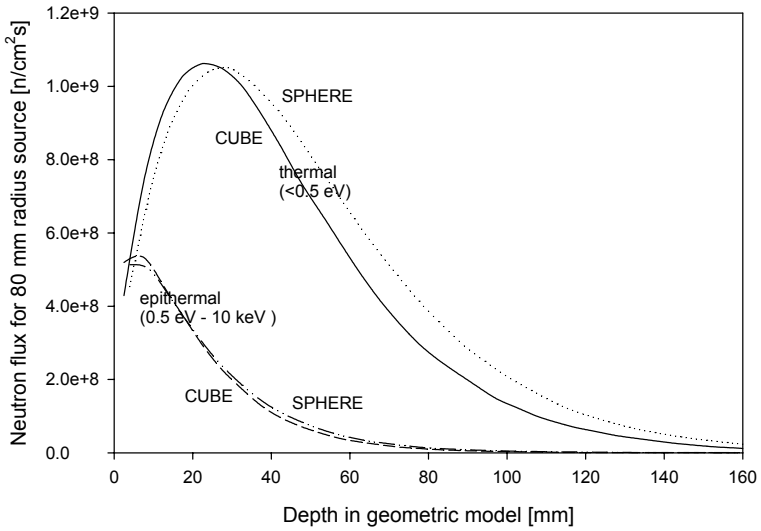

Figure 4.1. The epithermal and thermal neutron flux along the beam centre-line as a function of distance in a cube and sphere of H_2O.

The fixed parameters in the existing Petten set-up are all source related: Energy and spatially dependent source intensity and a maximum radius R_{src} of the irradiation beam of 8.0 cm. At the edges of the Petten beam, the neutron intensity drops rapidly. An average liver has a weight of around 1.7 kg [91] and would fit in an imaginary cube with sides of 12.0 cm. From Figure 4.1 it can be seen that the liver would need to be irradiated from more than one side in order to get a flat neutron fluence distribution.

By extrapolating the idea of irradiating a body from more than one side, the step to irradiate a rotating body which is rotational-symmetric seems straightforward. The simulation of the rotation is discussed in subsection 4.1.2. A spheroid shaped liver holder with a polar axis R_{pol} and an azimuthal axis R_{azi} is chosen, see Figure 4.2. The advantage of a spherical design is that the intensity fall off near the edges of the beam is compensated by the presence of less liver material to irradiate near the

bottom and top of the sphere. R_{pol} can be chosen to be the same as R_{src}. The R_{azi} should be chosen to be a compromise between large enough to create space for the liver and still provide enough thermal neutrons at the centre of the liver. In fact the thermal neutron profile, as shown in Figure 4.1, is distributed over a volume resembling a torus due to rotation of the spheroidal liver holder.
At the edges of the liver holder the tori-volumes are larger, which will decrease even more the already low thermal neutron flux density since this flux is 'smeared out' over this larger volume. This has to be compensated by surrounding the holder by neutron- moderating and reflecting materials in order to increase the number of thermal neutrons at the edges. In addition to selecting appropriate materials, the dimensions of the materials are also variable. Typical dimensions that can be varied in order to optimize are *q1,q2,q3,q4* and *q5* as indicated in Figure 4.2.

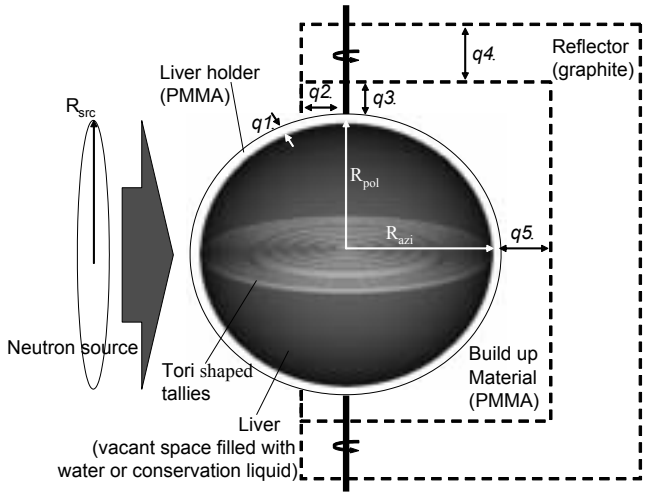

Figure 4.2. Schematic overview of the liver irradiation set-up with all the design parameters and some 3D drawn tori for tallying neutrons simulating rotation.

For moderation of the epithermal source neutrons, a scattering medium containing a lot of hydrogen should be selected. This requirement is met by the plastic polymethylmethacrylate (PMMA) which is solid and stiff. PMMA has a mass fraction for hydrogen which is around 20% less compared with liver tissue. This difference is reduced to 10% due to the higher density of the plastic. PMMA is non-toxic and transparent and therefore suitable for the liver holder. A disadvantage of hydrogen is the production due to neutron capture of 2.2 MeV gammas. For this reason the rotating liver holder is surrounded by sufficient PMMA to create the necessary thermal neutron build-up and supplemented by graphite for more scattering of the neutrons with less production of gammas. In Figure 4.2 these two materials are defined as build-up and reflector respectively. After selecting these materials, the Monte Carlo code MCNP [7] is used to simulate the neutrons and gammas through the geometry. By varying the parameters *q1* to *q5*, one at a time

and observing the changes, the optimum set-up can be approximated. During this phase the thermal neutron flux is monitored at certain characteristic positions, i.e. at the centre, the thermal maximum, the equator, top and bottom, to obtain a homogeneous neutron flux density. At the same time, it is desired to have as low as possible gamma production. When these criteria are closely met, the thermal neutron flux is calculated everywhere in the liver by simply programming many tori evenly distributed inside the liver. After calculating the entire thermal neutron field inside the liver holder for several combinations of promising parameter settings, the most homogeneous result is chosen. In the calculations the liver tissue composition is taken from ICRU 46 [8]).

4.1.2 Simulating rotation with the Monte Carlo code

By programming tori, only one MCNP calculation is needed in which the beam irradiates the liver from one direction. MCNP adds all the track lengths of the neutrons or gammas inside the torus volume and gives, when dividing by the volume of the torus (V_{torus}), the neutron and/or gamma flux. From another point of view, the flux can be seen as a time-averaged flux inside the rotating liver. Mathematically, the above explanation of the calculation of a flux in a rotating torus is as follows: Imagine the torus to be fixed and that the beam is rotating around it with a revolution time *T*. This means that the angular flux $\phi(\vec{r},\Omega,E,t)$, as defined in Bell and Glasstone [69] at $\vec{r}$ within the torus becomes a function of time *t*. The angular flux is also depending on the direction Ω and energy *E* of the neutrons. Integrating over time *T* and dividing by *T* gives a time averaged angular flux, as shown between the brackets in equation (4.1). In fact:

$$\bar{\phi}^{rev}_{V_{torus}} = \frac{1}{V_{torus}} \int_{V_{torus}} dV \int_{\Omega} d\Omega \int_{E} dE \left\{ \frac{1}{T} \int_{T} dt \phi(\vec{r},\Omega,E,t) \right\} = \bar{\phi}_{V_{torus}} \qquad (4.1)$$

gives the total flux averaged over V_{torus} per revolution (*rev*). This is in fact what MCNP calculates with the so called F4 tally [92].

4.1.3 Results of the designed liver facility at the HFR Petten

Two liver irradiation facility designs are discussed which represent the two extremes: As large as possible irradiated volume with acceptable homogeneity and the smallest acceptable volume with a high homogeneity. The first design has a volume of 2.4 litres and is restricted by the homogeneity demand of +/-20% in the thermal neutron fluence distribution. The second design has a volume of 1.6 litres and is restricted by the minimum volume of liver (together with the conservation liquid) that can be expected. After several MCNP calculations, the optimum parameter settings are obtained which are presented in Table 4.1.

Table 4.1. Optimal parameter settings for liver irradiation set-ups.

	$\mathbf{R_{pol}}$	$\mathbf{R_{azi}}$	***q1***	***q2***	***q3***	***q4***	***q5***
	[cm]						
1.6ℓ holder	8.0	7.0	1.0	3.5	3.5	15.0	1.0
2.4ℓ holder	8.0	8.5	0.5	3.0	3.5	15.0	1.0

Parameters *q1*, *q2*, *q3* are of direct influence in the Petten set-up while *q4* and *q5* are of little importance; as long as the graphite thickness *q4* > 15.0 cm. The graphite increases by up to 15% of the thermal neutron flux at the edge of the holder volume. It appeared that the build up PMMA around the holders almost doubles the number of thermal neutrons inside the holder. Figure 4.3 shows the cross sections of the thermal neutron flux distributions in the two liver holders and Table 4.2 contains an overview of the characteristic thermal neutron flux, the maximum weighted dose rates and the resulting irradiation times.

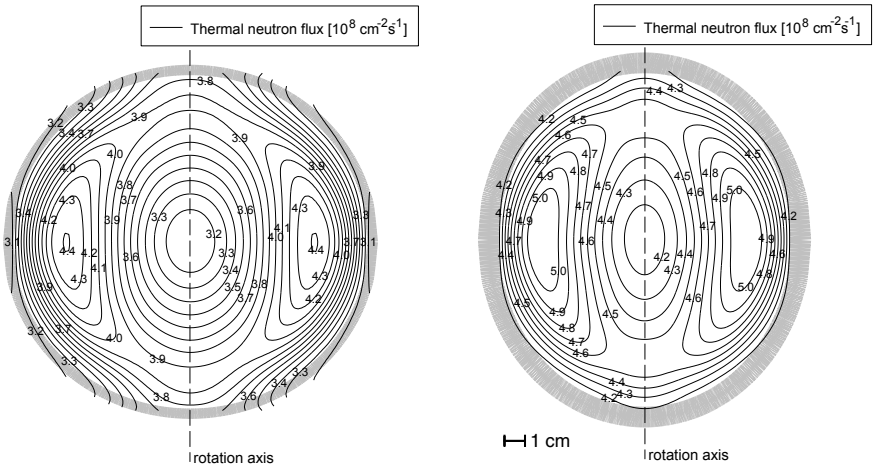

Figure 4.3. Left: The thermal neutron flux in the 2.4 litres liver holder. Right: same for 1.6 litres holder.

Table 4.2. Characteristic fluxes and weighted dose rates in both liver holders.

Description:	**2.4ℓ holder**	**1.6ℓ holder**
Average thermal neutron flux	3.8×10^{8} $cm^{-2}s^{-1}$ -20% minimum +17% maximum	4.7×10^{8} $cm^{-2}s^{-1}$ -12% minimum +9% maximum
Time to deliver 4×10^{12} cm^{-2}	175 min	142 min
Maximum weighted dose rate (point) 8 ppm ^{10}B	5.8 Gy h^{-1}	6.5 Gy h^{-1}
Time to deliver 15 Gy maximum dose	155 min	138 min

It is due to the smaller R_{azi} in the 1.6 litres holder that a better homogeneity can be obtained. In both holders the minimum flux is at the edge and centre of the liver volume and the maximum is as to be expected at the position near to the thermal maximum (see Figure 4.3). The thermal maximum is still present and recognizable in both holders. However in the largest holder, the ratio of maximum over minimum within 8.5 cm is 1.5 instead of almost 4 as seen in Figure 4.1. The 2.4 litres holder is

sufficient to hold livers up to 2.1 kg, which do exist (private communication M. Malago and W. Sauerwein, University Hospital Essen, Germany).
In the 1.6 litres holder, the time to deliver the thermal neutron fluence and the time after which the tolerance dose is exceeded is roughly in agreement. For the largest holder, there seems to be no improvement in homogeneity over the Pavia thermal neutron flux distribution; it has to be recalled that the Petten beam is rather small for such a large organ. Although the required fluence of $4x10^{12}$ cm^{-2} can be given within 180 minutes, the maximum prescribed dose will be exceeded when applying this fluence. This is partly caused by the higher photon dose rate, compared with Pavia, due to the beam photons. Nevertheless, this result is promising enough to proceed first with dosimetry and after that animal studies.

4.2 Optimum neutron beam design and holders for extra-corporal BNCT irradiations

The facility described in section 4.1 for irradiating an extra-corporal liver with epithermal source neutrons, tailored specifically for the HFR in Petten, is designed around a given source description. The 'Forward SCX technique' (see Chapter 3) that gives the expected detector contribution of the source particles which is numerically the same as the result of the adjoint method, can be applied for the inverse exercise: To find a neutron source distribution and spectrum that provides a homogeneous thermal neutron field in a given volume.
Actually, the best shape of the holder, i.e. cuboid, cylindrical or spherical (see Figure 4.4) has a direct dependence on the design of a new optimum neutron beam. It is chosen to study these models with volumes of 2, 4 and 6 litres. Despite of the previous sections, in all models, it is chosen to surround the liver only by PMMA and omit the graphite in order to simplify the set-up at this stage. The holder thicknesses are 0.5 cm while a surrounding PMMA block for build up and scattering of neutrons, is 50x50 cm^2 (width x height). In case of the cylinder and sphere, the block starts 2 cm before the rotation axis.
The new beam exit is chosen to be shaped according to the cross-sectional area of the model: this means a rectangular shape for the cuboid and cylinder and circular for the spherical holder. In the calculations, the dimensions of the beam exit (width and height or diameter) are chosen such that there is always sufficient overlap to each side of the cross-sectional area of the maximum investigated liver volume; 30x40 cm^2 for the cuboid, 25x39 cm^2 for the cylinder and a diameter of 32 cm for the sphere. In fact, these dimensions ensure that the beam area is two times the cross-sectional area of the largest holder (see dimensions of the 6 litres holders in Figure 4.4). The new beam will have a zero divergence and the desired neutron energy in the liver volume is <0.5 eV and the liver tissue contains 15 ppm of ^{10}B homogeneously distributed in the liver.

4.2.1 Set-up of the holder models

In the simulation, every holder model contains smaller cells which are the MCNP detectors. In these cells, the expected detector contributions of the source neutrons are obtained. This is necessary to monitor the homogeneity in the entire model during optimisation as will be further explained in section 4.2.3. Due to symmetry

only a quarter of the cuboid model and half of the cylindrical and spherical models have to be filled by these cells. Figure 4.4 shows the holder models and the surrounding PMMA with on the left the defined neutron sources.

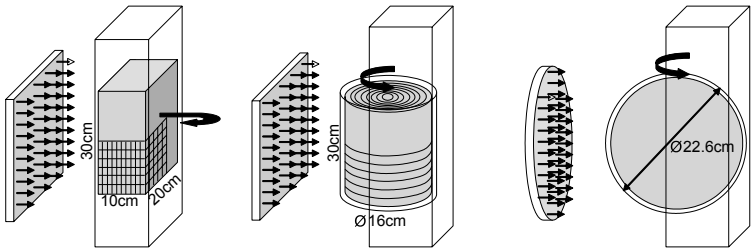

Figure 4.4. Cuboid shaped, cylindrical and spherical holder models (all 6 litres) in which the expected detector contributions are calculated together with the neutron beam exits.

The cell structure per model is organized in the following way:

* Cuboid: A quarter of the 6 litre cuboid model is filled with 300 rectangular parallelopiped shaped cells; width x height x depth=5 x 6 x 10 cells. The cuboid holder is irradiated from two sides (see arrow in Figure 4.4). In reality, the holder is turned half-way the irradiation time. For the 2 and 4 litre holders, the optimisation is performed over fewer cells; the outside cells are not taken into account whereby the thickness remains always 10 cells=10 cm. Separate MC calculations for these smaller volumes are not performed since the effect of the presence of 10% more hydrogen in liver tissue compared with PMMA is regarded to be insignificant compared with other influences such as the actual environment and beam characteristics.
* Cylinder: Half of the cylinder consists of 48 ring-shaped cells; diameter x height=8 x 6 rings. The cylindrical holder is rotating along a vertical axis. Similar to the cuboid model: the volume of the cylindrical holder is decreased by not taking into account the lowest 16 and 32 rings for the 4 and 2 litre holders, respectively, during the optimisation process.
* Sphere: The top half of the sphere is filled (not drawn) with 13 tori-shaped cells. The 4 'tori' along the vertical rotation axis are actually spheres. In every volume, the tori fill the space evenly. The straight arrow, drawn in the spherical holder model, in Figure 4.4 indicates that the diameter of the holder can be decreased, whereby the tori will be redistributed.

4.2.2 Expected contributions of the source neutrons inside the models

The forward source is chosen to have two uniform spectra; of 33 and 43 energy groups between the limits $1x10^{-5}$ eV to 27.4 keV and $1x10^{-5}$ eV to 19.6 MeV, respectively. These values of the upper limits come from the XMAS energy structure. By investigating these two spectra, the optimum source spectrum is obtained with and without the influence of the damaging fast neutrons. The energy groups are condensed groups of the 172 energy groups library described in Chapter 3. Everywhere, the statistical uncertainties in all the calculations presented are <5%

(95% confidence interval). In order to keep the graphs surveyable, only 10 cells of the cuboid model and 8 rings of the cylinder are considered. The results for the 6 litre holder models are presented in the Figures 4.5 to 4.7.

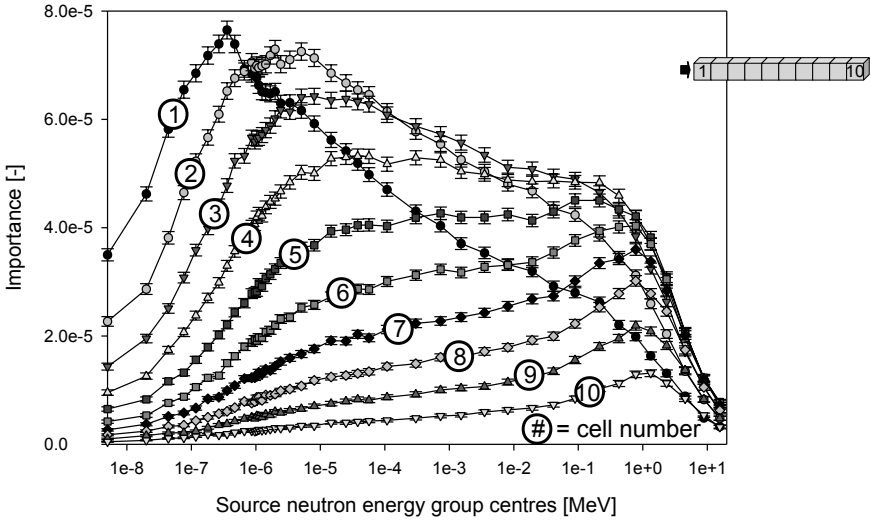

Figure 4.5. Expected detector contributions of the source neutrons of 10 cells along and nearest to the beam centreline inside the cuboid model when irradiated from one side.

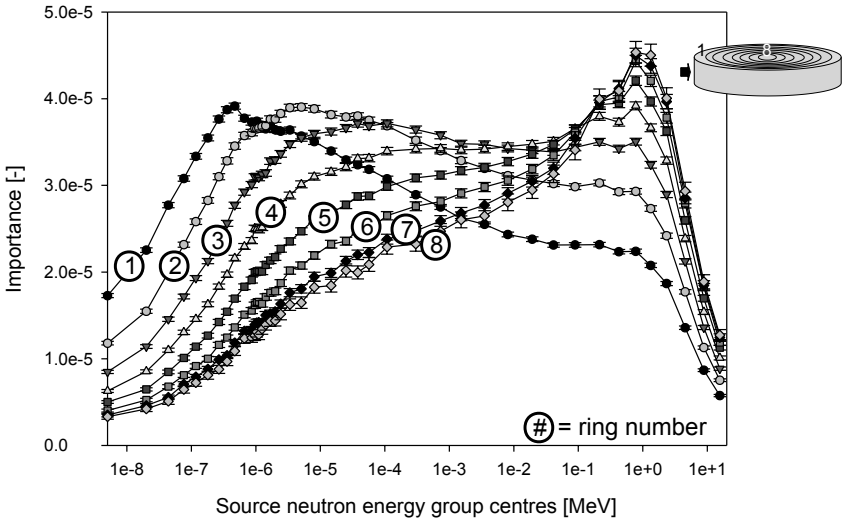

Figure 4.6. Expected detector contributions of the source neutrons of 8 rings nearest to the beam centreline inside the cylindrical model.

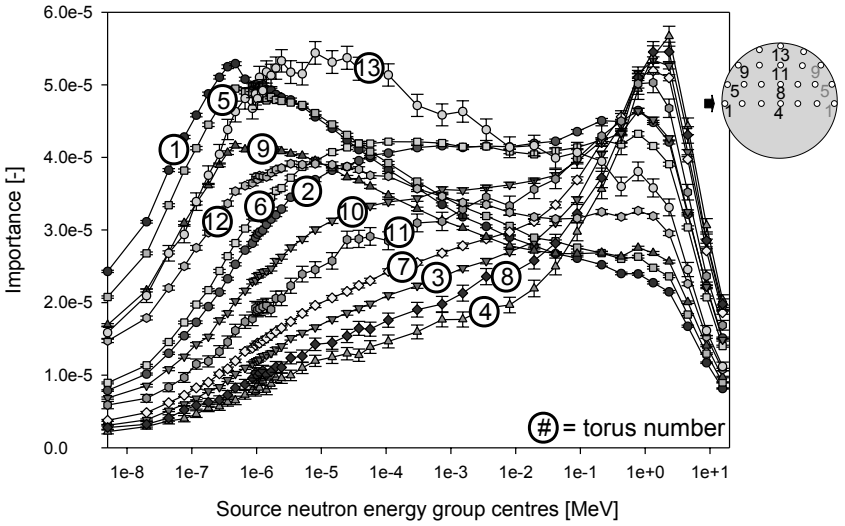

Figure 4.7. Expected detector contributions of the source neutrons of 9 tori and 4 spheres.

In Figure 4.5, 10 cells from the cuboid model, indicated at the upper right, are the nearest to the beam centre line and their expected detector contributions of the source neutrons are shown. Cell 1 is defined here as closest to the beam exit which explains the peaked preference at around 0.5 eV source neutrons. The accompanying importance value of 8.0×10^{-5} implies that for every 12,500 source neutrons of around 0.5 eV leaving the 1200 cm^2 source with 43 energy groups, only 1 neutron contributes to neutrons <0.5 eV in this cell 1. Cell 10, farthest away from the beam exit, has a preference for 1 MeV source neutrons. In Figure 4.6, the expected detector contributions of the source neutrons of 8 coaxial rings nearest to the beam centre line are shown. The outer ring has a preference for thermal source neutrons while the thermal neutrons in the centre ring come mainly from fast source neutrons. The expected detector contributions of the source neutrons of the rings in-between are shaped according to a transition from thermal to fast with plateau-shapes for ring 3 and 4. All the expected detector contributions of the source neutrons of the 13 tori of the spherical model (diameter of 22.6 cm) are given in Figure 4.7. There is a great similarity with the expected detector contributions of the source neutrons obtained in the cylindrical model, e.g. the curves are sharply peaked at the fast source neutrons in the tori (actually spheres) at the centre of the models.
Since the cuboid holder will be irradiated from two sides, the curves shown in Figure 4.5 are added such that cell 1 and cell 10 are added, cell 2 and cell 9, etc. The result is presented in Figure 4.8 for cells 1 to 5. The other 5 cells are similar due to symmetry.

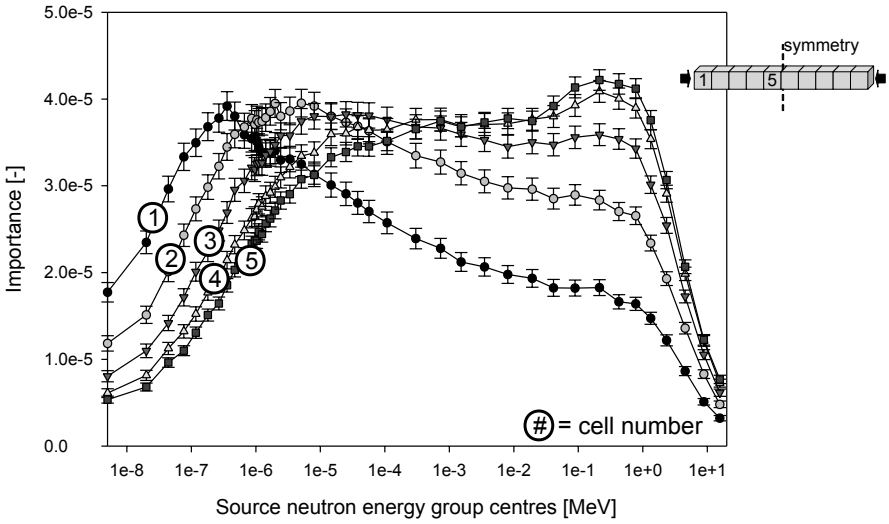

Figure 4.8. Expected detector contributions of the source neutrons when 10 cells are irradiated from two sides. Due to the symmetry only 5 cells are shown. The cells are along and nearest to the beam centreline inside the cuboid model.

4.2.3 Optimum source neutron energies

In order to realise homogeneity in the holder models, it is desirable to produce the same number of thermal neutrons (E<0.5 eV) in every cell. It is not to be expected that a high homogeneity can be obtained by using a single source neutron energy group. Therefore, it is shown here that by combining the contributions of source neutrons of different energy groups k with weight a_k, a better homogeneity is attained. The contributions are labelled as the 'importance' (*imp*) and the sum of the weighed importances over all energy groups in every cell j is called WI_j. Due to the direct relation between the number of source neutrons and importance, homogeneity can be defined as:

$$Homogeneity = \frac{\min_{j=1,J}\left(WI_j\right)}{\max_{j=1,J}\left(WI_j\right)}, \quad where \; WI_j = \sum_{k=1}^{G} a_k \cdot imp(k,j)$$

The closer to unity the better is the homogeneity. The minimum and maximum are selected after summing the weighed importances up to G energy groups in every cell j (J cells in total); G is 33 or 43 energy groups. The weighs a_k of the source energy groups are determined by using a linear optimisation scheme. The so-called Simplex method (described in [93-95]) can maximise an objective function Z under the constraints provided, whenever there is a solution. The scheme to solve is:

Objective function:

$$Z = \max\left(\sum_{j=1}^{J} WI_j\right)$$

3 constraints:

$$WI_j < L$$

$$WI_j \geq Homogeneity \cdot L \quad \text{with } 0 < Homogeneity < 1$$

$$\sum_{k=1}^{G} a_k = 1$$

That is: the optimization process will provide the maximum number of thermal neutrons in the liver under the constraint that the ratio of the minimum and maximum WI_j, among all cells, is between the *Homogeneity* and unity. Similar to the a_k's, L is a variable that will be solved during the optimisation. It is needed to prevent setting an absolute constraint which is already done with constraint 3; this keeps the total number of source neutrons constant. The system is solved each time with a given *Homogeneity* that increases in small steps from 0 towards 1. The maximum homogeneity is found for the last value of the *Homogeneity*, for which the Simplex method is able to provide a solution; if the *Homogeneity* increases further, the constraints cannot be satisfied.

In Figures 4.9 and 4.10, the Simplex solution vectors are shown containing the weights a_k of the energy groups, for the three holder models and three volumes. Figure 4.9 shows the result when source neutrons up to 19.6 MeV may be used while Figure 4.10 is limited up to 27.4 keV.
It is clear from both figures that the maximum homogeneity is reached when using the 'lowest' in combination with the 'highest' neutron energy groups, regardless of the holder model or volume; one exception is the 6 litre spherical holder when no fast neutrons may be used (see Figure 4.10).
For the results of all the "homogeneity vs. neutron source spectrum", the calculations are summarised in Table 4.3. The last two columns of Table 4.3 give the obtained homogeneities for the spectra shown in Figures 4.9 and 4.10.

Table 4.3. Obtained optimal homogeneities in the models for different neutron source spectra.

Model	Volume (litres)	Petten spectrum	Uniform source spectrum			Optimum source spectrum (Simplex)	
Energy range →		0eV-19.6MeV	0eV-27.4keV	<1eV	>1keV <27.4keV	0eV-27.4keV	0eV-19.6MeV
CUBE	2	0.63	0.77	0.48	0.54	0.96	0.98
	4	0.63	0.77	0.48	0.54	0.95	0.97
	6	0.62	0.76	0.47	0.52	0.93	0.95
CYLINDER	2	0.67	0.46	0.26	0.73	0.82	0.99
	4	0.67	0.46	0.26	0.72	0.81	0.99
	6	0.67	0.46	0.26	0.65	0.78	0.88
SPHERE	2	0.62	0.45	0.31	0.60	0.72	0.87
	4	0.44	0.30	0.19	0.55	0.65	0.90
	6	0.36	0.23	0.12	0.44	0.52	0.91

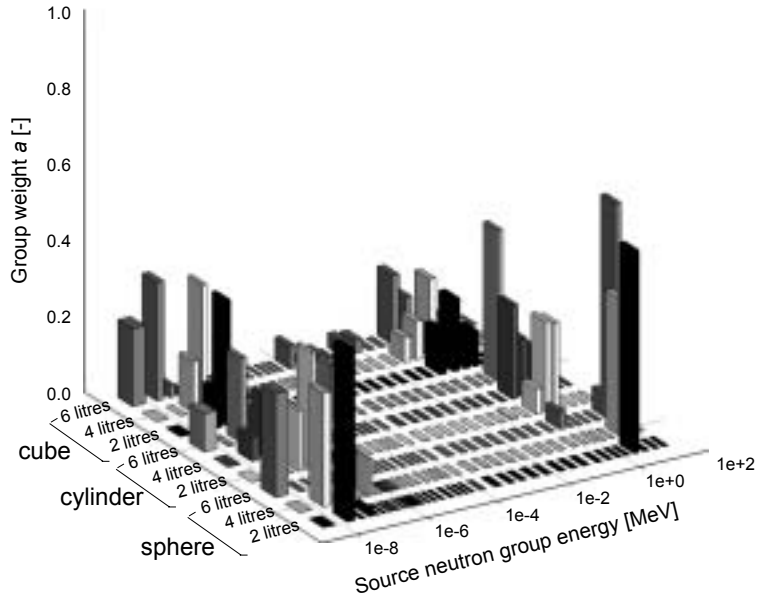

Figure 4.9. The optimum source neutron spectra with a 19.6 MeV upper limit for the 3 geometrical models (3 volumes) to obtain the maximum homogeneity.

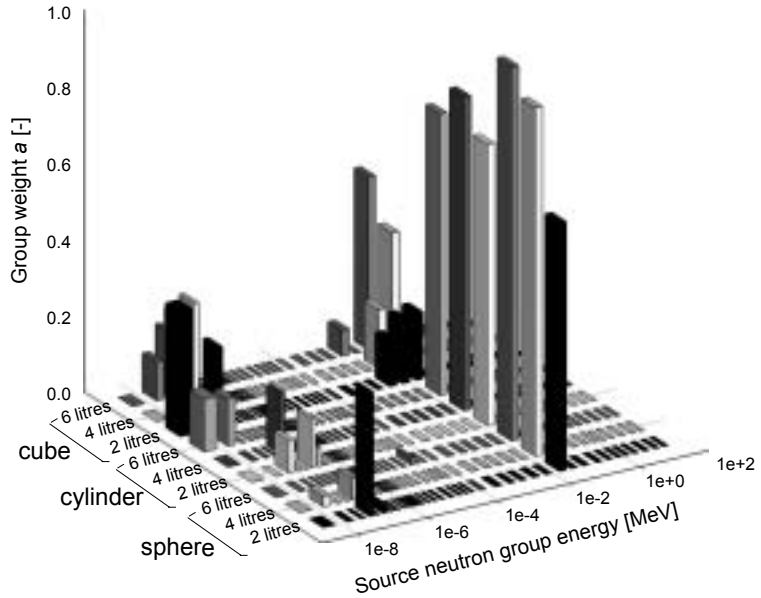

Figure 4.10. The optimum source neutron spectra with a 27.4 keV upper limit for the 3 geometrical models (3 volumes) to obtain the maximum homogeneity.

It can be seen that the cylindrical and spherical holders improve significantly whenever fast source neutrons are allowed. The cuboid liver holder provides the best homogeneous thermal neutron field. In studying all Simplex outcomes, it is concluded that the homogeneities will not change significantly compared to the optimum solution when another nearby energy group is selected or the weights are slightly changed. The numbers presented in the last two columns of Table 4.3 are the arithmetical optima. The table also shows the maximum homogeneities when using source neutrons with either a uniform spectrum up to 27.4 keV, or only thermal or only epithermal energy groups. For all spectra in Table 4.3, the fact that the homogeneity of the cuboid and cylindrical models does not vary greatly with decreasing volume suggests that the dimensions of the beam exit can be reduced. Furthermore, Table 4.3 shows that the Petten design presented in section 4.1, might have been improved by choosing a cylindrical liver holder instead of the spherical one. Unfortunately, this is not possible due to the rather small beam opening in Petten.The right choice for the spherical design in the Petten set-up is also conferred when taking into account the minimum summed weighed importance (WI_j) obtained in the holder model; this means a minimum number of delivered thermal neutrons. In Figure 4.11, this minimum WI_j is shown for every solution of the Simplex method (27.4 keV upper limit case) somewhere in the liver as a function of *Homogeneity*.

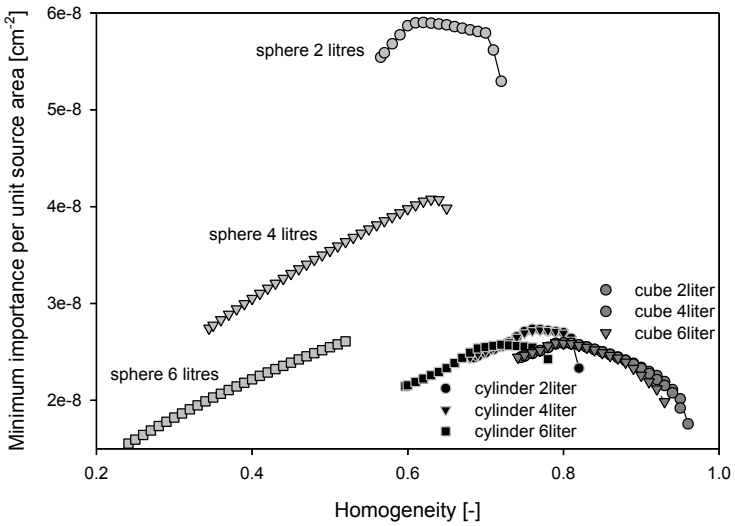

Figure 4.11. The minimum reached importance in a certain cell inside the 3 geometrical models, for 3 volumes each, as a function of the homogeneity.

Normalised to per source area, this minimum WI_j is highest in the 2 and 4 litre spherical holder models. In these models, the source neutrons can be said to be at their most effective. Therefore, given the small existing beam opening and intensity, as in Petten, the spherical holder seems from this graph to be the best choice. The curves in Figure 4.11 are based on the source areas as defined in section 4.2. In order to have the same ratio of beam area to cross-sectional area for all models with the

same volume, the curves for the spherical holders of 2 and 4 litres have to be multiplied with 0.67 and 0.84, respectively. It can be seen that even then, the contributions of the source neutrons in these spherical models are still higher.
Describing Figure 4.11 in terms of the Simplex method: For low values of the *Homogeneity* in the constraints, the objective function is maximised by having large WI_j's in many cells at the cost of low WI_j's in a small number of cells. For the 2 litres spherical and for all the cylindrical and cuboid shaped holders, it can be seen that the minimum WI_j somewhere in the holders, first increase then decrease towards the maximum homogeneities. This means that for the maximum homogeneities, the source neutrons are less effective and more source neutrons are needed to reach a certain effect. This does not mean immediately that it will take longer to irradiate since that depends on the available source neutron energy spectrum in combination with the source strength.

4.3 Conclusions

To conclude, it seems that the cuboid shaped model would be the best option when a new neutron beam is to be designed and constructed. The investigated thickness of 10 cm is sufficient for both livers and other similarly shaped volumes, such as for example the irradiation of cell cultures, for which also a homogenous thermal neutron field is required. The disadvantage, namely the rather large beam exit, can be circumvented by transporting the cuboid holder up and down (or left and right) through a smaller neutron beam with a high intensity. Furthermore, for neutron sources that may have relatively low strength, the 2 and 4 litre spherical holder models would be the preferred configuration which is practically the case with the present epithermal neutron beam in Petten. Note that the obtained homogeneity in the 2.4 litre spheroid liver holder (0.68) of section 4.1 is close to the optimum, as can be concluded from the spherical results in Table 4.2; the spheroid shape improves the result even further.

Chapter 5

Conclusions

The quest for the optimal source neutrons for BNCT was investigated from three viewpoints:

* In the first point of view, as there is no consensus among radiobiologists about the proper values of the parameters influencing the biologically weighted dose, e.g. RBE values and tolerance doses, almost all of these parameters were varied. For brain tumours located between 20 mm up to 80 mm from the skin it was found that for most parameter configurations, epithermal source neutrons, between 1 keV and 10 keV, are optimal. Only the parameters related to ^{10}B and fast neutrons result in diverging optimal source neutron energies. For example, low values for the ^{10}B concentrations and the accompanying CBE for the boron dose result often in lower than modal source neutron energies to be optimal. Smaller values for the RBE of the fast neutron dose enable higher source neutron energies to be optimal and thus more destructive in the tumour. These parameters are of influence in the tissue in which the tolerance dose is reached first. This is depending on the ratio of the tolerance dose set for skin to brain. It is likely that in the future, boron compounds will be available which give ^{10}B concentrations close to zero in skin and other healthy tissues. Furthermore, it is possible that in the future BNCT treatment modalities (e.g. extra-corporeal, at low temperatures) the recoil protons are found to be less damaging for the cells. Of course this needs to be investigated.
This parameter study shows that having three neutron beams, one nearly thermal (5 eV) and two epithermal (500 eV and 10 keV), assures an optimal treatment, no matter what the influencing biologically weighted dose parameter values may be.

* Two newly developed adjoint Monte Carlo (MC) techniques, the Legendre Expansion Technique (LEXT) and the Adjoint Point Detector Technique (APDT), enable the simulation of mono-directional gamma, as well as neutron, beams. When the beam diameters are larger than 5 cm, the results for 1020 beams are calculated 1.8 up to 20 times faster than when compared with results from forward MC. Overall, for small diameter neutron and gamma beams (around 5 cm), the adjoint MC techniques are preferred when thousands of different locations and orientations of a mono-directional beam need to be calculated and when there are no more than ten tumours and/or organs at risk (OAR). For larger beam diameters is adjoint MC preferable up to hundreds of regions of interest whenever even a ‘few’ hundred of mono-directional beams are investigated. Overall, in order to take advantage of the adjoint technique, the user has to be interested in beam positions at many locations around the irradiated patient or phantom. Apart from BNCT, the LEXT and APDT are of value in conventional radiotherapy since most of the treatment beams are mono-directional or have just a small divergence. Thereby, the conventional radiotherapy community would be interested to implement MC for dose

calculations, since the results are closer to the measurements than the results of other dose calculation techniques. For the LEXT, it is expected that other base functions than Legendre polynomials, will give improvements whenever they are more appropriate to describe the angular adjoint functions in a certain problem (e.g. particle type, geometry). At present, the divergence of a beam is easy to simulate with the APDT, just by changing the position of the adjoint point detector. However, a problem occurs when the optimal source neutron energy is investigated with adjoint MC because by definition the optimal source neutrons give a high contribution to the tumours and a low contribution to the OAR. As a consequence, the values of interest in the OAR have a large relative error, and no judgement can be given on the outcome. Nevertheless, preliminary results for a model with ten tumours in the brain showed that only thermal and low epithermal source neutrons can give significant improvements to the ratio of the thermal neutron flux in tumours to the thermal neutron flux in the OAR, when compared with the ratio resulting from the Petten BNCT beam. Further analysis in the field of treatment planning optimisation is obviously the next step.

* The last point in this thesis is the investigation to obtain the optimal source neutrons for future BNCT applications such as the extra-corporeal irradiation of organs (e.g. liver). The first part of this research shows that it is possible to irradiate a large liver, with a volume of 2.4 litres, at the current BNCT facility in Petten. This requires rotation of the liver in a spheroid holder in order to obtain thermal neutron fluence as homogeneous as possible with the rather small epithermal beam. The homogeneity is defined as the ratio of the minimum to the maximum thermal neutron flux in the liver holder. Simulation of the doses and fluxes in the rotating liver was performed with MCNP by programming torus shaped tallies in the liver and irradiating from one side. Averaging the flux and/or dose over the volume of the torus provides the answer as if the torus is rotating around the symmetry axis. The homogeneity in the designed and constructed 2.4 litre liver holder is 0.68. Since more researchers are interested in a volume with a homogenous thermal neutron field, e.g. for cell experiments, a systematic investigation was started in which also the neutron source could vary in shape and energy. In cubic volumes a homogeneity of around 0.95 can be realised when the source neutrons are mixed in a composition of around 30% thermal (around 0.1 eV) and 70% epithermal (around 10 keV). In spherical volumes the homogeneities cannot exceed 0.72, but these spherical shapes are prefered when high effectiveness per source neutron is required. This is necessary in case of a low source strength in combination with a limited irradiation time.

To conclude: in 1941, Zahl *et al.* {REF} proposed the use of epithermal instead of thermal source neutrons in BNCT. The outcome of the three parts of this thesis has shown that 3 neutron energy regimes should be prescribed. Besides the 10 keV epithermal source neutrons, low epithermal source neutrons of around 1 eV and thermal source neutrons with energies of 0.1 eV must also be used. With these source neutrons available, BNCT treatment planning can be optimised, whatever the biological factors may be, wherever the tumours are located, or wherever the patient

or the patient's organ is situated. This work shows that significant improvements in the delivery of a therapeutic radiation dose can be given if a new neutron filter is designed in order to provide a variable neutron spectrum as described above.

APPENDIX

Normalisation of adjoint MCNP results for mono-directional detector contributions

In Monte Carlo calculations, the probability that adjoint particles cross a certain detector with a certain angle is nearly zero. Knowing even that more of these particles are necessary to improve the statistics of the result indicates that it will be impossible to calculate such tasks with standard Monte Carlo. Therefore, a forward calculation concerning mono-directional source particles cannot be derived with the adjoint method by means of 'basic' MCNP. Figure A.1 shows schematically this forward set-up with a disc shaped source and spherical tumour as a detector. This figure and also the Figures A.2, A.3 and A.4 contain the parameter descriptions as used throughout this appendix and the characteristics as will be later used in Table A.1

In fact, a surface crossing estimator (EST_{sc}) should have been used for mono-directional adjoint particles. So the detector response function should be like

$\frac{1}{A_{src}}\delta(\Omega+\Omega_{src})\delta(y-y_{src})$ with (x, z) within the detector area.

Although it can be performed with 'basic' MCNP, this is not a feasible estimator for a Monte Carlo calculation, as no particle (like the grey arrow in Figure A.2) will have exactly the direction $-\Omega_{src}$. Therefore, a next-event estimator would be required which calculates from a given collision site the probability of scattering $p(-\Omega_{src})$ in the right direction and the attenuation $e^{-\xi}$ to get to the source disc as illustrated in Figure A.3. ξ is the number of mean free paths from the collision point to the detector (in fact to the source plane). Hence, the required estimator should be

$$EST_{sc} = p(-\Omega_{src})\frac{e^{-\xi}}{A_{src}} \qquad \text{(a.1)}$$

As such an estimator is not present in MCNP, this estimator is replaced by the next-event point detector estimator of MCNP, as illustrated in Figure A.4. The point detector estimator (EST_{pd}) gives for a particle entering a collision

$$EST_{pd} = p(\Omega_{\det})\frac{e^{-\xi}}{s^2} \qquad \text{(a.2)}$$

where $p(\Omega_{det})$ is the probability of scattering into the direction Ω_{det} towards the point detector and s is the distance between the collision site and the detector. This is provided with the F5 tally in MCNP [7]. If the position of the point detector is sufficiently far away, Ω_{det} will be sufficiently equal to the (opposite) source direction Ω_{src}. If the system dimensions are small compared to the

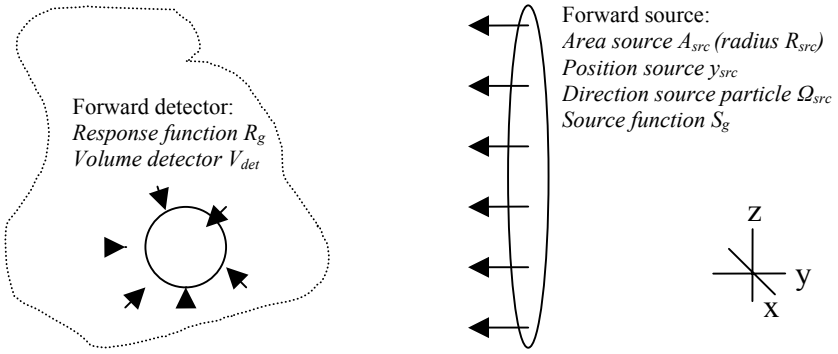

Figure A.1. Forward set-up.

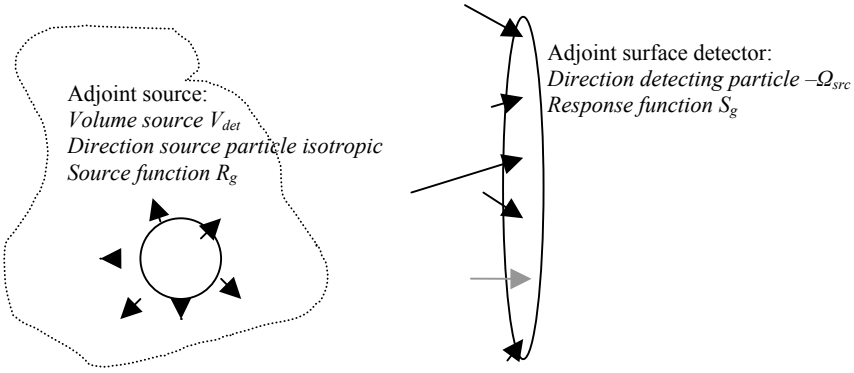

Figure A.2. Adjoint 'basic' set-up.

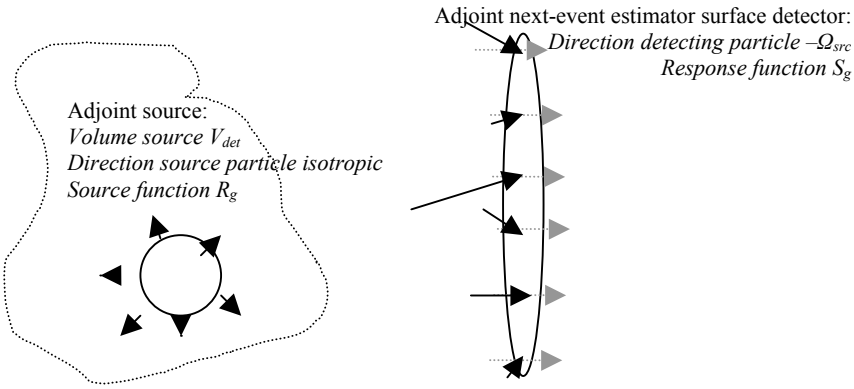

Figure A.3. Adjoint 'required' set-up.

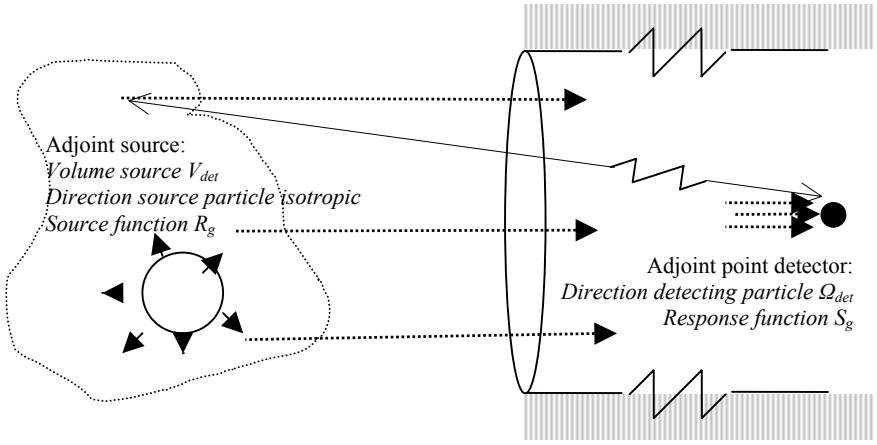

Figure A.4. Adjoint 'point detector' set-up.

distance to the detector, s can be considered constant and equal to the distance between the centre of the system and the point detector.
According to the methodology introduced by Wagner *et al* [70], Table A.1 can be composed for the geometry drawn in the Figures A.1 up to A.4 with the volume averaged flux in the tumour as the forward detector. Practically, after filling in the source and detector densities in Table A.1, the normalization factor is the product of the entries in the forward problem column divided by the product of the entries in the adjoint problem column.
The 3 columns for an adjoint calculation are (by approximation) equivalent with respect to the intention of the estimator. Comparing the results from the columns for the forward and the 'basic' adjoint equation (for a flat source spectrum and a flat detector energy response) a multiplicative normalization factor in the adjoint equation should be 4π. The estimator suggested for the adjoint 'required' calculation is equivalent to adjoint 'basic' and here also the normalization factor 4π results. By approximation this estimator is also equivalent to the adjoint point detector, but from comparison of the relevant columns, the factor s^2 must be compensated, as well as a factor A_{src}. Hence, for the actually calculated adjoint point detector the normalization factor F_{norm}, with which the result of the adjoint calculation must be multiplied becomes

$$F_{norm} = \frac{4\pi}{A_{src}} s^2 = \frac{4}{R_{src}^2} s^2 \qquad \text{(a.3)}$$

Note that here the situation is given for the total response over energy. If the response for one group is required, the adjoint source is limited to this group and the source density in energy is 1 instead of $1/G$ where G is the number of energy groups. This gives another factor $1/G$ in the normalization.

Table A.1. Normalisation form for the sample problem illustrated in the Figures A.1 up till A.4

dimension	forward	adjoint 'basic'	adjoint 'required'	adjoint 'point detector'
SOURCE				
space	$\frac{1}{A_{src}}\delta(y-y_{src})$	$\frac{1}{V_{\det}} \quad r \in V_{\det}$	$\frac{1}{V_{\det}} \quad r \in V_{\det}$	$\frac{1}{V_{\det}} \quad r \in V_{\det}$
direction	$\delta(\Omega-\Omega_{src})$	$\frac{1}{4\pi}$ (isotropic)	$\frac{1}{4\pi}$ (isotropic)	$\frac{1}{4\pi}$ (isotropic)
energy	$S_g / \sum_{g'} S_{g'}$ $= 1/G$ for flat source	$R_g / \sum_{g'} R_{g'}$ $= 1/G$ for flat response	$R_g / \sum_{g'} R_{g'}$ $= 1/G$ for flat response	$R_g / \sum_{g'} R_{g'}$ $= 1/G$ for flat response
DETECTOR				
space	$\frac{1}{V_{\det}} \quad r \in V_{\det}$	$\frac{1}{A_{src}}\delta(y-y_{src})$	$\frac{e^{-\xi}}{A_{src}}$	$\frac{e^{-\xi}}{s^2}$
direction	1	$\delta(\Omega+\Omega_{src})$	$p(-\Omega_{src})$	$p(\Omega_{\det})$
energy	R_g =1 for flat response	S_g =1 for flat source	S_g =1 for flat source	S_g =1 for flat source

Acknowledgement
The exact derivation of the normalisation factors presented here is performed by J.E. Hoogenboom.

NOMENCLATURE

A	surface area	m^2
a	weigh of source energy group	-
C	concentration	ppm
CBE	compound related biological effectiveness factor	-
d	coefficient of orthonormal basis functions	-
D	physical dose	Gy
E	energy	eV
EST_{pd}	next-event point detector estimator	m^{-2}
EST_{sc}	surface crossing estimator	m^{-2}
f	arbitrary function	-
F_{norm}	normalization factor for adjoint results	-
G	number of energy groups	-
J	number of cells	-
L	variable	-
N	number of samples	-
p	direction probability function	-
Q	source function	$cm^{-3}\ s^{-1}$
q1:q5	dimensions (thickness, distance)	m
r	position	-
R	radius	m
RBE	relative biologically effectiveness factor	-
R_g	group wise response function	-
s	distance between collision site and detector	m
S_g	group wise source function	-
T	revolution time	s
t	time	s
V	volume	m^3
w	weight of Monte Carlo particle	-
WI	sum of weighed importances	-
x	spatial coordinate	m
y	spatial coordinate	m
Z	objective function	-
z	spatial coordinate	m

Greek symbols

ϕ^+	adjoint function	-
ϕ	forward flux	$cm^{-2}\ s^{-1}$
$\bar{\phi}_V$	volume averaged forward flux	$cm^{-2}\ s^{-1}$
α	arbitrary angle	rad
β	arbitrary angle	rad
δ	Dirac-function	-
λ	ratio source gammas to source neutrons	-

ξ	number of mean free paths to detector	-
Σ_d	detector response function	cm^{-1}
ψ	orthonormal basis functions	-
Ω	direction	ster

Subscripts

azi	azimuthal
B	boron-10
bγ	beam gamma related
det	detector
i	index for samples
j	index for cells
k	index for energy groups
l	index for coefficients
m	index for coefficients
n	fast neutron related
p	thermal neutron related
pol	polar
rev	revolution
src	source
w	biologically weighted
γ	induced gamma related

ABBREVIATIONS

APDT	Adjoint Point Detector Technique
BNCT	Boron Neutron Capture Therapy
BNL	Brookhaven National Laboratory
BPA	Borono-phenylalanine
BSH	Borocaptate Sodium
CBE	Compound related Biological Effectiveness
DNA	Deoxyribonucleic acid
EELS	Electron Energy Loss Spectroscopy
EORTC	European Organisation for Research and Treatment of Cancer
EST	Estimator
FET	Functional Expansion Technique
HFR	High Flux Reactor
IAEA	International Atomic Energy Agency
ICRU	International Commission on Radiation Units & measurements
JRC	Joint Research Centre
KERMA	Kinetic Energy Released per unit Mass
LET	Linear Energy Transfer
LEXT	Legendre EXpansion Technique
MC	Monte Carlo
MCNP	Monte Carlo N-Particle transport code
MIT	Massachusetts Institute of Technology
OAR	Organs At Risk
PMMA	Polymethyl Methacrylate)
PNR	Physics of Nuclear Reactors
RBE	Relative Biological Effectiveness
ROI	Regio Of Interest

REFERENCES

1. T. HARTMAN, J. CARLSSON, “Radiation dose heterogeneity in receptor and antigen mediated boron neutron capture therapy,” Radiother Oncol. 31(1), 61-75 (1994).
2. J. A. CODERRE, J. C. TURCOTTE, K. J. RILEY, P. J. BINNS, O. K. HARLING, W. S. KIGER, III, “Boron Neutron Capture Therapy: Cellular Targeting of High Linear Energy Transfer Radiation,” Technology in Cancer Research & Treatment Volume 2, Number 5, October (2003).
3. J.J. DUDERSTADT, L.J. HAMILTON, Nuclear reactor analysis, John Wiley & Sons Inc, New York (1976).
4. International Atomic Energy Agency IAEA: Current status of neutron capture therapy. IAEA-TECDOC-1223. Vienna (2001).
5. J.A. CODERRE, G.M. MORRIS, “The radiation biology of boron neutron capture therapy,” Rad. Res., 151, 1-18, (1999).
6. E.H. ELOWITZ, R.M. BERGLAND, J.A. CODERRE, D.D. JOEL, M. CHADHA, A.D. CHANANA, “Biodistribution of p-boronophenylalanine in patients with glioblastoma multiforme for use in boron neutron capture therapy,” Neurosurgery 42(3), 463-8 (1998).
7. J.F. BRIESMEISTER, MCNP - A General Monte Carlo N-Particle Transport Code, Version 4C. LA-13709-M (2000).
8. ICRU 46. Photon, electron, proton and neutron interaction data for body tissues. International Commission on Radiation Units and Measurements. Bethesda. MD (1992).
9. G. M. MORRIS, J. A.CODERRE, J. W. HOPEWELL, P. L.MICCA, M. REZVANI, “Response of Rat Skin to Boron Neutron Capture Therapy with p-boronophenylalanine or Borocaptate Sodium,” Radiother. Oncol. 32, 144-153 (1994).
10. A.H. SOLOWAY, H. HATANAKA, M.A. DAVIS, “Penetration of Brain and Brain Tumor. VII. Tumor-binding Sulfhydryl Boron Compounds,” J. Med. Chem., 10:714-717, (1967).
11. H. C. MILLER, N. E. MILLER, E. L. MUETTERTIES, “Synthesis of Polyhedral Boranes,” J. Am. Chem. Soc. 85(23), 3885 – 3886 (1963).
12. H.R. SNYDER, A. H. REEDY, W.LENNARZ, “Synthesis of Aromatic Boronic Acids. Aldehydo Boronic Acids and a Boronic Acid Analog of Tyrosine,” J. Am. Chem. Soc. 80, 835-838 (1958).
13. Y. MISHIMA, C. HONDA, M. ICHIHASHI, H. OBARA, J. HIRATSUKA, H. FUKUDA, H. KARASHIMA, T. KOBAYASHI, K. KANDA, K.YOSHINO, “Treatment of Malignant Melanoma by Single Thermal Neutron Capture Therapy with Melanoma-seeking 10B-compound,” Lancet II, 388-389 (1989).
14. K.H.I. PHILIPP, Tolerance of normal brain tissue to Boron Neutron Capture Irradiation, PhD Thesis, Katholieke Universiteit Nijmegen (2004).
15. J. CHADWICK, “The Existence of a Neutron,” Proc. Roy. Soc., A,

136, 692-708 (1932).
16. E. RUTHERFORD, “Nuclear Constitution of Atoms,” Proc. Roy. Soc. A97, 374-400 (1920).
17. H.J. TAYLOR, M. GOLDHABER, “Detection of nuclear disintegration in a photographic emulsion,” Nature (Lond.) 135, 341-348 (1935).
18. G.L. LOCHER, “Biological effects and therapeutic possibilities of neutrons,” Am. J. Roentgenol. Radium. Ther. 36, 1-13 (1936).
19. P. G. KRUGER, “Some Biological Effects of Nuclear Disintegration Products on Neoplastic Tissue,” Proc.Natl.Acad.Sci.26, 181-192 (1940).
20. P.A. ZAHL, F.S. COOPER, “Physical and biological considerations in the use of slow neutrons for cancer therapy,” Radiology 37, 673-682 (1940).
21. P. A. ZAHL, F. S. COOPER, J. R. DUNNING, “Some in vivo Effects of Localized Nuclear Disintegration Products on a Transplantable Mouse Sarcoma,” Proc.Natl.Acad.Sci. 26, 589-598 (1940).
22. P. A. ZAHL, F. S. COOPER, “Localization of Lithium in Tumor Tissue as a Basis for Slow Neutron Therapy,” Science, 64-65 (1941).
23. L.E. FARR, W.H. SWEET, J.S. ROBERTSON, S.G. FOSTER, H.B. LOCKSLEY, D.L.SUTHERLAND, M.L. MENDELSOHN, E.E. STICKEY, “Neutron Capture Therapy with Boron in the Treatment of Glioblastoma Multiforme,” Am. J. Roentgenol., 71, 279-291 (1954).
24. W. H. SWEET, “Medical aspects of boron slow-neutron capture therapy,” In: Workshop on Neutron Capture Therapy, Report BNL-51994, eds. R.G. Fairchild, V.P. Bond (Brookhaven Natl. Lab., Upton, NY), 173-177 (1986).
25. H. HATANAKA, Y. NAKAGAWA, “Clinical results of long-surviving Brain Tumor Patients who underwent boron neutron capture therapy,” Int .J.Radiat.Oncol.Biol.Phys. 28, 1061-1066 (1994).
26. H. HATANAKA, “Clinical results of boron neutron capture therapy,” Basic Life Sci. 54, 15-21 (1990).
27. R.L. MOSS, “Progress towards boron neutron capture therapy at the High Flux Reactor Petten,” Basic Life Sci. 54, 169-83 (1990).
28. G. DETLEF, R. MOSS, editors, Boron neutron capture therapy: toward clinical trials of glioma treatment (HB), Plenum Press, New York (1992).
29. R.L. MOSS, O. AIZAWA, D. BEYNON, R. BRUGGER, G. CONSTANTINE, O. HARLING, H.B. LIU, P. WATKINS, “The requirements and development of neutron beams for neutron capture therapy of brain cancer,” J. Neuro-Onc. vol 33, 27-40 (1997).
30. L. KANKAANRANTA, T. SEPPÄLÄ, M. KALLIO, J. KARILA, C. ASCHAN, T. SEREN, M. KORTESNIEMI, P. KOTILUOTO, E. JÄRVILUOMA, M. KULVIK, J. LAAKSO, A. BRANDER, J. JÄÄSKELÄINEN, J. VÄHÄTALO, I. AUTERINEN, S. SAVOLAINEN, M. FÄRKKILÄ, H. JOENSUU, “First clinical

results on the Finnish study on BPA-mediated BNCT in glioblastoma," - NCT Osaka 2000. 9th International Symposium on Neutron Capture Therapy for Cancer, Program & Abstracts. Osaka, JP, 2 - 6 Oct., 31-32 (2000).

31. J. CAPALA, B.H. STENSTAM, K. SKOLD, P.M. AF ROSENSCHOLD, V. GIUSTI, C. PERSSON, E. WALLIN, A. BRUN, L. FRANZEN, J. CARLSSON, L. SALFORD, C. CEBERG, B. PERSSON, L. PELLETTIERI, R. HENRIKSSON, "Boron neutron capture therapy for glioblastoma multiforme: clinical studies in Sweden," J.Neurooncol. 62(1-2), 135-44 (2003).
32. B.T.S. THIRUMAMAGAL, X.B. ZHAO, A.K. BANDYOPADHY, S. NARAYANASAMY, J. SAMUEL, R. TIWARI, D.W. GOLIGHTLY, V. PATEL, B.T. JEHNING, M.V. BACKER, R.F. BARTH, R.J. LEE, J.M. BACKER, W. TJARKS, "Receptor-Targeted Liposomal Delivery of Boron-Containing Cholesterol Mimics for Boron Neutron Capture Therapy (BNCT)," Bioconjugate Chem. 17 (5), 1141 -1150 (2006).
33. J. CARLSSON, E.B. KULLBERG, J. CAPALA, S. SJÖBERG, K. EDWARDS, L. GEDDA, "Ligand Liposomes and Boron Neutron Capture Therapy, " J.Neuro-Oncology 62, Number 1, 47-59 (2003).
34. G.C. KRIJGER, M.M. FRETZ, R. CARVALHO, O. STEINEBACH, W. JISKOOT, G. STORM, G.A. KONING, "Tumor targeted lipsomes for neutron capture therapy," Radiochim.Acta 93, 589-593 (2005).
35. G.A. KONING, M.M. FRETZ, U. WORONIECKA, G. STORM, G.C. KRIJGER, "Targeting liposomes to tumor endothelial cells for neutron capture therapy," Appl. Radiat. Isot. 61 (5), 963-967 (2004).
36. R.A. WATSON-CLARK, M.L. BANQUERIGO, K. SHELLY, M.F. HAWTHORNE,E. BRAHN, "Model studies directed toward the application of boron neutron capture therapy to rheumatoid arthritis: Boron delivery by liposomes in rat collagen-induced arthritis," Proc.Natl.Acad.Sci. 95, 2531–2534 (1998).
37. J.C. YANCH, S. SHORTKROFF, R.E. SHEFER, S. JOHNSON, E. BINELLO, D. GIERGA, A.G. JONES, G. YOUNG, C. VIVIEROS, A. DAVISON, C. SLEDGE," Boron Neutron Capture Synovectomy: Treatment of Rheumatoid Arthritis Based on the 10B(n,alpha)7Li Nuclear Reaction," Medical Physics (26)3, 364-375 (1999).
38. P. VAN LENT, "Selective Elimination of Synovial Macrophages by Boron Neutron Capture Therapy prevents onset of Murine Experimental Arthritis," 12th International Congress on Neutron Capture Therapy, Proceedings of ICNCT-12 Takamatsu, JP, 9 – 13 Oct. (2006).
39. Y. SAKURAI, K. ONO, S. MIYATAKE, A. MARUHASHI, "Improvement effect on the depth-dose distribution by CSF drainage and air infusion of a tumour-removed cavity in boron neutron capture therapy for malignant brain tumours," Phys. Med. Biol. 51, 1173-

1183 (2006).
40. K. YOKOYAMA, S. MIYATAKE, Y. KAJIMOTO, S. KAWABATA, A. DOI, T. YOSHIDA, T. ASANO, M. KIRIHATA, K. ONO, T. KUROIWA, "Pharmacokinetic study of BSH and BPA in simultaneous use for BNCT," J. Neuro-Oncology 78 Number 3, 227-232 (2006).
41. J. MICHEL, G. BALOSSIER, A. WITTIG, W. SAUERWEIN, K. ZIEROLD, "EELS spectrum-imaging for boron detection in biological cryofixed tissues," Instr.sci.technol. 33 no6, 631-644 (2005).
42. K.J. RILEY, P.J. BINNS, D.D. GREENBERG, O.K. HARLING, "A Physical Dosimetry Intercomparison for BNCT," Med.Phys. 29 (5), May (2002).
43. P.J. BINNS, K.J. RILEY, O.K. HARLING, W.S. KIGER 3RD, P.M. MUNCK AF ROSENSCHOLD, V. GIUSTI, J. CAPALA, K. SKOLD, I. AUTERINEN, T. SEREN, P. KOTILUOTO, J. UUSI-SIMOLA, M. MAREK, L. VIERERBL, F.SPURNY, "An international dosimetry exchange for boron neutron capture therapy. Part I: Absorbed dose measurements," Med.Phys. 32(12), 3729-36 (2005).
44. J. BENCZIK, T. SEPPÄLÄ, M. SNELLMAN, H. JOENSUU, G. M. MORRIS, J. W. HOPEWELL, "Evaluation of the Relative Biological Effectiveness of a Clinical Epithermal Neutron Beam Using Dog Brain," Radiat. Res. 159, 199–209 (2003).
45. J. GUEULETTE, P.J. BINNS, B.M. DE COSTER, X-Q. LU, S.A. ROBERTS, K.J. RILEY, "RBE of the MIT fission converter beam for crypt cell regeneration in mice," Radiat. Res. 164, 805-809 (2005).
46. R.G. FAIRCHILD, "Development and Dosimetry of an Epithermal Neutron Beam for Possible Use in Neutron Capture Therapy, I. 'Epithermal' Neutron Beam Development," Phys.Med.Biol. 10 No. 4, 491-504 (1965).
47. R.G. FAIRCHILD, "Development and Dosimetry of an Epithermal Neutron Beam for Possible Use in Neutron Capture Therapy, II. Absorbed Dose Measurements in a Phantom Man," Phys.Med.Biol. 11 No. 1, 15-30 (1966).
48. O.AIZAWA, "Research on neutron beam design for BNCT at the Musashi Reactor," Basic Life Sci. 54, 109-24 (1990).
49. G. TRACZ, L. DABKOWSKI, D. DWORAK, K. PYTEL, U. WOZNICKA, "The filter/moderator arrangement-optimisation for the boron-neutron capture therapy (BNCT)," Radiat. prot. dosim.110 no1-4, 827-831 (2004).
50. J.M. VERBEKE, A.S. CHEN, J.L. VUJIC, K.N. LEUNG, "Optimization of Beam-Shaping Assemblies for BNCS Using the High-Energy Neutron Sources D-D and D-T," Rad.Biol.Med. 134(3), 278-293 (2001).
51. T. KOBAYASHI, Y. SAKURAI, K. KANDA, Y. FUJITA, K. ONO,

"The Remodeling and Basic Characteristics of the Heavy Water Neutron Irradiation Facility of the Kyoto Univesity Research Reactor, Mainly for Neutron Capture Therapy," Rad.Biol.Med. 131(3), 354-378 (2000).
52. T. MATSUMOTO, H.B.LIU, R.M.BRUGGER, "Design studies of an epithermal neutron beam for neutron capture therapy at the Musashi reactor," J. Nucl. Sci. Technol. 32 no2, 87-94 (1995).
53. H.B. LIU, R.M. BRUGGER, D.C. RORER, P.R. TICHLER, J.P. HU, "Design of a high-flux epithermal neutron beam using 235U fission plates at the Brookhaven Medical Research Reactor," Med Phys. 21(10), 1627-31 (1994).
54. J.C. YANCH, X.L. ZHOU, G.L.BROWNELL, "A Monte Carlo Investigation of the dosimetric properties of monoenergetic neutron beams for neutron capture therapy," Radiat.Res.126, 1-20 (1991).
55. J.C. YANCH, O.K. HARLING, "Dosimetric Effects of Beam size and collimation of epithermal neutrons for Boron Neutron Capture Therapy," Rad.Res. 135, 131-145 (1993).
56. E. BISCEGLIE, P. COLANGELO, N. COLONNA, P. SANTORELLI, V. VARIALE, "On the optimal energy of epithermal neutron beams for BNCT," Phys.Med.Biol. 45, 49-58 (2000).
57. D.L. BLEUEL, R.J. DONAHUE, B.A. LUDEWIGT, J. VUJIC, "Development of a Neutron Energy-Biased In-Air Figure of Merit for Predicting In-Phantom BNCT Neutron Beam Characteristics," In: Proceedings of the 8th International Symposium on Neutron Capture Therapy for Cancer, La Jolla, CA, Sep. 13-18, (1999).
58. H.D. THAMES, J.H. HENDRY, Fractionation in Radiotherapy, Taylor & Francis Books Ltd., London (1987).
59. J.F. FOWLER, "Biological factors influencing optimum fractionation in radiation therapy," Acta Oncologica 40(6), 712-717 (2001).
60. D.T. GOODHEAD, J. THACKER, R. COX, "Effects of radiations of different qualities on cells: molecular mechanisms of damage and repair," Int.J.Radiat.Biol. 63, 543-556 (1993).
61. E.J. HALL, A. GIACCIA, Radiobiology for the Radiologist, Lippincott Williams and Wilkins, Philadelphia, San Francisco, Sixth Edition (2005).
62. A.L. BROOKS, G.J. NEWTON, L.J. SHYR, F.A. SEILER, B.R. SCOTT, "The combined effects of alpha-particles and X-rays on cell killing and micronuclei induction in lung epithelial cells," Int.J.Radiat. Biol. 58, 799-811 (1990).
63. Y. FURUSAWA, M. AOKI, M. DURANTE, "Simultaneous exposure of mammalian cells to heavy ions and X-rays, Advances in Space Research," 30, 877-884 (2002).
64. A. WITTIG ET AL., Early phase II study on BNCT in metastatic malignant melanoma using the boron carrier BPA, EORTC protocol 11011 (2003).
65. W. SAUERWEIN ET AL., Postoperative Treatment of glioblastoma

with BNCT at the Petten Irradiation Facility, EORTC Protocol 11961 (1999).
66. K. HIDEGHETY, W. SAUERWEIN, A. WITTIG, C. GOTZ, P. PAQUIS, F. GROCHULLA, K. HASELSBERGER, J. WOLBERS, R. MOSS, R. HUISKAMP, H. FANKHAUSER, M. DE VRIES, D. GABEL, "Tissue uptake of BSH in patients with glioblastoma in the EORTC 11961 phase I BNCT trial," J.Neurooncol. 62(1-2), 145-56 (2003).
67. D.W. NIGG, "Some recent trends and progress in the physics and biophysics of neutron capture therapy," Progr. In Nuclear Energy 35 No 1, 79-127 (1999).
68. C. VROEGINDEWEIJ, F. WHEELER, F. STECHER-RASMUSSEN, R. HUISKAMP, "Microdosimetry Model for Boron Neutron Capture Therapy. II. Theoretical Estimation of the Effectiveness Function and Surviving Fractions," Rad. Res. 155, 498-502 (2001).
69. G. I. BELL, S. GLASSTONE, Nuclear Reactor Theory, Van Nostrand Reinhold Company, New York, NY (1970).
70. J.C. WAGNER, E.L. REDMOND II, S.P. PALMTAG, J.S. HENDRICKS, "MCNP: Multigroup/Adjoint Capabilities," LA-12704, Los Alamos National Laboratory (1994).
71. J.E. HOOGENBOOM, "Methodology of Continuous-Energy Adjoint Monte Carlo for Neutron, Photon, and Coupled Neutron-Photon Transport," Nucl. Sci. Eng. 143, 99-120 (2003).
72. F.C. DIFILIPPO, "Forward and adjoint methods for radiotherapy planning," Med. Phys. 25(9), 1702-10 (1998).
73. J.V. SIEBERS, M. LAUTERBACH, S. TONG, Q. WU, R. MOHAN, "Reducing dose calculation time for accurate iterative IMRT planning," Med.Phys. 29(2), 231-237 (2002).
74. W. ULMER, J. PYYRY, W. KAISSL, "A 3D photon superposition/convolution algorithm and its foundation on results of Monte Carlo calculations," Phys.Med.Biol. 50, 1767-1790 (2005).
75. Q. WU, D. DJAJAPUTRA, M. LAUTERBACH, Y. WU, R. MOHAN, "A fast dose calculation method based on table lookup for IMRT optimization," Phys.Med.Biol. 48, N159-N166 (2003).
76. C.M. MA, E. MOK, A. KAPUR, T. PAWLICKI, D. FINDLEY, S. BRAIN, K. FORSTER, A. L. BOYER, "Clinical implementation of a Monte Carlo treatment planning system," Med.Phys. 26(10), 2133-2143 (1999).
77. J.J. DEMARCO, I.J. CHETTY, T.D. SOLBERG, "A Monte Carlo tutorial and the application for radiotherapy treatment planning," Med.Dosim. 27(1), 43-50 (2002).
78. R. JERAJ AND P. KEALL, "Monte Carlo-based inverse treatment planning," Phys. Med. Biol. 44,1885-96 (1999).
79. M. GOLDSTEIN, "The adjoint Monte Carlo - a viable option for efficient radiotherapy treatment planning," Proc. of the 19th Conf. of

the Israeli Nucl. Soc. 11-2 (1996).

80. S. YOO, M.E. KOWALOK, B.R. THOMADSEN, D.L. HENDERSON, "Treatment planning for prostate brachytherapy using region of interest adjoint functions and greedy heuristic," Phys.Med.Biol. 48, 4077-90 (2003).
81. B. WANG, M. GOLDSTEIN, X.G. XU, N. SAHOO, "Adjoint Monte Carlo method for prostate external gamma beam treatment planning: an application to 3D patient anatomy," Phys.Med.Biol. 50, 923-935 (2005).
82. R.A. LILLIE, "BNCT filter optimisation using two-and three-dimensional discrete ordinates," In: Proceedings of the 3-D Deterministic Radiation Transport Computer Programs: Features, Applications and Perspectives, vol. 1, Paris, France, 379 (1996).
83. B.L. BEERS, V.W. PINE, "Functional Expansion Technique for Monte Carlo Electron Transport Calculations" IEEE Trans. Nucl. Sci. 23, No. 6 (1976).
84. D.P. GRIESHEIMER, W.R. MARTIN, "Monte Carlo Based Angular Flux Distribution with Orthogonal Function Expansion," Trans. Am. Nucl. Soc. 89 (2003).
85. J.P. BOYD, Chebyshev and Fourier spectral method, Dover Publications, New York (2000).
86. J.T. WEST III, "SABRINA, an Interactive Three-Dimensional Geometry-Modeling Program for MCNP," Los Alamos National Laboratory Report LA10688M (1986).
87. K.A. VAN RIPER, "A CT and MRI scan to MCNP input conversion program," Rad.Prot.Dos. 115 No. 1–4, 513–516 (2005).
88. T. PINELLI, A. ZONTA, S. ALTIERI, S.BARNI, A. BRAGHIERI, P. PEDRONI, P. BRUSCHI, P. CHIARI, C. FERRARI, C. ZONTA, "TAOrMINA: From the first idea to the application to the human liver," In: W. Sauerwein, R. Moss, A. Wittig, eds Research and Development Neutron Capture Therapy. Bologna: Monduzzi Editore, 1065-72 (2002).
89. T. PINELLI, S. ALTIERI, F. FOSSATI, A. ZONTA, C. FERRARI, U. PRATI, L. ROVEDA, S. NGNITEJEU TATA, S. BARNI, D.M. FERGUSON, "Operative modalities and effects of BNCT on liver metastases of colon adenocarcinoma," In: M.F. Hawthorne, K. Shelly, R.J. Wiersema, eds. Frontiers in Neutron Capture Therapy. New York: Kluwer Academic, Plenum Publishers, 1427-40 (2001).
90. R. NANO, S. BARNI, P. CHIARI, T. PINELLI, F. FOSSATI, S. ALTIERI, C. ZONTA, U. PRATI, L. ROVEDA, A. ZONTA, "Efficacy of boron neutron capture therapy on liver metastases of colon adenocarcinoma: optical and ultrastructural study in the rat," Oncol.Rep. 11, 149-153 (2004).
91. H. GRAY, Anatomy of the Human Body. Philadelphia: Lea & Febiger; 1918. Thoroughly revised and re-edited by WH. Lewis New York: Bartleby.com (2000).

92. J.A. FAVORITE, Memorandum: Proposed Changes to the Tallies Section of the MCNP4C Manual, Chapter 2, Secs. V.A-V.C, X-5:02-017(U), LA-UR-02-1892 (2002).
93. G.B. DANTZIG, Linear Programming and Extensions. Princeton, NJ Princeton University Press (1963).
94. Numerical Recipes in Fortran 77: The art of scientific computing. Copyright (C) 1986-1992 by Cambridge University Press.
95. T. COLEMAN, M. A. BRANCH, A. GRACE, Optimization Toolbox For Use with MATLAB, User's Guide Version 2, The MathWorks, Inc. (1999).

ACKNOWLEDGEMENT

I am willing to defend the proposition that says that without any of you mentioned in the acknowledgement, there would have been no thesis and list of propositions at all! One could argue that some people are not directly involved but I would reply that these people enjoy(ed) my life which is most important when trying to achieve something like a Ph.D. While writing this acknowledgement at the last moment (of course), I am afraid that I might forget to thank someone which would destroy my latest proposition immediately. Therefore, as a solution:
Many thanks to …….....! How could I ever forget you? Sorry.
As you can imagine, it is impossible for me to start thanking all the persons in an order of 'importance'. There are the people who coached and helped me scientifically and there are the people who supported me privately in the dark moments I went through during this Ph.D. adventure. To be honest, I was at one moment close to giving up. I choose the 'proven' and therefore 'safe' order of thanking you which is roughly arranged from work-related friends to private friends to closest family.
In Delft, I want to thank the Professors Hugo van Dam and Tim van der Hagen for their trust, advice and support over the years. I learned a lot in the monthly meetings in which often one of you attacked my work while the other one protected me. Fortunately, Dr.ir. Jan Leen Kloosterman was always at my side in these meetings. However, outside the meetings Jan Leen pushed me hard to keep track of an imaginary schedule. Thank you for that, I know now that it is absolutely necessary. Always interested in my work was Dr.ir. Danny Lathouwers; the man with whom I baked bitterballen and vlammetjes during our duty in the IRI-bar (thank you Ruben for teaching us)! Let me continue with thanking Dr.ir. Eduard Hoogenboom, Ine, Riny, Piet, Camiel, Dick, August and Martin. Of course, we started more or less together, and finished it: Alexander, Marek and the Húngàrian guy I forgot the name of (C15?). All students from PNR thank you for letting me feel welcome during my monthly returns to Delft.
In Petten, I want to thank our director Professor Kari Törrönen, Dr. Roberto May and Dr. Marc Becquet. Thank you Dr. Ray Moss. Of course, very important, Gerda, thank you for all your support. Mentioning Gerda, with tears in my eyes: where would I have been without TIM, TAS, Conge, WAB and Sysper2! Thank you all people of the JRC's administration and IT department for making impossible things possible. All my fellow colleagues and agents: Antoaneta, Jim, Arthur, Josselin, Lucien, Giuseppe, Günther, Andrzej, Yuan-DHL, Bart, Alain, Finn, Klaas, Anton and Francois. I really appreciate the friendliness and interest of all the people from NRG working around the reactor. Thanks und grüsse to the Essen crew in the persons of Professor Wolfgang Sauerwein, Dr. Andrea Wittig and Dr. Reinhard Hentschel. Thank you all BNCT colleagues and friends worldwide: Super Cecile, Silva, Andrea, Stead, Jingli, Stuart, Kent, Ray, Hiroaki, Saverio, Grazia, Simone, The Elisabettas, Jerome, Marjan, Gerard and Gerben. Thanks to Wilko and Corine for your Dutch BNCT support. Not to forget the people who encouraged me during my graduation work and motivated me to continue: Professor Rob Mudde, Dr. Hans

van Maanen and Jaap Beekman. Also related to this is Hanneke who encouraged me to go for it. Many thanks!
Okkebas, Het Eiland (Allan, Jan and Maikel) and Thijs G thanks for the great time. Please let me repeat it once again: no Cris and Haipo, no coffee, no thesis. Harold and Zoe thanks for also helping me with the linear programming. I will never forget the man who gave me a lot of support and who will make me feel very welcome in Hungary, whenever I go there: David!
Let me now thank my parents and family. Joop and Hedy, you are always there for me and this was once again proven as you helped us after the birth of Anna and Sofie. This was a very hectic period. Let me immediately add the name of Joke Wilkes. Many many thanks! Side support was given by Bert, Jorine, Eveline and Yvonne. I appreciated the support and understanding I received from my supervisors in Delft and Petten in this time.
My dear beloved Sabine, Anna and Sofie. I am very grateful to live my life with you every day. You gave me all the support possible to finish this thing. I am really looking forward to continue with you without having a thesis on my mind. This is for you!

Finally, I include here the first school-pictures of our daughters of whom we can be proud. With these pictures they have also something to look at in my thesis!

Petten, 10th of May 2007,
Sander

CURRICULUM VITAE

Victor Alexander Nievaart

Call name: Sander
Date of birth: June 19, 1973
Place of birth: Apeldoorn, The Netherlands

1985-1992:	High school “Veluws College” in Apeldoorn; HAVO and VWO.
1992-2000:	M.Sc. in applied physics at the Delft University of Technology, The Netherlands. Majored in the Transport Phenomena group on Laser Doppler Anemometry in multiphase flows.
2000-2004:	Ph.D. student within a cooperation of the Section Physics of Nuclear Reactors of the Faculty of Applied Sciences of the Delft University of Technology and the Institute for Energy of the Joint Research Centre of the European Commission in Petten, The Netherlands. Ph.D. topic is ‘Spectral tailoring for Boron Neutron Capture Therapy’.
2004-2007:	Continuing Ph.D. and involved in treatment planning in the BNCT clinical trials in Petten, investigating BNCT treatments of extra-corporeal livers and rheumatoid arthritis.

PART II

PAPERS I-III

INSTITUTE OF PHYSICS PUBLISHING PHYSICS IN MEDICINE AND BIOLOGY

Phys. Med. Biol. **49** (2004) 4277–4292 PII: S0031-9155(04)75598-0

A parameter study to determine the optimal source neutron energy in boron neutron capture therapy of brain tumours

V A Nievaart[1,2], R L Moss[2], J L Kloosterman[1], T H J J van der Hagen[1] and H van Dam[1]

[1] Reactor Physics Department, Delft University of Technology, Mekelweg 15, 2629JB Delft, The Netherlands
[2] Joint Research Centre of the European Commission, Postbus 2, 1755ZG Petten, The Netherlands

E-mail: victor.nievaart@jrc.nl

Received 3 February 2004
Published 3 September 2004
Online at stacks.iop.org/PMB/49/4277
doi:10.1088/0031-9155/49/18/006

Abstract

The values of the parameters used in boron neutron capture therapy (BNCT) to calculate a given dose to human tissue vary with patients due to different physical, biological and/or medical circumstances. Parameters include the tissue dimensions, the ^{10}B concentration and the relative biological effectiveness (RBE) factors for the different dose components associated with BNCT. Because there is still no worldwide agreement on RBE values, more often than not, average values for these parameters are used. It turns out that the RBE-problem can be circumvented by taking into account all imaginable parameter values. Approaching this quest from another angle: the outcome will also provide the parameters (and values) which influence the optimal source neutron energy. For brain tumours it turns out that the ^{10}B concentration, the RBE factors for ^{10}B as well as fast neutrons, together with the dose limit set for healthy tissue, affect the optimal BNCT source neutron energy. By using source neutrons of a few keV together with neutrons of a few eV, it ensures that, under all imaginable circumstances, a maximum of alpha (and lithium) particles can be delivered in the tumour.

1. Introduction

Boron neutron capture therapy (BNCT) is a promising treatment for various types of cancer. Basically, BNCT treatment consists of two parts: firstly the tumour is loaded with the isotope boron-10 (^{10}B) and secondly the tumour is irradiated with thermal neutrons. When a thermal

neutron is captured [illegible] produces an alpha and a lith[illegible] principle, can break the DNA [illegible] cell, thus ca[illegible]th. BNCT is distinct from conventional radiation [illegible] the [illegible] presence of more ^{10}B resulting in a higher loca[illegible]lation. In th[illegible] cells can be spared.

In recent years, in sever[illegible] worldwide, clinical trials have been performed ly deal with the treatment o[illegible] life threatening brain tumours, n[illegible] lastoma multiforme. Although, quite [illegible]mising BNCT results have d in the treatment of other types of cancer[illegible] of the body (e.g. eatment of liver cancer reported by Pinelli *et al* (2[illegible]lts are for the glioblastoma trials, which seem to suffer fr[illegible] a chall[illegible] ^{10}B to the right location inside the brain and [illegible]e head without remo[illegible] studies (recent related publication[illegible]timal when as many neu[illegible]t with the boron atoms inside the t[illegible]ame time [illegible]ible damage as possible to the vital parts of the b[illegible] [illegible]in (skin, eyes, ears, glands, etc). The tissue d[illegible] [illegible] an equivalent dose which, when a preset eq[illegible] (tolerance dos[illegible] indicates when treatment should be ha[illegible]ding the equivalent dose be considered that neutrons en[illegible]e (mainly consisting of hydroge nd nitrogen) introduce [illegible]. In BNCT, the equivalent dose is usua[illegible] to be made up [illegible]ributions, namely the ^{10}B reaction producing [illegible] nitro[illegible]ducing protons; the hydrogen reaction producing and [illegible]rotons. The resulting total equivalent dose follow[illegible] the absorb[illegible] have been weighted with particle-dep[illegible]ative biological effectiv[illegible]damage caused by a proton is different from [illegible] particle with the same energy. The RBE [illegible] V gammas, of whi[illegible]own from conventional gamma therapy.

[illegible] to be no worldwide agreement among the BNC[illegible] the co[illegible] RBE factors or what should be the right proc[illegible] them. Discussio[illegible] using them at all, to providing values to tw[illegible] cimal places. These uncer[illegible]rd for a nuclear physicist who is look[illegible] optimal energy of the neutrons, com[illegible] to irradiate a patient by BN[illegible] NCT literature, when dealing with the o[illegible]tron energies, the re[illegible] based on one set of RBE factors, according to [illegible] Yanch *et al* [illegible]2000, Bleuel *et al* 1998). As such the question a[illegible] the in[illegible] RBE factors on the optimal source neutron energ[illegible] variation o[illegible]ch as the thickness of [illegible] as the values of the allowed to[illegible]nsive overview on the correlation bet[illegible]tron energy. It takes into con[illegible]ged ranges of parameters [illegible]searchers el[illegible]oretical nature of this investigation has allowed us [illegible] in [illegible]ed manner. This means that there is an interest i[illegible] [illegible]rameter configuration.

In the next section (section 2) we describe [illegible]source neutron energy [illegible]raints of a tolerance dose in tissue [illegible]is section also gives more deta[illegible] physical or absorbed dose [illegible] deals with the calculation set-up, s[illegible] metry and the m[illegible]is section the chosen parameter ranges are pr[illegible]

and how the post p… …provides the results
for both t… …ron energy and any improve… …energies.
C… …n section 5.

…ory

…ptimal source neutron energy in B… …rs is determined by calculati…
…lent dose at every location along a beam … …roduction at every l…
…umour is expected. In this parameter study, th… …H_i at ever…
… is calculated using

$$H_i = (C_{\ldots} \ldots \cdot \mathrm{RBE_N} \cdot (D_N)_i + (\mathrm{RBE_H} \cdot D_{\ldots}) \ldots \gamma i \qquad (1)$$

where $\mathrm{CBE_{10B}}$ is th… …roducts of ^{10}B,
which is l… …ed for the characteristics of the comp… …^{10}B
ator… …r healthy cells. The parameters C_{10B} and D_{10B} a…
…d ^{10}B dose, respectively. D_N is the absorbed do… …rodu…
… of thermal neutrons with nitrogen and RBE… …g factor to tra…
into an equivalent dose. The two oth… …al effectiveness factors …
…r the proton recoil of hydroge… …gammas. D_H is the absorbed prot…
se, also known as fast n… …γ represents the induced absorbed gam…
…n gammas, pr… …e reactor core (as in Petten reported by Ver…
… …ver … …e $D_{b\gamma}$ term. The index i shows that all elemen…
the … …d on the position in tissue. The $\mathrm{RBE_N}$ translates on…
effect of th… …protons from the nitrogen reacti… …ame
in all tissues. The s… …MeV gammas
from the hydrogen reaction … …beam gammas does not
exceed 10 MeV … …rence, it is
chose… …ect with a location-independent RBE_γ. The re… …m
h… …the energy of the incoming neutrons and depend o…
… Conse… …hosen to be location dependent. Due to the stru…
tissues, such as to… …tion of blood vessels, the boron concentra…
as the $\mathrm{CBE_{10B}}$, differs from …
…lculation of the optimal source neu… …ally searching for the maxim…
…duction under limiting conditions, which … …as

$$\max_{E} \left\{ \left(\frac{H^{\mathrm{tolerance}}}{H(E)} \right)_{\text{somewhere healthy tissue}} \cdot \alpha(E)_{\text{tumour}} \right\}$$

with the dimensions

[total number … …tron].

… …(E) represents the alpha production in the tumour f… …n
…e term $H(E)$ is defined as the total equivalent do… …on
…efore, the fraction on the right-hand side is th… …source neutro…
…ach the tolerance dose ($H^{\mathrm{tolerance}}$) at a p… …issue. The energy E_k, at
…ximum of alphas is produced i… …hosen such that the product of s…
…ons with energy E_k, nee… …olerance dose in the healthy tissue (H^{tc}…
number of alp… …on with energy E_k, is a maximum.

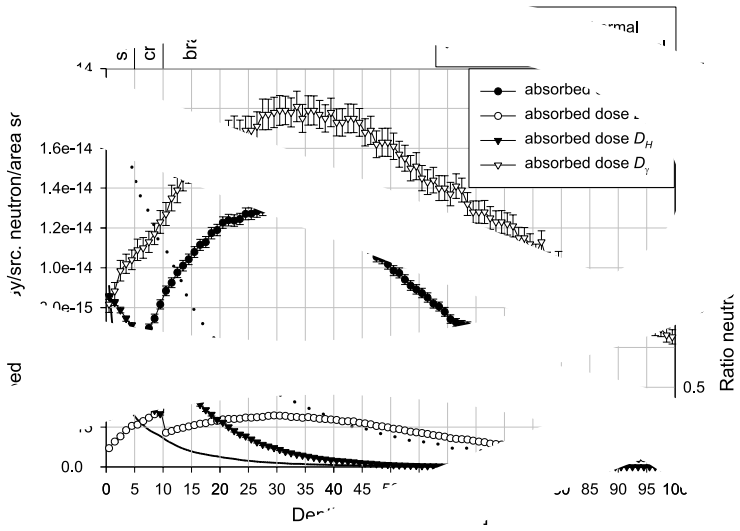

Figure 1. The four maj… …% confidence intervals) together with the neu… energy groups … …antom (10 ppm ^{10}B in all tissues) due to 10 keV s… neutrons

2.1. Physica…

By studying the equiva… …masqueraded by the multiplicati… …logically or me… …ole quantities.

…beam gammas $D_{b\gamma}$, although slightly decreasing… …idered as …

four major absorbe… D_H and D_γ which arise in the head due t… neutrons, are presented in … …on of depth for the case when skin … are both 5 mm. This figure shows … neutron case, with 10 ppm … tissues. The data in figure 1 are extracte… …s with the Monte C… …P (Briesmeister 2000) in a cubic head model (… …h is disc…

…lines give the ratios of the fast:epithermal and … …al energy group…, … …defined in Sauerwein *et al* (1999). The … …the phantom and most of them would h… …rties of water with which … …best compared. The diffusion leng… …and the … defined as the root mean square distance a neutron … a … to its capture as a thermal neutron, is 58.4 mm (… …al. …s clear that all dose contributors, except for … …e to thermal … …ough the probability of a neutron scatter… …decreases for higher en… …nergy, and likewise the absorbed … …g protons will be significantly h… results in a proton recoil … …gh in the skin and decreases rapidly … phantom.

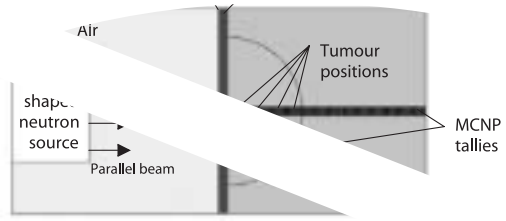

Figure 2. Cross section of the head phantom. The ladder-sha
ak of the particles in MCNP (called tallies). The tum
d
0 and

Furthermor
n the other
tissues i
igure 1. For increasing source neutron ene
of
th
maximum within the phantom, the values of D
ne D_H in skin increases rapidly. The location o
xima
unction of source neutron energy. A more d
hat the D_{10B}, D_N
ma can even be shifted slightly with r
for the same source neut

e next section, physic
d here, will be used as a basis to perform
tudy.

3. Ca

The calculation of the o
different parameter
configurations consi
post-processing
calculation
ode MCNP calculates the de
which
the
determined with changing parameters such as bo
factors and parameters affecting the influence o
urthermore,
ssing, a ratio concerning the tolerance dose r
n is varied using presc

NP calculation

ned phantom, filled with brain tissue, was mode
ns of 24
mm (width × depth × height) using MCNP4c2.
figure
by air. A disc-shaped neutron source, with 60 r
ed
centrally, 15c
are layers
of skin and cranium. The
ried over three MCNP
calculations usin
7 mm. These values
are ext
ption of the head of the reference
which it
i
ead possesses the greatest variety of tissue thickn
hat
ition and density of skin are very similar to those
e
e unlikely skin thickness of 7 mm should h
osition of thes
ing the cranium. All tissue composition
e taken from ICRU 46 (
During the MCNP transport calc
, cranium and brain possess 10 p
which is homogeneously
here is an effect when ^{10}B is homogen
ted in the tissue
considered if this would affect this study sign

The 7 mm phant… …ith the maximum values
of 80 … …e skin, cranium and brain, … …urce neutron
… turns out that at 50 mm from the skin there is a … …ce of
… …flux between a phantom really loaded with the ac… …'s
…3 and the ac… …e. Note that it affects only the proportion
…rmal effects and the … Fortunately, for low source neutron energ…
…e deviation becomes larger, the … very small fast component. Toge…
…e presence of statistical uncertainties … …to the conclusion that a c…
…ld complicate the investigation unnecessar…
will be seen later, the preset dose limit in brain … …s an …
…e of the brain. Therefore, half a sphere is modelled … …age
br…
The … …e are 22 discrete,
even logarithmic… …n to 1 MeV. This
results … …eV and
1… …ge it is shown that only hydrogen and nitrogen deliv… …y,
…ur, major BNCT dose contributors. Source neutr… …y of
…ive negligible dose contributors due to thresh… …other nuclides
tissues. As described in Bleuel *et al* … …CT neutron source can
…osed 'straightaway' by regardin… …of the calculated mono-energeti…
…directional results. This … …bility that the position of the maximum
…sue is shifted … …mponents in the spectrum. This effect is kept
…th…
…ructured ladder-shaped geometry shows the locat… …
tallies. … …defined regions in which the code re… …uctions.
In order to investi… …20 mm, 40 mm,
60 mm and 80 mm from th… …delled as brain tissue). The
MCNP talli… …ith individual
volu… …For MCNP4c2 calculations, the standard ENDF… …library
…of chlorine where the ENDF/6.8 evaluation is used,
…tions co…

Post processing

…very output of the three MCNP calculati… …cranium thickness
…n) a data file containing the four absorbed dose… …on as a f…
…hantom and source neutron energy, is created. Th…
fun… …ree neutron energies, all absorbed doses per sou… …brain
averaged o… …absorbed do… …energies are
discussed later). Since th… …uation, the $D_{b\gamma}$ as given in
equation (1) h… A Fortran code is
writt… …ad file and multiply every value … …arameter(s)
…quation (1). Table 1 presents all the parameters … …levant
…s, as varied in this study.

All the choices concerning the parameter ra… …based on a bo…
…dy (Hideghéty *et al* 2003), the current P… …as used in Petten (Sauer…
…99, Wittig *et al* 2001) combine… …values that can be found in th…
…erature (e.g. Nigg 1999)… …meter ranges are extended so that the bo…
…ain 'highly un… Moreover, all RBEs can have the value 1 w…

Table 1 [illegible] and step sizes.

		CBE_{10B} (–)	RBE_N (–)	RBE_H[a] (–)	RBE_γ (–)	[illegible] (–)
	[illegible]	[illegible] 1	1–5 step 1	1–6 step 1	0.5–1	1, 5 and
[illegible]m	0–20 ste[illegible]			1–6 step 1	step 0.5	10
[illegible]n	0–30 step 10	[illegible]		1–6 step 1		

[illegible]he RBE_H cannot exceed its previous tissue [illegible].

Table 2. Number of parameter configurations.

[illegible]	RBE_N	RBE_H	RBE_γ	Beam gamma energy [illegible]
[illegible]				[illegible]000

[illegible]resence of each parameter value in the 4 527 600 configura[illegible]

[illegible] CBE_{10B}		RBE_N	RBE_H					[illegible]$\varepsilon\gamma$			
Cranium	Brain	All tissues	[illegible]			[illegible]	tissues	All tissues		All tissues	
	[illegible]ry	Ever[illegible]		[illegible]	18%	38%		1	43%	0	
			3	11%	21%	27%	Every				
3[illegible]		[illegible]%	4	18%	21%	18%	value	5	29%		
			5	27%	18%	11%	50%				
						5%				[illegible]0	43%

the idea of [illegible]. Note that in the [illegible] ncerning the ^{10}B [illegible]ant difference whether the compound carrying [illegible] BSH [illegible]s *et al* 2001).

[illegible]he sake [illegible] post-processing calculation, the C_{10B} and t[illegible] are combined to ave[illegible]. The RBE_H is chosen to be at least adjust[illegible]e since the recoiling proton e[illegible] the neutron energy which decreases [illegible]eutron travels deeper into the phan[illegible] Goudeweij *et al* 2000). The[illegible] RBE_H value for deeper lying tissue cannot e[illegible] tissue value.

RBE_γ, defined to be unity for gamma energies [illegible] above, is [illegible]ter setting of 0.5 as well, since it is possible that [illegible] fo[illegible] [illegible]mas (see Kuni 1998). The beam gammas in th[illegible] with discrete en[illegible] [illegible] and 10 MeV. M[illegible] Brakel 2002) show a dose rate of 1 Gy [illegible]ation at the thermal neutron peak. A MCNP [illegible] dose rate, there is one beam [illegible] source neutrons. Taking this result [illegible] extreme $\lambda_{b\gamma}$ [illegible]1/10 are selected. Again, to avoid duplicate value[illegible] [illegible]rgies [illegible]are combined. Table 2 shows the resulting total [illegible] [illegible]. The range of the parameter values combined [illegible]ions to speed [illegible]ocessing affects directly the number of [illegible] parameter value is prese[illegible] the total number of configurations [illegible] We present percentages (rounded [illegible]rameter value. For inst[illegible] $\lambda_{b\gamma}$ can be either 0.5 or 1, it is immedia[illegible] each value wi[illegible] [illegible] of all the 4 527 600 configurations.

Due to the rest[illegible] the presence of the RBE$_H$ dif[illegible] brain, table 3 shows that no[illegible] present in th[illegible] can be regarded as a bias. Although this issue wi[illegible] the [illegible] main that the main interest of this study is to inves[illegible] parameter a[illegible] all settings.

The final part of the p[illegible] ulation is the choice of the tolerance [illegible] e. This study follows the Pet[illegible] the sense that limits are set for th[illegible] brain: a point tolerance dose for skin [illegible] as a volume tolerance d[illegible] The latter is actually the same as allowing [illegible] ints. For the rat[illegible] dose in point skin:point brain, as well as the po[illegible] brain, t[illegible] en: 1/5, 1/3, 1, 3 and 5. Note that it is actua[illegible] depe[illegible] ource strength, which is cancelled out in th[illegible] e dose ratio approac[illegible] interest in the absolute equivalen[illegible] can also be interprete[illegible] bers on how the dose components a[illegible] To obt[illegible] in reasonable time, the 'point dose' in this paper [illegible] ume (78.5 mm^3).

[illegible] discussing the results, it should be point[illegible] only the follo[illegible] rs were varied or not varied in this s[illegible] iers varied were the tis[illegible] s, the RBEs, the ^{10}B concentra[illegible], the tolerance dose and the tumo[illegible] n principle, this study is [illegible] ed on the discrete source neutron ener[illegible] ware shape of [illegible] source intensity distribution and the field si[illegible] varie[illegible]

4. Results

In figures 3–7 [illegible] e the source neutron [illegible] 3.1) will be rounded to integer values.

[illegible] ures, the statistical uncertainties are omitted i[illegible] le re[illegible] ation. In all figures the relative statistical unc[illegible] vant results are [illegible]

e optimal source neutron energy

[illegible] ws the optimal source neutron energy for a pla[illegible] f skin ar[illegible] c[illegible] function of the four tumour depths and according to [illegible] skin:p[illegible] The colour in this figure is a measure of the per[illegible] ter configuratio[illegible]

Figure 3 is the result o[illegible] erpolation of the discrete values belongin[illegible] mour depths. This graph [illegible] 50% of the parameter configurati[illegible] neutron [illegible] keV, 5 keV and 10 keV for tumours at 20, 40, 60 [illegible] in, [illegible]. Because of the limited colour resolution, which [illegible] olved in redness, the regions between 0% and [illegible] with grey cont[illegible] xample, at a tumour depth of 20 mm. th[illegible] all a few per cent of pa[illegible] igurations having an optimal sou[illegible] of 5 eV (between the grey lines a[illegible] 0 eV). At the other end [illegible] tumours at 80 mm are optimally irra[illegible] 0 keV source [illegible]

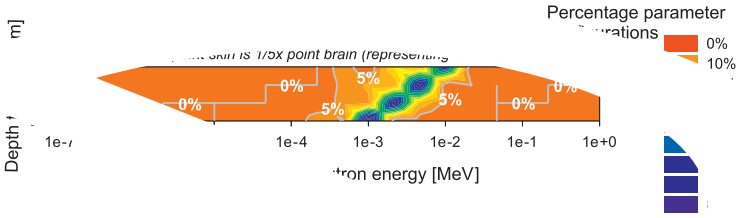

Figure 3. Percentage of all parameter config… optimal source r… energy as a function of tumour depth. The tolerance do… point brain…

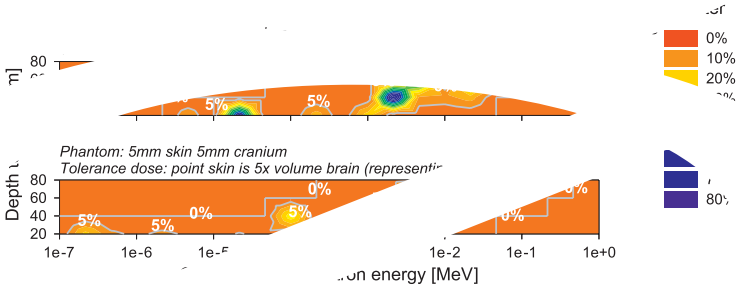

…(5 mm skin and 5 mm cranium phantom) but for two othe…

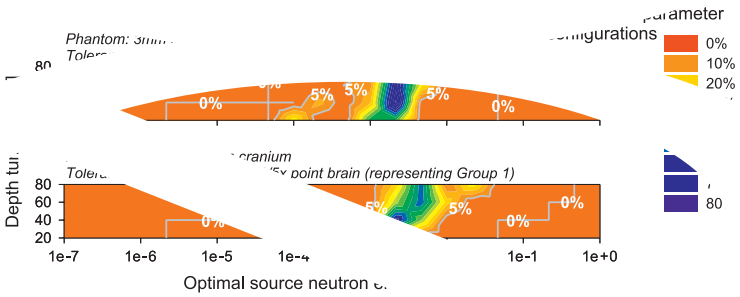

…5. Percentage of parameter configurations having a certain … …nce ratio but two different phantoms.

After studying the … the other tolerance dose ratios … groups. As s… epresentative of the ratios of point skin:point br… …in, of 1/5, 1/3 and 1. In this group, the majori… …all tumour positions lie between 1 keV and 1… …pattern exa… in figure 3. The remaining four tolerance… …be split into two gro… ng to whether they are defined o… …olume brain. For the phant… nm skin and 5 mm cranium… …se ratios, representing these two grou… …in figure 4.

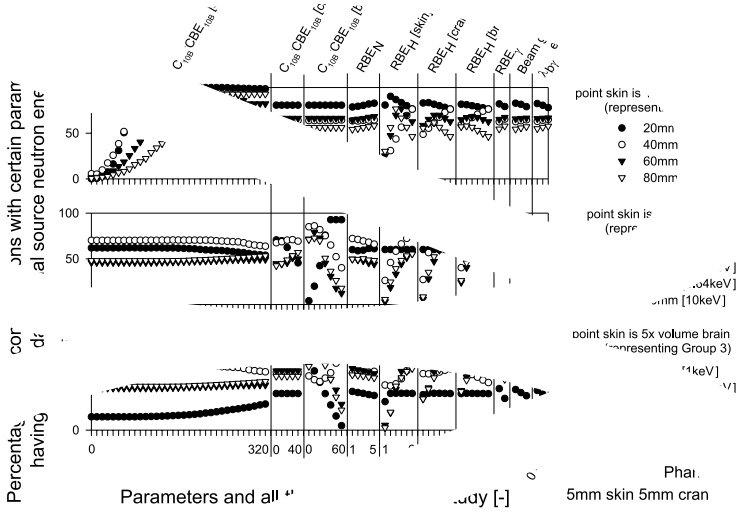

Figure 6. Influence (shown on the *x*-axis) for all configurations, cau
the modal o ergy (on the *y*-axis) for four tumour positions, tolerance
for th ue 5 mm phantom.

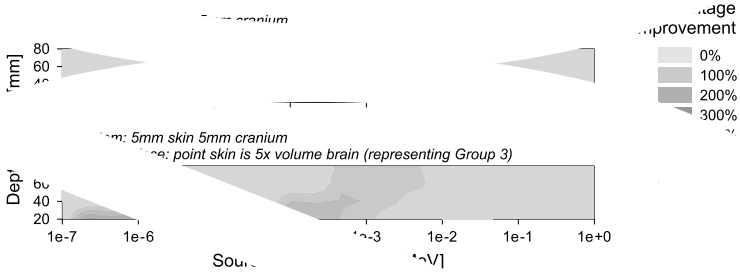

Figure 7. Maximum percentage improvement o oduced with the
source neutron energy in comparison with the numbe th 10 '
trons, for the case of a phantom with 5 mm skin and 5 mm
d 3.

For the case t brain (top graph
of figu ce ratio of 5), there is a clear de tumour
r a source neutron energy of 20 eV; for the 60 mm ng
ons pointing at 5 keV, as well as 20 keV; and f
rance dose gives mainly 10 keV and for 2 resulting gra
nce dose which is higher in point ski ain (bottom graph of fi
s the tolerance ratio of 5) looks r ix of the already described gro
nce ratios. For tumour owing number of configurations towar
l source neutro he explanation for this is that lower source

Table 4. The th… …ed tolerance dose ratios.

	…ation	
	…tolerance dose in point skin is *lower than or equal* …nce dose in *point* brain or *volume* brain	1/5, 1/…
Group 2	…in point skin is *higher* than … …int brain	3/1 and 5/1
Group 3	The tolerance … *higher* than the tolerance dos…	3/1 and 5/1

energie… …best to react with ^{10}B situated at shallow … …in. For tolerance ra… …man brain, it will most likely be that … …is averaged over a volum… …such the dose limit in brain. Becau… …hat extrem… …eutron energies can produce, under certain condit… nu… …in the tumour.

…discussion accompanying figures 3 and 4. It … …d that the resu… …studied tolerance ratios can be divided … …, which is summarized in…

…are, of course, transitio… …the groups due to the fact that another …e ratio can sh… …here the tolerance dose will be reached. … a … so… …gy generating more alphas at the tumour posit… sudden…

Neverth… …ds that the optimal source neutron e… …of parameter variations s… …n and brain. For the other phantom calculatio… …ing to the ten tolerance dose ratios, is als… …2, but now for the 3 … …mm skin and cranium thicknesses, respectiv…

…graphs of figures 3 and 5, it is of no doubt that th… …d cranial … …ant influence on the optimal source neutron e… …tumours positio… …20 mm from the skin, the differences are s… …ficant but for the shallowe… …ted tumours a transition can be seen …e of the 20 mm tumour, with incr… …anium thickness, the majority …nal source neutron energies 'move' from … …100 eV towards 1 ke… 500 eV for the 7 mm phantom. For the 80 … …nsition tow… hig… …rce neutron energies is observed. In fact, huge d… in the o… …ic results. The basic mechanism causing this de… thickness origi… …components: the thicker th… …ations of the D_H within the skin … …, which are tissue thickness independent … …the D_H value at the surface of th…

…ing parameters

…e clear indications presented above, it is … …cribe which parameters …cause the most significant deviat… …e this, the resulting optimal sou… energy is scored for ev… …ue. For each of the three phantoms, e… dose ratio and e… …mour, a plot has been made indicating the nu…

Table 5. [illegible] source neutron energies in a 5 mm [illegible] the square brackets [illegible] tissue that the parameter is set for.)

Phantom: 5 mm skin 5 mm cranium			
[illegible] our	Modal energy	[illegible]	Deviating higher energy
[illegible] rance dose: point skin 1/5 × point brain [illegible]			
[illegible] m	1 keV	21 eV: $C_{10B} \cdot CBE_{10B}$	
[illegible]	2.15 keV	464 eV: $C_{10B} \cdot CBE_{10B}$ [skin]	[illegible] keV: RBE_H [skin]
	4.64 keV	464 eV: $C_{10B} \cdot CBE_{10B}$ [skin] < 20	[illegible] RBE_H
	10 keV	464 eV: $C_{10B} \cdot CBE_{10B}$ [skin] < 20	
Toleran[illegible]		[illegible]t brain (representing group 2)	
20 mm	[illegible]		[illegible]$_{10B} \cdot CBE_{10B}$ [brain] < 20
40 mm	2.15 [illegible]		CBE_{10B} [brain] >
60	[illegible]		21.5 [illegible]
	10 keV		[illegible]$_{10B} \cdot CBE_{10B}$, RBE_H [all] < 2
[illegible]e dose: point skin 5 × volume brain (represe[illegible]			
	1 keV	0.215 eV: [illegible]	[illegible] < 40
	2.15 keV	10[illegible]	[illegible]skin] < 40
	4.64 keV		21.5 keV: $C_{10B} \cdot CBE_{10P}$ [illegible] 40; RBE_H [all] < 3
[illegible]			46.4 keV: C_{10}[illegible] 40; RB[illegible]

of occurrences [illegible] [illegible]utron energies. It wo[illegible] [illegible] present all the resulting 120 plots, i.e. [illegible] [illegible]rance [illegible] [illegible]positions. Fortunately, it is already seen that the [illegible] [illegible]nto t[illegible] [illegible]ns. Therefore, three representative tolerance ra[illegible] [illegible]ed. Furthermore, [illegible]om seems sufficient to represent the other p[illegible]

Practically, the parameter value [illegible] split into two parts, which w[illegible] [illegible]sed separately in the following subsectio[illegible]

[illegible]ers and values causing non-modal optimal source [illegible]

the [illegible] [illegible]rce neutron energy is given, as well as the dev[illegible] [illegible]gher energies and [illegible] [illegible] [illegible]ne deviating source neutron energies [illegible] [illegible] of a parameter value and the energies rel[illegible] [illegible] [illegible]are not met, then the devi[illegible] [illegible]eutron energy mentioned in table [illegible] [illegible] 5, and similar data found from the 3 mm and 7 [illegible]ears optimal source neutron energy in each toleranc[illegible] [illegible]ce [illegible]meters. The following results are therefore [illegible] [illegible]e thickness [illegible] [illegible]nium. In the case of group 1, the C_{10B} [illegible] [illegible]$_H$ parameters, all for sk[illegible] [illegible]e the influencing parameters. In t[illegible] [illegible] post processing, the location as t[illegible] [illegible] limit is reached inside t[illegible] [illegible] recorded. Indeed, for group 1, by far, [illegible]eached in skin [illegible] [illegible] cranium. Furthermore, in the case of group [illegible]

and CBE_{10B} for bra[illegible]going parameters. In recordin[illegible]quivalent dose limits, most pe[illegible]al neutron fl[illegible]0 mm and 40 mm.

[illegible]roup 3, a mixture of C_{10B} and CBE_{10B} for both s[illegible]nd the RBE_H [illegible]s the influencing parameters.

Although it is clear w[illegible]re important in each group, there seem[illegible]ystematic behaviour when the [illegible]ualities are interpreted (see table [illegible]lieved that this is caused due to va[illegible]' effects and actions invol[illegible]ting the optimal source neutron energy.

[illegible]ms that the value of the RBE_N parameter plays a[illegible]'st for [illegible]ll phantoms, there is a notable influence at 20 m[illegible]and [illegible].

4.2.2. Par[illegible]ing to the modal optimal [illegible] The para[illegible]s in table 1 are chosen in such a way that they c[illegible] BNCT of brain tumours. As discussed in se[illegible]ctions influence the presence of each parame[illegible]ight influe[illegible]ce of certain optimal source neutron ene[illegible]he intention of this s[illegible] conclude that the modal optima[illegible]ergy is the 'best' source neut[illegible]t is interesting to see how [illegible]s contribute to the modal optimal sou[illegible]ergy. To indica[illegible] schematically, figure 6 shows in how man[illegible]nfigur[illegible]n parameter value, there is a contribution to th[illegible] op[illegible]gy. The values displayed in figure 6 are for the 5 [illegible] for thre[illegible]resenting the three groups and at four tum[illegible]dal optimal source n[illegible]

To explain these curves, a[illegible]0 mm which has a modal optimal source ne[illegible] $CBE_{10B}[skin] =$ 320 con[illegible] neutron energy. As another example, n[illegible]r at 40[illegible]al optimal source neutron energy of 2.15 ke[illegible], [illegible]s wi[illegible]- 4 contribute to this modal neutron energy. [illegible], for RBE_H[bra[illegible]his occurs in 11% of the 4 527 600 configura[illegible]6 also allows the reade[illegible]ides drawing conclusions on influen[illegible]ters written in the last subsectio[illegible]' effects. That is in group 1, [illegible], it seems that the modal optimal sourc[illegible]are caused by all valu[illegible]$_{10B}$[skin] > 100. Except in the case of the 4[illegible]increasing v[illegible] concerning ^{10}B in the skin, the optimal source [illegible]tow[illegible]ev: it results every time, like clipped, in the same [illegible], energy. Th[illegible]en in groups 2 and 3 for some [illegible].

Generally spea[illegible]m and 40 mm is contrary and different f[illegible]our positions.

[illegible]nt of the optimal source neutron energies

[illegible]esults presented above show a wide spectrum [illegible]neutron energ[illegible], the question as to whether this study c[illegible]s regarding an optimal [illegible]ron energy. To investigate this [illegible] of alphas generated by each o[illegible]e neutron energy is com[illegible]mber of alphas generated by a neutron [illegible]eV. The choic[illegible]source neutrons as a reference comes from

that most BNCT fac[illegible] around this energy (Moss *et*

comparison, representing groups 1 and 3, are [illegible] 7

e improvement is shown for the case of a phanto[illegible]

5 mm crani[illegible] om group 2 are somewhere in between.

or example, focusing [illegible] roup 1 (top graph), it is clear that for a t

mm, there is a parameter co[illegible] ing an optimal source neutron ene

V, which produces 600% more alp[illegible] V source neutrons. As a

e, for group 3 and a tumour at 60 mm: t[illegible] keV indicates th

rations in which this source neutron energy de[illegible] more

neutrons. Note that the improvement for parame[illegible]

optim[illegible] ergy at 10 keV is of course 0%.

Althoug[illegible] the maximum improvement is aro[illegible] nth), all other tumour po[illegible] then 200% improvements. The [illegible] mum impr[illegible] group 1, which is due to the fact that in this, the [illegible]

[illegible]. Decreasing the parameter values related to the [illegible] dec[illegible] [illegible]olution of lower energy neutrons to skin. Th[illegible] [illegible]eutrons to pro[illegible] nas in the tumour than the 10 keV sou[illegible] suffer from the rather h[illegible] ecoil dose in skin. In groups 2 [illegible] ain that is set as the more sensiti[illegible] these groups, for tum[illegible] deeper, it matters little whether the alr[illegible] e produced by [illegible] ons, which reach the dose limit in deeper br[illegible] part[illegible] by lower energies, which reach a dose limit in s[illegible] brai[illegible] eutrons produce, in the end, a corresponding num[illegible]

As we[illegible] improvements, for single parameter [illegible] rage improvements were [illegible] configurations resulting in the same optim[illegible] a phantom with 5 mm skin and 5 mm [illegible] 7 but now rangin[illegible]

7 is representative of all other improvement out[illegible] ins. The [illegible] ment for the 3 mm phantom and 7 mm phanto[illegible] % and 350%, res[illegible] imum improvement for both phantoms ra[illegible] 0% and 500%, respectively.

all phantom cases, the improveme[illegible] l source neutron energies bel[illegible] ly in the case of the 7 mm skin and cranium [illegible] e cases in which a so[illegible] rgy of more than 100 keV gives an improve[illegible] a tumour [illegible]

5. Conclusions

This parameter st[illegible] T. By varying many of the [illegible] involving ones directly (e.g. RBE, [illegible] ometry) [illegible] valent dose, insight can be gained into the behavi[illegible] e [illegible]gy in BNCT of brain tumours. In selecting su[illegible] up to realistic maxima, there was a certain ar[illegible] ther such an [illegible] would lead to conclusive results. An [illegible] of values, gathered fr[illegible] ture, was chosen. By ignoring [illegible], mostly zero values, and obvi[illegible] ng physically impossible [illegible] number of possible configurations co[illegible] significantly [illegible] unprejudiced, the resulting optimal source

energies of the [illegible] Nevertheless, the modal [illegible] energies can be seen as good [illegible] energies.

[illegible] described above, it is clear that there is a signi[illegible] of the [illegible]um for all parameter configurations. There is [illegible]

[illegible]our of the [illegible] a certain optimal source neutron energy for [illegible] 40 mm deep seated t[illegible] [illegible]ison with the 60 mm and 80 mm ones. L[illegible] [illegible]ects, the optimal source neutr[illegible] [illegible]urs at 40 mm from the skin, for a[illegible] [illegible]antom cases and tolerance dose ratios, [illegible]round 2 keV.

Furthermore, the optimal source neutron e[illegible] [illegible]strongly influen[illegible] [illegible]of the tolerance dose in skin and brain. In this [illegible] [illegible]s di[illegible] [illegible]teristics in the results, could be identified accordi[illegible] [illegible]os:

- G[illegible] [illegible]lerance dose in every point i[illegible] [illegible]al or equal to the tolerance [illegible] [illegible]me of the brain. The skin t[illegible] [illegible]limiting tissue.
- [illegible] [illegible]has a higher tolerance dose in every point of the s[illegible] [illegible]oint [illegible]al. The brain turns out to be the treatment limiti[illegible]

[illegible]oup 3, which is the same as group 2, exc[illegible] [illegible]ce dose in brain is se[illegible] [illegible]e whole volume of the brain. Bot[illegible] [illegible]rain can be the treatment lim[illegible] [illegible]ssue.

[illegible]rns out that [illegible] [illegible]al the tolerance dose is reached first, determ[illegible] [illegible]amount of deviation in the source neutron ene[illegible] pa[illegible] [illegible] are the ^{10}B concentration (C_{10B}), the adjusted [illegible]al effectiv[illegible] [illegible]CBE[illegible]) and the biological effecti[illegible] [illegible]oil recoil (RBE_H). In gener[illegible], [illegible]dual optimal source neutron energies are n[illegible] [illegible]roton recoil parameters. Lower opti[illegible] [illegible]gies are prevalent as [illegible] [illegible]raction with ^{10}B [illegible]wer values of the C_{10B} as well as the CBE_{10B} fac[illegible] [illegible]f the [illegible]roton production of nitrogen, the induced gamma[illegible] [illegible]seem unl[illegible] [illegible]ptimal source neutron energy.

[illegible]is clear that many [illegible] varied in this study give very different [illegible]e optimal source neutron en[illegible] [illegible]from the perspective of designing [illegible]on filter, this conclusion is overshad[illegible] [illegible]s at the improvement in gen[illegible] [illegible]particles with the optimal source neutron [illegible]rison with 10 keV [illegible]The improvements are insignificant for sour[illegible] [illegible]1 keV [illegible]ity in modal source neutron energies occurs as a [illegible] thi[illegible] [illegible]neutrons lower than 1 keV, it is possible to achi[illegible] [illegible]ents. On averagi[illegible] [illegible]ow 1 keV can improve the alpha produc[illegible] [illegible]the 10 keV case. Without averaging, as i[illegible] [illegible]to 700%. Although furth[illegible] [illegible]matters, it is apparent already fro[illegible] [illegible]ce neutron [illegible]10 eV and 100 eV will increase the alpha prod[illegible] [illegible]many [illegible] configurations at all tumour positions and inde[illegible] [illegible]se [illegible]ular, the treatment of shallow situated tumou[illegible] [illegible]al the availabi[illegible] [illegible]wer source neutrons.

As an overall conclusion, the r[illegible] [illegible]eals that no matter what the inve[illegible] [illegible]ameter values are or wi[illegible] [illegible], a source neutron energy of a few keV [illegible]a source neutr[illegible] [illegible]der of tens of eV will cover all configurations

the best alpha production possible in BNCT. A logical next step and future study will be to ignore the non-influencing parameters and investigate new parameters such as, for example, the field size.

References

Bisceglie E, Colangelo P, Colonna N, Santorelli P and Variale V 2000 On the optimal energy of epithermal neutron beams for BNCT *Phys. Med. Biol.* **45** 49–58

Bleuel D L, Donahue R J, Ludewigt B A and Vujic J 1998 Development of a neutron-biased in-air figure-of-merit for predicting in-phantom BNCT neutron beam characteristics *The 8th Int. Symp. on NCT for Cancer (Ja Jolla, CA, 13–18 Sept. 1998)*

Briesmeister J F (ed) 2000 MCNP—A General Monte Carlo N-Particle Transport Code, Version 4C, LA-13709-M

Duderstadt J J and Hamilton L J 1976 *Nuclear Reactor Analysis* (New York: Wiley)

Hideghéty K *et al* 2003 Tissue uptake of BSH in patients with glioblastoma in the EORTC 11961 phase I BNCT trial *J. Neurooncol.* **62** 145–56

ICRP 1975 *Reference Man: Anatomical, Physiological and Metabolic Characteristics* (Oxford: Pergamon) ICRP Publication 23

ICRU 46 1992 *Photon, Electron, Proton and Neutron Interaction Data for Body Tissues* (Bethesda, MD: International Commission on Radiation Units and Measurements)

Kuni H 1998 The concept of equivalent dose and dose limits—urgent improvements *STOA Workshop (Brussels)*

Moss R L, Aizawa O, Beynon D, Brugger R, Constantine G, Harling O, Liu H B and Watkins P 1997 The requirements and development of neutron beams for neutron capture therapy of brain cancer *J. Neurooncol.* **33** 27–40

Nigg D W 1999 Some recent trends and progress in the physics and biophysics of neutron capture therapy *Prog. Nucl. Energy* **35** 79–127

Pinelli T *et al* 2002 TAOrMINA: from the first idea to the application to the human liver *Research and Development Neutron Capture Therapy* ed W Sauerwein, R Moss and A Wittig (Bologna: Monduzzi Editore) pp 1065–72

Sauerwein W *et al* 1999 EORTC BNCT Study Group, Phase I clinical trial with BNCT for patients with glioblastoma at the European High Flux Reactor Petten (EORTC 11961) *(11th Int. Congress of Radiation Research (Dublin)) Radiat. Res.* **1** 26 (Congress Abstracts)

Tanaka K, Kobayashi T, Sakurai Y, Nakagawa Y, Ishikawa M and Hoshi M 2002 Irradiation characteristics of BNCT using near-threshold ^{7}Li(p,n)^{7}Be direct neutrons: application to intra-operative BNCT for malignant brain tumors *Phys. Med. Biol.* **47** 3011–32

van Vliet-Vroegindeweij C, Wheeler F, Stecher-Rasmussen F and Huiskamp R 2000 Microdosimetry model for boron neutron capture therapy: II. Theoretical estimation of the effectiveness function and surviving fractions *Radiat. Res.* **155** 498–502

Verbakel W F A R 2002 Design and validation of a γ-ray telescope for *in vivo* dosimetry during BNCT *PhD Thesis* NRG, Petten

Wittig A *et al* 2001 Early phase II study on BNCT in metastatic malignant melanoma using the boron carrier BPA, EORTC BNCT study group *Protocol 11011*

Yanch J C, Zhou X L and Brownell G L 1991 A Monte Carlo investigation of the dosimetric properties of monoenergetic neutron beams for neutron capture therapy *Radiat. Res.* **126** 1–20

Ye S J 1999 Boron self-shielding effects on dose delivery of neutron capture therapy using epithermal beam and boronophenylalanine *Med. Phys.* **26** 2488–93

Application of adjoint Monte Carlo to accelerate simulations of mono-directional beams in treatment planning for Boron Neutron Capture Therapy

V. A. Nievaart[a)]
Department of Applied Sciences, Delft University of Technology, Lorentzweg 1, 2628CJ Delft, The Netherlands and Joint Research Centre of the European Commission, P.O. Box 2, 1755ZG Petten, The Netherlands

D. Légràdy
Department of Applied Sciences, Delft University of Technology, Lorentzweg 1, 2628CJ Delft, The Netherlands

R. L. Moss
Joint Research Centre of the European Commission, P.O. Box 2, 1755ZG Petten, The Netherlands

J. L. Kloosterman
Department of Applied Sciences, Delft University of Technology, Lorentzweg 1, 2628CJ Delft, The Netherlands

T. H. J. J. van der Hagen
Department of Applied Sciences, Delft University of Technology, Lorentzweg 1, 2628CJ Delft, The Netherlands and Reactor Institute Delft, Delft University Technology, Mekelweg 15, 2629JB Delft, The Netherlands

H. van Dam
Department of Applied Sciences, Delft University of Technology, Lorentzweg 1, 2628CJ Delft, The Netherlands

(Received 12 May 2006; revised 8 February 2007; accepted for publication 8 February 2007; published 16 March 2007)

This paper deals with the application of the adjoint transport theory in order to optimize Monte Carlo based radiotherapy treatment planning. The technique is applied to Boron Neutron Capture Therapy where most often mixed beams of neutrons and gammas are involved. In normal forward Monte Carlo simulations the particles start at a source and lose energy as they travel towards the region of interest, i.e., the designated point of detection. Conversely, with adjoint Monte Carlo simulations, the so-called adjoint particles start at the region of interest and gain energy as they travel towards the source where they are detected. In this respect, the particles travel backwards and the real source and real detector become the adjoint detector and adjoint source, respectively. At the adjoint detector, an adjoint function is obtained with which numerically the same result, e.g., dose or flux in the tumor, can be derived as with forward Monte Carlo. In many cases, the adjoint method is more efficient and by that is much quicker when, for example, the response in the tumor or organ at risk for many locations and orientations of the treatment beam around the patient is required. However, a problem occurs when the treatment beam is mono-directional as the probability of detecting adjoint Monte Carlo particles traversing the beam exit (detector plane in adjoint mode) in the negative direction of the incident beam is zero. This problem is addressed here and solved first with the use of next event estimators and second with the application of a Legendre expansion technique of the angular adjoint function. In the first approach, adjoint particles are tracked deterministically through a tube to a (adjoint) point detector far away from the geometric model. The adjoint particles will traverse the disk shaped entrance of this tube (the beam exit in the actual geometry) perpendicularly. This method is slow whenever many events are involved that are not contributing to the point detector, e.g., neutrons in a scattering medium. In the second approach, adjoint particles that traverse an adjoint shaped detector plane are used to estimate the Legendre coefficients for expansion of the angular adjoint function. This provides an estimate of the adjoint function for the direction normal to the detector plane. In a realistic head model, as described in this paper, which is surrounded by 1020 mono-directional neutron/gamma beams and from which the best ones are to be selected, the example calculates the neutron and gamma fluxes in ten tumors and ten organs at risk. For small diameter beams (5 cm), and with comparable relative errors, forward Monte Carlo is seen to be 1.5 times faster than the adjoint Monte Carlo techniques. For larger diameter neutron beams (10 and 15 cm), the Legendre technique is found to be 6 and 20 times

 0094-2405/2007/34(4)/1321/15/$23.00

faster, respectively. In the case of gammas alone, for the 10 and 15 cm diam beams, both adjoint Monte Carlo Legendre and point detector techniques are respectively 2 and 3 times faster than forward Monte Carlo. © *2007 American Association of Physicists in Medicine*.
[DOI: 10.1118/1.2712573]

Key words: adjoint Monte Carlo, mono-directional beams, treatment planning, BNCT

I. INTRODUCTION

In [illegible] ...ument planning, the treatment ...parameters such as the ...acteristics, the ...be used, their ...and orientation, together w... ...and ...gans at risk (OAR). The next step is to ...lan by adjusting the weights and/or shapes of ... ...beams such that the target volume receives the re... ...lose without exceeding the tolerance doses of the ...the first step, it would already be an improvem... ...direction, energy, and shape) were sele... ...ciple, possible ... ...joint transport theory ...ical description of the adjoint ...ided in this paper and the reader is re... ...literature.[1–3] Furthermore, this paper deals ...nerapy treatment planning in the field of Boron ...apture Therapy (BNCT). A brief desc... ...iven in Sec. II A. At this st... ...CT patients are ... ...ed radia... the ...hat treatment plans can only ...arlo (MC) based programs. In normal MC tra... source, lose energy while traveling ... ...tered when passing a ... as forward ... ...ward particles travel from the ...ector. This way of trav... ...versed and ...int MC. So... ...nt particles start at the so... ...al s, gaining energy before they are re... ...e forward source. Actually, in adjoint MC the ... ...or becomes the adjoint source and the forward ...the adjoint detector. (In the remaining text, whe... "source," "detector," or "particle" is written, the ... ...is in the real world is meant. With the additive ... ...tor or particle is suggested by ... While there ... ...ward" is some... tim... ...in order to improve the readability. ...djoint" is always written whenever simulated ...rticles travel from the adjoint source to the adjoint ...r.) With the adjoint method the user obtains at ... ...t detector the adjoint function which re... ...nition given by Bell and Glas... ...me ...e" of a forward ...ributing to ... ...The adjoint function wh... ...ec. II B. For treatment planning, the adjoint fun... ...ther informa... tion about the position, angle, ...

...ors and OAR. Instead of performing a great num... ...to find the optimal irradiation conditions, the ad... ...in a few calculations. The adjoint approach is ... ...n the number of beam exits (adjoint detectors) ...r than the number of tumors and OAR (adjoi... ...l advantage depends on the number and ...P and on the number and si... exits.

As stated ... ...ni and Difilippo[6–8] can be rev... ...the applica... ...ing. Although they and ... ...it is applicable, the adjoint MC method is stil... ...linical community.

Most of the ... ...this is Carl... ...ode system MCNP ... ...aboratory.[11] Furthermore, in the ...ories, the irradiated bodies are all surrou... spherical or cylindrical surface, which is segme... adjoint detector areas. Such a set-up implie... functions are determined at fixed po... ...NP calculation. The adjoint ... ...have the ... ...a lattice of smaller ...senting an array of pencil beams. This ...if the lattice is fine struc... tured in size, energy, and ... ...an would a superposition of the pencil beams, i... ...eam opening, make sense. Even with present co... computer power, this fine structure approach ... ...ible due to the time required to achieve dece... ...ber large lattices need to be used pr... ...coarse grid of optim... irradiate from ... ...f Iera... ... shown that this approac... ...tep, is already a great im... ...n plan.

...ped adjoint detector segments ...of the contribution for a certain beam. This artic... ...beam shaped adjoint detector segments and ...me its asso... ciated probl... ...to be ex... ...adjoint particles a... ...ible phase space coordinates a... ...ment beam has for instance an angular 2 degrees, only adjoint particles hitting the plane within 2° to the normal are valuab... ...e adjoint particles travel in the oppo... ...e par... ticles in the treatment be... ...take a long time ... ...obtained for a specific ...hase space coordinates. Such an approach

is applied by Wang *et al.*[5] wh
of the treatment
the bea
jr
ods are developed and applied to enable a
ent planning.
method is based on next event estimators and the
is based on the expansion of the adjoint func-
tic
second
technique (FE
Legendre expansion in Mo
particles can contrib
contributio
OAR
h
ent.

LS AND METHODS

starts by giving mor
the adjoint
the
approac
with Legendre po
IV, the two developed meth
amples. The first example shows the va
joint MC methods and
of the Legend
head
ar
preferred over
speed. Finally, the optimu
a neutron beam are presented which m
n introductory step for further investigations
n of treatment planning.

A. of Boron Neutron Capture Therapy

Boron Neutron C
thermal neutrons are delivered a
taining much more boro
healthy cells
^{10}B, h
produced that, in principle, can
. Consequently, healthy cells containing
lower doses and will be spared. This non-
is a result of the thermal neutrons creating sec-
articles due to hydrogen and nitrogen reactio
. This could give an unwanted dose in
its the irradiation time. In BN
ed with epitherm
ne neu-
aliz
n intermediate
tiss
he aim is to have a lot of
thermal n
f the cancer. In reactor
based BNCT, as m

gammas originating from the re-
erform the calcula-
tions also for this type
utrons and
gammas are both important in BN
ques
presented in this paper will be demonstrat
irradiation. More details on BNCT can be
publications.[13,14]

n forward flux and adjo

In gene
is prefe
ward detector is sim
joint
particles that start at a s
ve a larger
source, from which
the adjoint function) can be
obtained.
particles start at
the tumor or at the OAR and
where
outside the body in ord
and orientatio
large ac
but m
be modeled. The t
called the forward neutron or
$r,E)$ and the adjoint function $\phi^+(\underline{r},\underline{\Omega},E)$,
ly. Both quantities are a function of the positi
direction $\underline{\Omega}$ and the energy E of the (adjoint)
interest. From Williams and Engle,[15] ϕ may be
quantity related to the "particle distrib
be interpreted as the "effect
detector
or neutrons and
Boltzmann equation. In the
and notation of this equation
can be writte
erator L. This
operator includes the characte
d scat-
tering terms operating on the flux ϕ.
transport equation can be defined with a mat
joint transport operator L^+ operating on ϕ^+. Bet
the important relation between the forward flu
tion ϕ^+, the forward and adjoint transp
ith accompanying boundary c
Using
fter Bell and Gl
relevant forwa
ssed
defined by

$$L\phi(\underline{r},\underline{\Omega},E)=0 \tag{1}$$

$$r\in S,\underline{\Omega}\cdot\hat{n}<0, \tag{2}$$

where ψ
source and S, of
which $\hat{n}$ is the unit outw
boundary
surface of volum
In
this pape
have a p
particles crossing S
relevant adjoint problem for ϕ^+ s

$$L^+\phi^+(\underline{r},\underline{\Omega},E)=-\Sigma_d(\underline{r},E),\quad \underline{r}\in V,$$

$$\phi^+(\underline{r},\underline{\Omega},E)=0,\quad \underline{r}\in S,\underline{\Omega}\cdot\hat{n}>0,$$

where L^+ is the adjoint transport
he de-
tector response functi
given by a
the adjoint calcula-

tion the source of the adjoint
illustrate that the
boundary
solution" involves a specific
and ϕ^+ is given by

$$\int_V \Sigma_d(\underline{r},E)\phi(\underline{r},\underline{\Omega},E)dE$$

$$=\int_{\Omega<0}\int_0^\infty |\underline{\Omega}\cdot\hat{n}|\phi^+(\underline{r},\underline{\Omega},E)\phi^b(\underline{r},\underline{\Omega},E)dEd\Omega dS, \quad (5)$$

ived following the literature on the adjoint
tech
Introduction. Interpreted for treatment plan
integral of the adjoint
function multiplied
source function over the surf
beam exit is loca
ming inward vol-
ume V, ar
the left-hand side of Eq. (5),
the
se. This total detector response is the
treatment beam to the flux or dose in, for
or. This is when the adjoint source is located
with a source spectrum Σ_d according to the flu
e in this paper the focus is on incid
tely or nearly mono-direct

$$\phi \quad (6)$$

where δ is the
the direction of the
particles in the beam.

MCNP tracks adjoint neutrons, as well
but the adjoint MC implem
multigroup cro
ultigroup libraries
are prob
noted that MCNP adjoint
real treatment
ialization is des
[16] and
horough description of
be found in Lewis and M
[18]

erhaps confusing, the reader has to be in-
possible to calculate adjoint functions with
fo
sibility is applied in Example I (Sec. III). The
rgy dependent adjoint function
in forward mo
at the forward detector all those scores of
from the same energy group at the so
sums for each source
joint functi
This method is similar
to th
ribution function which is defined
contribution of source particles to the
course, it is still a forward MC calculation and,
he statistical uncertainties of an estimate can only
when a forward particle reaches the detect

ent estimator appro
nique

bability that adjoint MC
particles
tor plane perpendicularly
is virtually zero.

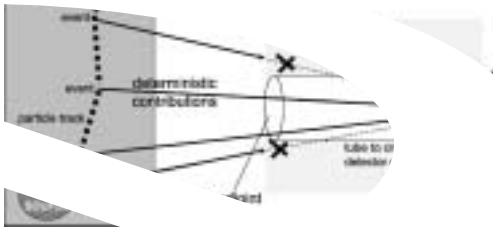

FIG. 1. Adjoint Point Detecto
detector far
away from the phant
outions of adjoint
entrance. This entrance is

detecting all adjoint par
tions. However
culation
good
adjoint particles w
djoint detector. A solution for th
e to force the flight direction along the p
e just before it crosses the adjoint detector plane
has a next-event estimator that closely meets th
ment. The technique is called DXTRAN, w
terminology stands for Deterministic TP
it involves deterministically
events
ighborhood of a
contributions to the detector
user-defined sphere is taken
to be infinitely
tain many particles in a point of interest tha
impossible to sample. MCNP tally type 5 is
detector. DXTRAN can be used with both
joint particles. In this work, the contributions
tector are only from adjoint particles. Following
MCNP-forum,[19] it is recommended to
very far away from the phan
that an
are parallel. Using
outside of whi
historie
fectively creates an adj
the
beam exit. This technique
adjoint
ustrated in Fig. 1.
sed in this work, a distance of
the phantoms and the adjoint
point detect
effect disappear
and simulate only parall
nce is related to the size
the
diameter
the adjoint
point detector in the
e of incidence. This means that an
beam can be simulated by changing the loc
point detector. Due to its forced nature, the re
tainty in the APDT decreases rapidly as a
number of adjoint particle histories/ever
tribution can be made. For the
the examples described in th
uction in cal-
point detectors in one

single MC run when com-
adjoint point
to b
ng a so-called heating time, but
ulation time.

for angular interpolation.
nsion Technique

basic idea behind the functional expansion techniq
to describe a detector response by a series expan-
C samples for estimating the coefficients. Since
[12] the FET technique has been applied to
various
[20–24] and its convergence proper-
ties analyzed.
pressed by

$$f(\cdot) \qquad (7)$$

set of coordinates in the phase space, ψ_n are
d basis functions, and d_n are coefficients given b
product of

).

imulati
sampling an
im
unction (pdf) φ. A
sample is
the phase space (x) and the
statistical weight o
can usually be described as an
chosen detector function
mation of the

$$(9)$$

mber of (x_i, w_i) samples. If the
of the implicitly sampled pdf at a coord
unction is selected as $h = \delta(x - x_0)$. Normally, no
les fall exactly at x_0, unless forced by next-event
the number of non-zero scores (and, conse-
qu
ce rate) is extremely low. This was
already
duction. After applying the
general formula
an estimate for the d_n expansio
some low number, M),
to estimate

$$\sum_{j=0}^{\infty} \psi_j(x_0) \int \varphi(x)\psi_j(x)dx\psi_j(x_0) \approx \frac{1}{N}\sum_{i=1}^{N} w_i \sum_{j=0}^{M} \qquad (10)$$

In the
simulation, the estimator of
the importance
surface, for a certain solid angle

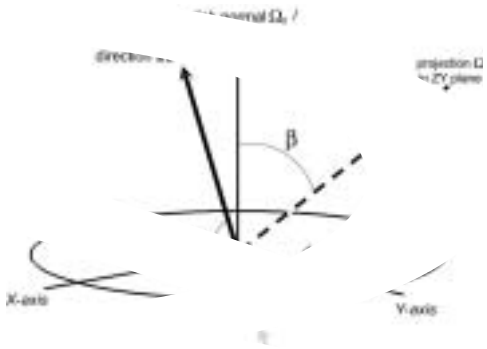

FIG. 2. Adjoint detector
tor
of the crossing
and α an

, by applying Eq. (10). As is explain
detail in the next section, Ω_0 is decomposed into
pendent angular variables (α and β) and, ther
dimensional base function set $\psi_{l,m}(x,y)$ ha
For the base functions the product of
nomial (P_l) expansions is used
(β),
where
As the Legendre
on $L^2(-1,1)$, the angular coordi-
med to $(-1,1)$. While only Leg-
endre poly
it is more appro-
priate to introduce the term
Technique
(LEXT) instead of using the genera

E. Parameterization of the LEXT for mono
beams

ticles traveling parallel to the disk
mono-directional beam
adjoint de
ether wit
direction vector
isk.
According to the last sec
normal is
defined as
ever "normal" is
the adjoint detector disk is men-
pointing away from the phantom.
not return after cross-
ing the adjoint detec
importance is
only non-zero i
le. The
Legend
[26]
er poi
ndle of $(-1,1)$. The
the hemisphere of the angular c
ave the disk normal falling in the middle
both $\cos(\alpha)$ and β. Note that this requireme
that can be accomplished in several ways
chosen that the X- and Y-axis of the
are
defined within the disk plane
the nor-
mal. β is chosen
Z-axis and the
in the ZY plane. Since
pass the disk from one side, β is in

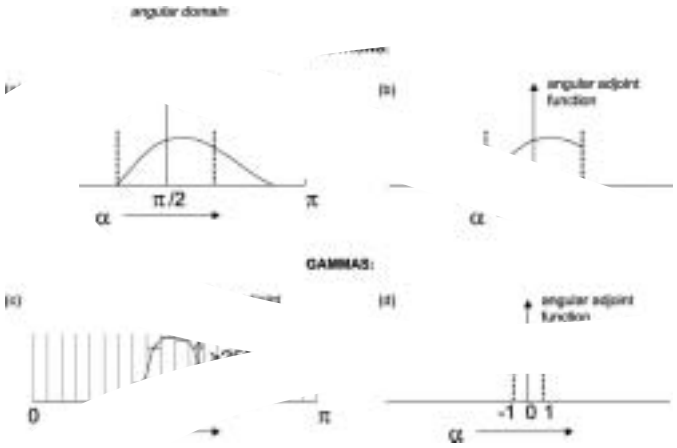

FIG. 3. Neutrons ... for different truncati... clude zero values or st... the angular adjoint func... cating the functions, f... polynomials are need... A typical adjoint ... ...ns is sh... ...). A ... function ...omains is shown ...).

...ith the normal direction ... ...negative for ne... ...so α is ... ...at the normal direction ... at $\pi/2$ in $[0,\pi]$. Both intervals can be ... ...egendre interval of $(-1,1)$. Rewriting Eq. (10), omitting all phase space coordinates but with both α and β linear...

$$\frac{1}{N}\sum_{i=1}^{N} w_i 4 \sum_{j=0}^{M}\sum_{k=0}^{K} \frac{2j+1}{2}\frac{2k+1}{2} \times P_j(\cos\alpha_i)P_k(\beta_i)P_j(\cos\alpha_0)P_k(\beta_0). \quad (11)$$

...tion provides a factor that belongs to the direc... ...for which the initial weight of the adjoint Mo... ...be corrected. After this weight correction, the ... deviation estimated in the regular ... outcome looks like a normal ...

This interpr... ...ity if the importance ... ...nction of the solid angle, and is ... ...the middle of $(-1,1)$. A more sophisticated ... requires more coefficients for an accurate de... ...creasing the polynomial order means higher fluctuations in the correction of the weight. Therefore, while the truncation error decreases, the estimated ... in the statistical sense.[25] ... the number of ... ...otherwise ... ...with zero values and, ... of the Legendre interval $(-1,1)$, ...chosen dependent on the particle type. This ...

...improvement of the LEXT by reducing the ... of coefficients

The number of Legendre coefficients ... expanding the angular adjoint ... ...s for α and β ... ...ating the angular ... ...ies and to some extent rapidly ... ...unction discontinuities may arise at the ... ...angle, adjoint particles from the tissue cannot ... ...r disk. Likewise the exclusion of rapid gradients ... hance the convergence at the cost of shrinking detector (disk) size, meaning less hits to utilize ...XT. After rescaling to the Legendre interval, the ... ...chosen to be at 0 where good pointwise ... ...the Legendre expansion is ex... already ...

The angular ... ...ehavior ... different for gammas and ... ...ces that are involved in this ... ...as scatter ... ...ow shaped angular ... ...mas whilst broad and flat for neutrons. ... of α and β intervals are performed differently ... ...ns. Two examples of typical angular adjoint ... ...gammas and the way that ... ...ncated are ... ...the proces... ... α. For β, it is the same ... ...the intervals are defined by the ... ...gular adjoint function closest to the norm. For example, in Fig. 3(a), the left zero value is $=\pi/2$ (normal direction of the adjoint detector) ... the symmetrical interval indicated by the ... interval is rescaled to $(-1,1)$ in ... ...an as illustrated in Fig. 3(b). ... ...s are defined ... ...adjoint function closest

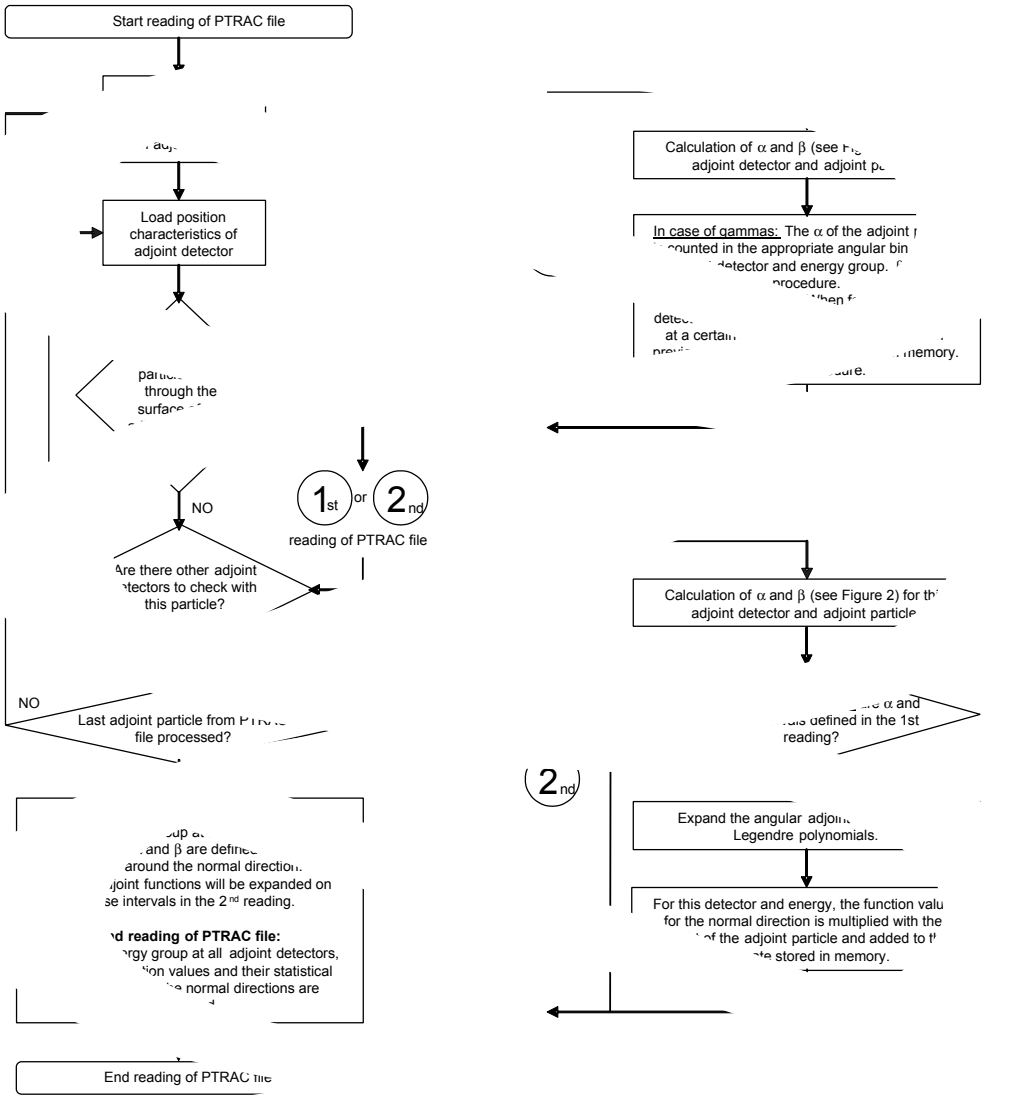

FIG. 4. [illegible] steps involved in the preprocessing for the LEXT. Note that all recorded adjoint [illegible] have to be

ial direction. The steep gradients can be found by course representation of the adjoint fu[illegible] interval for α is divided into [illegible] shows an example of [illegible] ogram. It is cl[illegible] gradient when the angular ad[illegible] successive angular bin dif-

[illegible]%. Therefore, in Fig. 3(c) the [illegible] side of the normal direction decreases [illegible]%, which causes the function to be expanded [illegible] ing within the two bins around the normal [see

Consequently, for the techniques des[illegible] gammas and neutrons it has to be cor[illegible] cat-ing the intervals for α and [illegible] ormation

outside the intervals is not
timate from t
sam
tion, it is chosen in this work to
for every energy group
detector
seems that the
d narrow-shaped ad
only
mes encounter this problem. In th
r bins are added until 50% of the sam

gh, the techniques and assumptions presented here
LEXT work fine for the examples discussed
it is worthwhile studying this aspect in
more de

G. Adjoint particle
the LEXT

the LEXT to determine the contribution
ctional beam to a specified region in a phan-
form an adjoint MC calculation without defining
detector. The adjoint source particles start in
a cell which can be a tumor or OAR
by traveling through the
e the phanto
the sur-
oss a sphere sur-
roun
y, the adjoint particles are
recorded whe
a radius of 50 cm.
The computer output fi
weight, and energy of the adjoint pa
called a PTRAC file
Particle TP
the user to gather each
ind
individual particle events
score
the estimate and
uncertainty of a
In or-
the size of the PTRAC file
filters. In this work only adjoint parti
ned sphere around the phantom pass the filter
d. This sphere will be further called the PTRAC

MC calculation is finished, custom made
Fortran
preprocessing. To obtain the
results, the PTR
adjoint par-
ticles, has to be read twice.
obtain for all adjoint detect
of the adjoint
direction
whic
or zero values as explained in
cond reading of the PTRAC file is per-
pand the angular adjoint function with Legendre
nals and to provide an estimate for the normal direc-
f all adjoint detectors for each energy group
overview of all steps involved in the pr
XT is given in Fig. 4. Apart fr
sing needs a list w
tion of all
ors th
, done with MCNP version
4C2 as
cessing codes written in For-
tran, are perform
a 3 GHz processor and 512 M

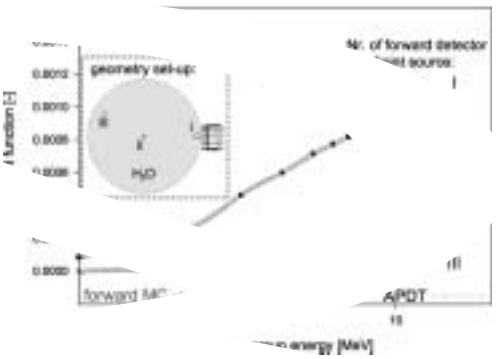

FIG. 5. Contributions of source
rey groups
which leave a 10 cm diam
ferent
cells in a light wate
with APDT
identical resu

mand shell. This information is given i
nterpret the absolute times given in the results
the calculation times given include the loadi
geometries (heating time).

III. EXAMPLE 1: W
ATED
ITY OF THE APDT
OF THE LEXT

to show that the
APDT and LEXT gener
can be ob-
tained with forward MC. This will be
the
adjoint functions calculated with the APDT
The way to calculate adjoint functions with
described in the last paragraph of Sec. II B. Furth
is used to illustrate the physical signific
Secondly, the APDT and LEXT
comp
how the LEXT r
towards the
corr
endre coefficients.

herical light water phantom is cho-
ctional gammas com-
ing from a 10 cm diam
oss section of
the geometry se
e water
sphere
al
and co
cal
of 2.0, 1.0, and 0.5 cm
and are positioned at different dis
ce. These cells are labeled I, II, and III,
the inset in Fig. 5. The goal is to obtain the er
adjoint functions in these three cells. In
set-up the three cells are forward det
ard
source is at the right side. T
forward
source particles is t
antom as indi-
arrows in the opposite
the adjoint particles of the adjoint calcu-

lation for the APDT. Thes
through the 1
10^4 c
. For both the APDT and LEXT,
int sources in which the
ie track
ections. For the
methods, the gamm
ions and
group structure from the ME
The forward and adjoint sources have a
ectrum over 12 energy groups between the limi
V up to 20.0 MeV. The detector response functions
rd and adjoint methods are similar and also
the 12 energy groups. In this example,
the g
d at the central energies of the
12 groups. In
volume tallies of the F4
APDT is of type
set, as
the adjo
ed in the PTRAC file when
pa
ere.

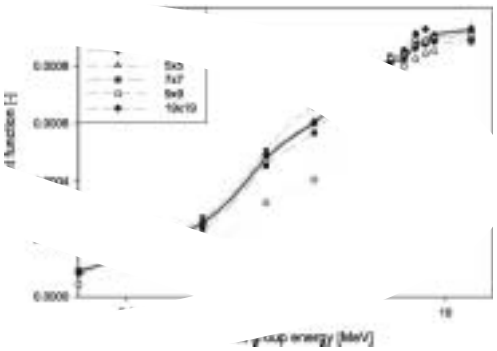

FIG. 6. The adjoin
EXT for different
numbers of Legendre coefficients
converges
towards the APDT, which
's or
more for α and β.

s: Comparison between the APDT and IC

in Fig. 5 show six
are
herical
forward MC
and
belong to the direc-
tion of t
detector disk. It can be
clearly seen that the
To obtain similarly averaged
95% confidence interval
0.3%, and 2%
takes 50.8 min
against
it is clear that adjoint MC
advantage for these
with rela
tectors com-
ne size of the forwa
djoint functions in Fig. 5 indica
mmas of a certain energy group leaving
perpendicularly that contribute to the cells I, II,
example, see the function value indicated with
5. At this point, per source gamma leaving
the
haped source, around 0.0012 source
gammas
9 and 20 MeV (the 12th
energy group) co
every 833 source gammas, there
an energy between 9 and
Concern
position of the
thr
at adjoint function I is the highest
ed closest to the source. Compared with
ells, many source gammas of all energy groups
ribute easily to cell I because they are not affected
water thickness (depth). Curve I is higher
a source energies, as these gammas
lity to scatter in the first few
ected towards cell
II, located
tanc
y the higher source
e
t of the lower energy gam-
mas ar
red in the water. The small-
est cell III is ra

e direct gamma beam. Only a very small
e source gammas having the highest energies
such that they can contribute to this cell.

C. Results: Convergence of

the adjoint func-
and APDT for cell II. For this
calculation for the LEXT is
started wi
starting in cell II.
This simulation and writing
file takes
131 min of CPU time. In Fig. 6, the
the
adjoint function obtained with the APDT
as the reference. To obtain the adjoint func
EXT, the correct number of Legendre coefficie
d. In this example, the M and K for α
as 1, 3, 5, 7, 9, and 19 coe
these
ients, the adjoint
shown in Fig.
agen
and one for β (writte
EXT
result does not agree wi
rises for 3
to 9×9, the adjoint
the LEXT has for this configuration
me sets of curves for the other
positions
it is observed that
all adjoint functions ha
nce with the
corresponding
re co-
efficie
rther expe
he
meter of the adjoint de
at using 7×7 coefficients contin
same adjoint functions as the APDT and
When even more coefficients are used, th
oscillate (see, for example, 19×19 in F
relative errors increase. The relative
nce
interval) of the above results
ne more
coefficients are used
error becomes.
of coefficients has to be

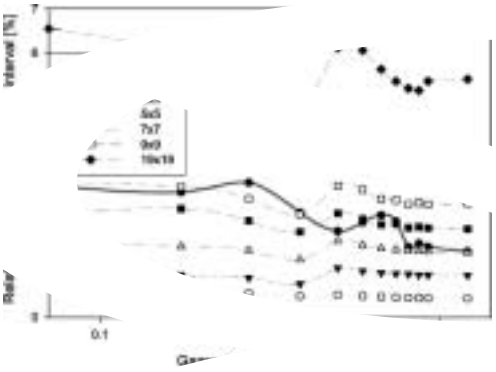

FIG. 7. The ... functions for the LEXT and APDT. The er... with increasing number of Legendre coef-fic...

...nat the result converges with the minimum ... ...'s approach is further discussed in ... ...parison with the LEXT ... ... 10^5 adjoin... ...that the aver... ...e LEXT with 7 ×7 coeffi... ...culation for one adjoint detector disk with ... ...was that the LEXT cannot compete regard... ... LEXT will start to profit when mo... ... involved because the c... ... the informati... ...of now it is concluded that th... ...identical results as f... ...at the ... certain ge-... ...pplying a tuned im...

LE 2: PHANTOM HEAD IRRADIATE... TRON AND GAMMA BEAMS

...illustrates how the APDT and LEXT per-fo... ...with forward MC in a real radiotherapy BNCT ... ...tion times of the three methods to obtain the re... ...the tumors and OAR are compared when irra... formed with neutrons and gammas ... three methods is disc... tions, the cr... ...ed and a preliminary resu... ...e the optimal neutron beams around ... After all, the goal of these adjoint methods ...the number of beam scenarios that can be cal-...a certain amount of time.

... Carlo set-up

...ample, the bound... ...q. (5)], ...atme... ...e BNCT trials at the ... Netherlands. The beam can be re... ...nal (angular divergence <2°) and consists ...

...in the source spectrum of the beam ... ...MC calculations, the detector response functio... ...d have an energy spectrum in accordance wi... ...ross-sections of ^{10}B, H, and N. These cross-sec... mon that at thermal energies, the probability i... orders of magnitude higher than at high neutron ... BNCT, determining the total detector r... ...rmal neutrons with energies < vic... of the main (therm... lated) dose ... the ... response function Σ_a ...n up to 0.5 eV. The optimizati... ...a plan from the ... ...getting a high ther-... ...nd a low thermal neutron flux in the C...

For the forward and adjoin... ...ons in this example, a new 172 ... structure based ... the libra... a tem... ...ne $S(\alpha,\beta)$ therma... ...gen is taken into account. In th..., the adjoint detector response function is ...he (forward) boundary source function ϕ^b whic... energy spectrum of the treatment beam in Petten ... groups representation. Vice versa, the adjoint ... is similar to the (forward) detector res... ...a this example, for the three m... ...ugs are ... ...e 1. This means ... ...e due to the flux of gammas in ... ...for a uniform gamma source with energy ... ...20.0 MeV. In this section, "total detector resp... ...sometimes shortened by mentioning only "the...

B. Geometry set-up

...25 CT images of a patient's head, a v... ...made using the program Scan... The he... ...1 cm, a height of 2... the distance fro... ...the h... measures 22.2 cm. Acco... ...el in the CT image, a threshol... ...material ... ...modeled as soft ...ue of skin, muscle, and fat. The ...520 voxels which contain only ... or mixtures ... ...e, and cranium. These tissue composition... ...ken from ICRU46.[30] In Fig... ...[32] of the head ... tissue ma...

...al tumor lesions, which is not un... ...with melanoma metastases in the brain, (dark colored), together with the ten OAR (ligh... defined in the BNCT protocol[33] used in Pe... eters of the tumors are all 1 cm. Simil... ...d OAR are modeled as spheres and ... inner ears, pituitary gland ... ...the thalamic ...diameters of the OAR

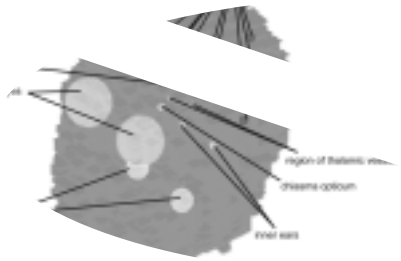

FIG. 8. Head phantom with all tissues
light and the ten tumors

.5 cm of which the last merely indicates a
20 tumors/OAR are the adjoint sources in the
chniques and forward detectors in the for
ns.
for the LEXT, there a
which are cl routed
sphe ter points are
20 cm aw phantom that is also the
center of the P d in azimuthal
and polar angles, as shown i
orientations of the 60 adjoint detecto
having the inner norm
tom. This is g. 9(b). In order to

ations, at each of the 60 center
nt orientations are
added.

As shown in Fig. 9(c), eight dis ving
angles of 10° with the initial disk normal,
numbered 2–9. Another eight normals make a
with the initial normal [numbered 10–17 in F
tra adjoint detectors are generated and n
tine for each of the 60 point
he orientations for
positions to tors a
function is determi 1020
"Petten" neutron/gamma ated. In the
sks are the forward
In the APDT these 1020
ad in Fig. 1. In
order to observe the influenc treat-
ment beam on the thre
beam exit dia m. In M
neutr ward detectors are n
e F4 type and the point detect
ype F5.

C. Strategy for comparing the calculation ti three methods

Comparison of the calculation MC
calculations the A d on a com-
ined in the tumors and
rtain number of beams. This rela-
nse as defined in
Sec. II B. The LEXT is ams with

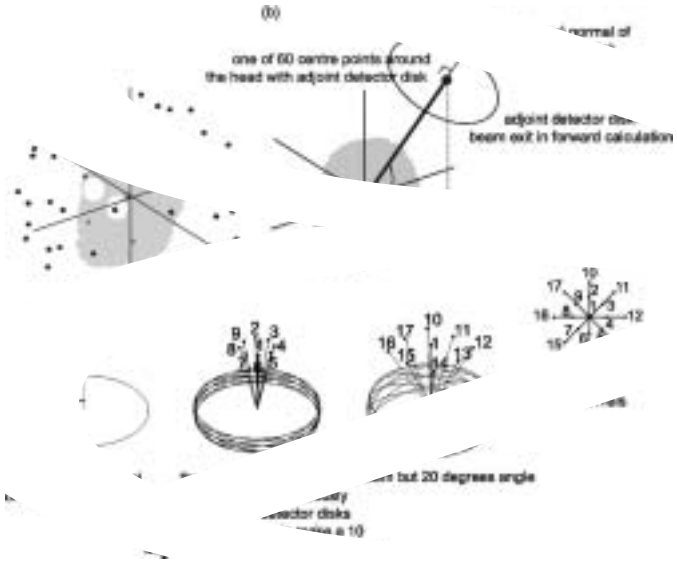

0 center points of the
djoint detector disks around the head.
(b) These points are described with
azimuthal angles. (c) Orien-
joint detector disks
s similarly
enter
. In t
=1020 beams sh
have diameters of 5,

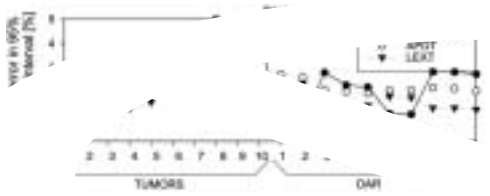

elative errors in the total detector responses due to the flux of (<0.5 eV) in all tumors and OAR. The errors for the three d to a maximum of 5% and averaged over 255 neu- tro.. ulation times of the methods can be adapted and com-

three different diameters
calculate all 102 ferent diameters for all meth suming. For this purpose, for eac' ue APDT and forward MC are only beams out of the 1020. These beams are tionally around the head and checked if the ations of the relative errors converge for th-

at the relative error in
root of the can be calc ic runs should be in or ror. The pre-processing time of the LEX ber of histories to be processed. It is chos relative error in the tumors and OAR to interval). The compari on the adapt LEXT to obtain the result d adapted calculation ti ns are multi-

Calculation times of the three me.

ase of the neutrons, for the LEXT, a 20 Gb written for the tumors and OAR. For the gam- ze of 130 Gb. More gamma samples are neede n" and "narrow" angular adjoint functions w ies. Since gammas are tracked faster, it take 130 Gb file in comparison with the ne time to obtain the optimum (in this exam for the gamm ue total time for reasons dis-

ves an example of the averaged relative errors eutron beams with a diameter of 15 cm, after he calculation times of the three methods in same maximum relative error. lative errors of the forward R 1, 2, 6, and 7 y large lar act that forward pa large detectors. Overall, Fig. 10 sh of the three methods are in the same range a

mes for the three methods for neutrons. All mmand shell on a personal computer with a Pentium th of memory.

Diameter of adjoint detector/ beam exit (cm)	Time n normalized Forward MC	AP.
	1.00(=140 days)	27.
	1.00(=113 days)	1
	1.00(=88 days)	

diameters and gam- similar to Fig. 10.

Table I the three meth- ods, for 1020 beams, to obtain ses of the thermal neutron flu relative error of ce inte the te ne calculation time. ters. Regarding Table I, due to eutron events, which are all tracked but e to the point detector, the APDT takes 27 to longer when compared with the forward calcula calculations would take years. For 1020 tumors/OAR, the calculation of the co with a diameter of 5 cm is h d cal- 15 cm can be LEXT. more than 6 and 20 times the advantage of the LEXT becomes meter becomes larger. In spite of the results o ple, it is demonstrated here that the LEXT be APDT whenever more beam positions are ca.

In Table II, the gamma results for the head p. ented. As there are far less gamma events in PDT improves greatly from that compa gamma beams with diameters 15 cm, XT are roughly 2 faster, respectiv Note will become advantage an 1020 beams are required I ocessing , to get similar sta- me has to be obtained which is

TABLE II. The total calc s. All calculations ar a com comp z processor and 512

Diameter of adjoint detector/ beam exit [cm]	Time to calculate 10 normalized to forw Forward MC		
5	1.00(=53 d		.7
10	1.6		0.55
15		0.33	0.30

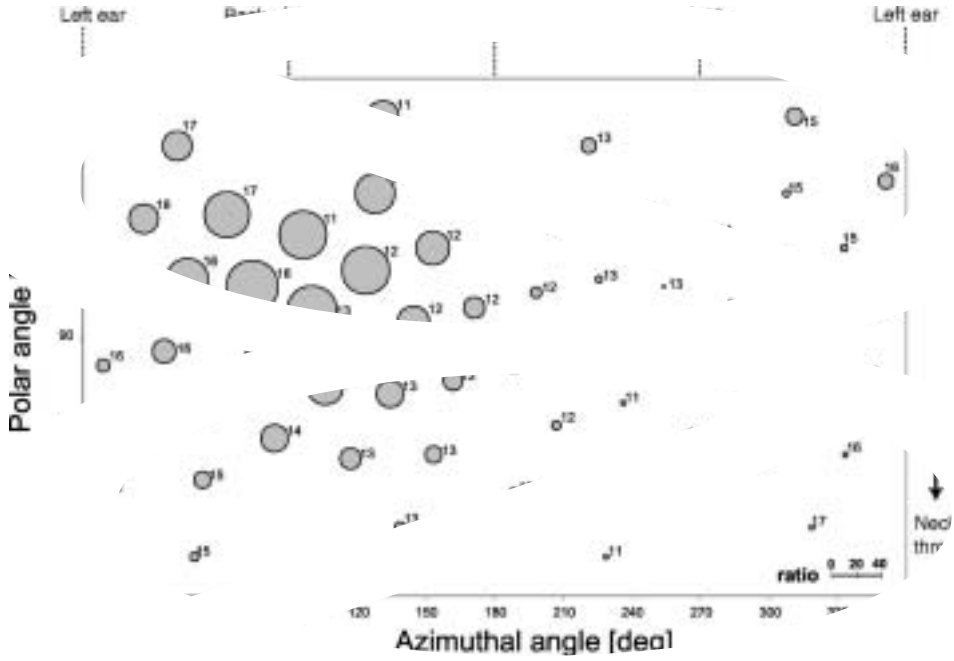

FIG. 11. An example outcome for treatment planning w... ...locations around the head, the maximum (=optimal) ratio of thermal neutrons in t... The larger the gray bubble the better is the ratio.

T... ...with ... ...5 cm diam- e... ...quickly obtained... ...4C

...timum neutron beams for irradiation

... the result of what are termed the best "Pe... ...(diameter 15 cm) out of 17 orienta- tions at ... ...ions are shown in Fig. 11. These in total 1020 ... ...lated with the LEXT, which is 20 times fast... gray bubble in Fig. 11, the larger is the average thermal neutron flu... thermal neutron ... ...large gray bubbles ... ...the tumor and a low dose in the ... ...tors of the ratios presented in Fig. 11 ...% confidence interval. The numbers writ- ...ach gray bubble correspond to the optimum ...he result is checked by the 255 forward calc... the differences are according to the

...rting at some po... ...the ... ...rig. 11, the averag... ...ound 35 times higher in the tumo... ...mall bubble indicated with "6" in the facial a...

the average thermal neutron flux in the tumors ... times less than in the OAR. Nevertheless, this is t... ...m out of 17 orientations from this position. To av... ...which the average flux in the tumors is sma... ...zero, which would give anyway ratio, ...ntation is chosen such t... or more of the ... ...mal neutron tumors is always prov...

For the optimization presente... ...est beams it is chosen t... ...rmal neu- ...and the thermal neutron ...AR. It needs to be investigated ...optimum) treatment plan when compared to ... ...bution of every beam to each tum... ...ing an optimization ... to t... subject ... ...rtheless, optimiz... ...with the LEXT and APDT ap...

...ISCUSSION

In this paper, two adjoint MC techniques ar... with an explanation on how perpendicular ... an adjoint detector plane can be ca... ...is the aim of this work to ... ...echniques ... ...on time per beam in

MC based radiotherapy treat
with forward MC
be calcu ..e treatment plans for mono-
d realistic scenarios, the
..l APDT ..nd proven in
..s. For the LEXT, so.. ..tions
which need some further au..
the next two sections.

efficient training

..alculation times of the LEXT, the times
to fin ..endre coefficients for which the
results conve.. ..t this number of
Legendre coefficients depe
and type of particle it
adjoint detec .. to be expected that
when ir ..utoms, such as head phantoms,
un ..ions, this "training for coefficients"
..e only once. Nevertheless, although this
necked for the geometries presented in Ex-
2, in which the adjoint sources are at var
rther investigation is necessary. In
al.[25] describe a first app
that autom ..e opti-
mun ..e tested and
implemen ..roperly for the radio-
therapy applicatio

B. Improvements

A way to im ..ugate other func-
tion ex ..al harmonics or Fourier
or ..ngular adjoint
..y definition. I.. ..n the
djoint functions between ..
the selection of a function expansi..
he particle type, will improve the outcome. Su..
..n, in conjunction with investigating how to
..mples for the estimates, as described in Sec.
II ..ber research. As well as improvements,
work ca.. ..t the LEXT such that it can be
used for more u.. ..EXT neutron beam in
Petten has a 2° angular di..
differences when simulated by a mon
beam. Actually, the d
for the dist ..eting and the irradiated
bod ..ve not been applied, as it was cho-
..e the methods by using Example 2, which
..t simplified. Note that in this respect, in Ex-
..e distance of the detector disks is chosen as fixed
ect to the center of the phantom instead of
he skin.

SION

..of the flux, dose or reac-
tion rate ..due to a known source,
can be obtained wi..

..t of the adjoint function and the
source ..pace variables pro-
vides this total (forwa.. ..In general,
whether an adjoint MC calculation ..er a
forward MC calculation, in terms of spe
number of sources, detectors, and their respe
example, the results for many large forward sou
..ll forward detectors (=adjoint sources),
..djoint MC. Apart from the e
..n the number of sou
and their si.. ..nges, i
ward to know whet.. ..djoint
MC or vice versa. It will ..ermine this
..his work can, there-
..arded as an example for ra-
diotherapy ..head. This ex-
ample shows that 20 adjoint s.. ..n still
be regarded as a "few"
(beams) are si
..adiotherapy treatmen..
..ions are impossible when the t..
..mono-directional. This is in despite of the
.. circumstances are in favor of the adjoint as d
above. The LEXT and APDT are two techniques
an estimate for the value of the angular adj
the direction of the adjoint detector's po..
of the LEXT is that for diff.. .. geom-
..has to be deter-
.. converged. The APDT is dis-
..many events which are not
contributing t.. ..ns in light wa-
ter.

From the BNCT example of a huma..
20 tumors/OAR and 1020 different positio..
directional neutron or gamma beam, it seems
..ms (exit diameters of 5 cm) are calculated mos
forward MC calculations. This result is
..neutrons. For the larger beam
and t.. ..e the adjoint MC
based on the LE.. ..s fas
than the forward MC. ..as,
both the LEXT and APDT ..than the
..ueless, the APDT
.. whenever fewer beam positions
..ms directed to the face in the
head phanto.. ..y, i.e., are unac-
ceptable.

To conclude ..ions
always s.. ..or MC b..
..suffered when mono-di..
..e considered. From the work pre
problem has now been solved and the opti
treatment plans and/or studying its mechanis
possible.

ACKNOWLEDGMENT

This work has been ..the Joint Re-
..ission.

[a]Electronic mail: victor.nievaart@jrc.nl

[1]G. B. Arfken and H. J. Weber, *Mathematical Methods For Physicists* (Academic, San Diego, 2005).
[2]B. Davison and J. B. Sykes, *Neutron Transport Theory* (Clarendon, Oxford, 1957).
[3]G. I. Marchuk, *Adjoint Equations and Analysis of Complex Systems* (Kluwer, Secaucus, New Jersey, 1995).
[4]G. I. Bell and S. Glasstone, *Nuclear Reactor Theory* (Van Nostrand Reinhold, New York, NY, 1970), pp. 252–313.
[5]B. Wang, M. Goldstein, X. G. Xu, and N. Sahoo, "Adjoint Monte Carlo method for prostate external gamma beam treatment planning: An application to 3D patient anatomy," Phys. Med. Biol. **50**, 923–935 (2005).
[6]F. C. Difilippo, "Forward and adjoint methods for radiotherapy planning," Med. Phys. **25**, 1702–1710 (1998).
[7]F. C. Difilippo, M. Goldstein, B. A. Worley, and J. C. Ryman, "Adjoint Monte Carlo methods for radiotherapy treatment planning," Trans. Am. Nucl. Soc. **74**, 14–16 (1996).
[8]M. Goldstein, "The adjoint Monte Carlo–a viable option for efficient radiotherapy treatment planning," *Proceedings of the 19th Conference of the Israeli Nuclear Society 11–2* (1996).
[9]D. L. Henderson, S. Yoo, M. Kowalok, T. R. Mackie, and B. R. Thomadsen, "The adjoint method for the optimization of brachytherapy and radiotherapy patient treatment planning procedures using Monte Carlo calculations," Final Report for DOE-NEER Grant: DE-FG07-99ID13774 (2001).
[10]R. Jeraj and P. Keall, "Monte Carlo-based inverse treatment planning," Phys. Med. Biol. **44**, 1885–1896 (1999).
[11]"MCNP–A general Monte Carlo N-particle transport code, version 4C," LA-13709-M , edited by J. F. Briesmeister (2000).
[12]B. L. Beers and V. W. Pine, "Functional expansion technique for Monte Carlo electron transport calculations" IEEE Trans. Nucl. Sci. **23**, 1850–1856 (1976).
[13]R. F. Barth, J. A. Coderre, M. G. H. Vicente, and T. E. Blue, "Boron neutron capture therapy of cancer: Current status and future prospects," Clin. Cancer Res. **11**, 3987–4002 (2005).
[14]Y. Nakagawa, K. Pooh, T. Kobayashi, Y. Sakurai, T. Kageji, S. Uyama, A. Matsumura, T. Yamamoto, and H. Kumada, "Clinical review of the Japanese experience with boron neutron capture therapy and a proposed strategy using epithermal neutron beams," J. Neuro-Oncol. **62**, 87–99 (2003).
[15]M. L. Williams and W. W. Engle, Jr., "The concept of spatial channel theory applied to reactor shielding analysis," Nucl. Sci. Eng. **62**, 92–104 (1977).
[16]J. C. Wagner, E. L. Redmond II, S. P. Palmtag, and J. S. Hendricks, "MCNP: Multigroup/adjoint capabilities," LA-12704, Los Alamos National Laboratory (1994).
[17]E. E. Lewis and W. F. Miller, Jr., *Computational Methods of Neutron Transport* (Wiley, New York, 1984).
[18]J. E. Hoogenboom, "Methodology of continuous-energy adjoint Monte Carlo for neutron, photon, and coupled neutron-photon transport," Nucl. Sci. Eng. **143**, 99–120 (2003).
[19]http://www-rsicc.ornl.gov/rsic-cgi-bin/enote.pl?nb=mcnp5&action=view&page=116; MCNP5 Notebook-page 116, F. Wasastjerna and T. Booth.
[20]A. Noel and H. S. Wio, "A new series-expansion approach in Monte Carlo: Application to neutron shielding," Ann. Nucl. Energy **11**, 225–227 (1984).
[21]D. P. Griesheimer and W. R. Martin, "Monte Carlo based angular flux distribution with orthogonal function expansion," Trans. Am. Nucl. Soc. **89**, 370–372 (2003).
[22]D. P. Griesheimer and W. R. Martin, "Two dimensional functional expansion tallies for Monte Carlo calculations," PHYSOR 2004—The Physics of Fuel Cycles and Advanced Nuclear Systems: Global Developments (2004).
[23]D. Legrady and J. E. Hoogenboom, "Midway Monte Carlo forward-adjoint coupling with Legendre polynomials," New Frontiers of Nuclear Technology: Reactor Physics, Safety and High-Performance Computing (2004).
[24]D. Legrady and J. E. Hoogenboom, "Visualization of space-dependency of responses of Monte Carlo calculations using Legendre polynomials," Proceedings PHYSOR 2004, Chicago, IL, April 25–29 (Elsevier Science, Chicago, 2004), pp. 1–7.
[25]D. P. Griesheimer, W. R. Martin, and J. P. Holloway, "Convergence properties of Monte Carlo functional/expansion techniques," J. Comput. Phys. **211**, 129–153 (2006).
[26]J. P. Boyd, *Chebyshev and Fourier Spectral Method* (Dover, New York, 2000).
[27]R. C. Little and R. E. Seamon, "New MENDF5 and MENDF5G," Los Alamos Internal Memorandum X-6:RCL-86–412 (1986).
[28]JEF-2.2 Nuclear Data Library, JEFF Report 17, Paris, France (2000).
[29]K. A. Van Riper, "A CT and MRI scan to MCNP input conversion program," Radiat. Prot. Dosim. **115**, 513–516 (2005).
[30]ICRU 46. Gamma, electron, proton and neutron interaction data for body tissues. International Commission on Radiation Units and Measurements, Bethesda, MD (1992).
[31]J. T. West III, SABRINA, "An interactive three-dimensional geometry-modeling program for MCNP," Los Alamos National Laboratory Report, LA10688M (1986).
[32]K. A. Van Riper, "New features in Sabrina," *Proceedings of the Topical Meeting on Radiation Protection for our National Priorities*, Spokane, WA, Sept. 17–21, (2000), pp. 316–323.
[33]EORTC protocol 11011 (version 2.0/February 2, 2004): Early phase II study on BNCT in metastatic malignant melanoma using the boron carrier BPA. European Organization for Research and Treatment of Cancer, Brussels (2004).
[34]R. H. Hardin, N. J. A. Sloane and W. D. Smith, "Tables of spherical codes with icosahedral symmetry," published electronically at http://www.research.att.com/~njas/icosahedral.codes/. These tables are copyright R. H. Hardin, N. J. A. Sloane, and W. D. Smith, 1994 (2000).

RADIATION RESEARCH **166**, 81–88 (2006)
0033-7587/06 $15.00

Design of a Rotating Facility for Extracorporal Treatment of an Explanted Liver with Disseminated Metastases by Boron Neutron Capture Therapy with an Epithermal Neutron Beam

V. A. Nievaart,[a,b,1] R. L. Moss,[b] J. L. Kloosterman,[a] T. H. J. J. van der Hagen[a,c] H. van Dam[a] A. Wittig,[d] M. Malago[e] and W. Sauerwein[d]

[a] *Department of Applied Sciences, Delft University of Technology, 2628CJ Delft, The Netherlands;* [b] *Joint Research Centre of the European Commission, 1755ZG Petten, The Netherlands;* [c] *Reactor Institute Delft, Delft University of Technology, 2629JB Delft, The Netherlands;* [d] *Clinic and Policlinic for Radiotherapy, Essen University Hospital, 45122 Essen, Germany; and* [e] *Department of General and Transplantation Surgery, Essen University Hospital, 45122 Essen, Germany*

Nievaart, V. A., Moss, R. L., Kloosterman, J. L., van der Hagen, T. H. J. J., van Dam, H., Wittig, A., Malago, M. and Sauerwein, W. Design of a Rotating Facility for Extracorporal Treatment of an Explanted Liver with Disseminated Metastases by Boron Neutron Capture Therapy with an Epithermal Neutron Beam. *Radiat. Res.* 166, 81–88 (2006).

In 2001, at the TRIGA reactor of the University of Pavia (Italy), a patient suffering from diffuse liver metastases from an adenocarcinoma of the sigmoid was successfully treated by boron neutron capture therapy (BNCT). The procedure involved boron infusion prior to hepatectomy, irradiation of the explanted liver at the thermal column of the reactor, and subsequent reimplantation. A complete response was observed. This encouraging outcome stimulated the Essen/Petten BNCT group to investigate whether such an extracorporal irradiation could be performed at the BNCT irradiation facility at the HFR Petten (The Netherlands), which has very different irradiation characteristics than the Pavia facility. A computational study has been carried out. A rotating PMMA container with a liver, surrounded by PMMA and graphite, is simulated using the Monte Carlo code MCNP. Due to the rotation and neutron moderation of the PMMA container, the initial epithermal neutron beam provides a nearly homogeneous thermal neutron field in the liver. The main conditions for treatment as reported from the Pavia experiment, i.e. a thermal neutron fluence of $4 \times 10^{12} \pm 20\%$ cm^{-2}, can be closely met at the HFR in an acceptable time, which, depending on the defined conditions, is between 140 and 180 min.

INTRODUCTION

The liver is the first major organ reached by the blood draining the gastrointestinal tract. Consequently, it is a common site of hematogenous metastasis from gastrointes-

tin- -ies. Colorectal cancer is the -ading
-ed death in developed coun- -he
alone, 14b,- -ses occur annually (*1*), o-
develop liver m- -nd in a third of the
will be the only site o- -s (*2*). Untrea-
olorectal metastasis has a po- -is, v- -
a- -l of 6–12 months (*3*). In sele- -gery
offers - -therapeutic opti- -o an im-
proved medi- -and a 20%
10-ye- -(3). However, in cases o- -mor
le- -icted to the liver that can- -
-epatectomy, chemother- -only trea-
-n be offered. Even - -newest chemot-
drugs have a r- -te of around 40%, the
-ival be- -een shown to be margina-
at- -to loco-regional techniques t- -a-
er with -surgical procedures m- -tially
curative. One su- -acorporal treat-
ment of the l- -py (BNCT).
Th- -ion presented here is mo- -suc-
c- -treatment using BNCT on o- -t
-a (Italy) - -48-year-old patient dev-
ronous diffuse l- -ases from an adeno-
of the sigmoid colo-, -ver metastases
after conventional chemo- -fter ir-
pre- -xperiments (*6*, *7*), the patie- -nl
of a 0.- -phenylalanine (BPA- -olution
(300 mg BPA p- -ugh the colic vein
over a p- - - -and tumor
sa- -taken to measure the boron -ration
-r to hepatectomy. The exp- -d
-and transported to the -eactor of t-
-ity of Pavia where i- -iated at the therm-
for 11 min -d neutron fluence of 4
-cm- -ter BNCT, the liver was tr- -d
ba- -ating theater and reimplante- -plete

[1] Address for correspondence: Joint Research Centre of the European Commission, P.O. Box 2, 1755ZG Petten, The Netherlands; e-mail: victor.nievaart@jrc.nl.

[2] Private communicatio- - -, A. Pinelli and S. Altieri.

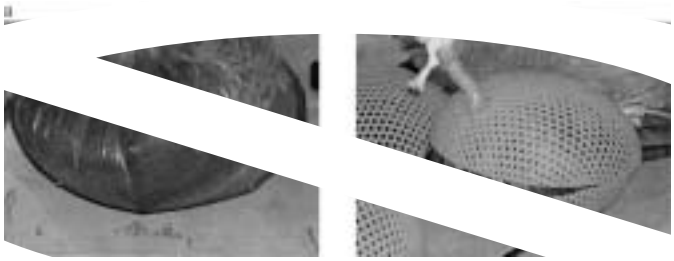

lastic bag, a liver takes the form of a spheroid. Panel b: Inser
liver ...

tumor respor ... an observation period of 12 ... the liver showed a normal liver v... lesions in the former tumor areas. Af... tumor recurrence was observed in the form utside the liver but in the area of the former . It was interpreted as iatrogenic due t... mor tissue prior to the liver e... emoved. An adju... as ad... his ir... onths after BNCT, ... ed shortly followed by intraperito... ent died in August 2005, 44 months after B... from diffuse liver metastases of a colo... treated following the same ... ter the auto-tr... ase problems that were ir... m prior chemotherapy. Th... ...te any viable ... (communicat... ervations stimulated not only ... but also similar studies in Finland (e... U.S. (*10*).

the reaction that occurs between the boron-... ermal neutrons. In this reaction, the ther-ma... d by the nucleus, and the resulting boron-11 ... the emission of high-LET and high-RBE α ... ticles are only 9 and 5 μm, re... particle traverses the cell nucl... death. With tar... cells, a se-lective ... ...s can be obtained (*11*). This ... possibility to treat multiple metastases ...ch more efficiently than with existing con-...erapies. Moreover, BNCT has the potential to very small metastases or satellite nodules that ... ...cally detectable and are often respons... ...sease. A prerequisite, how... ... of ^{10}B inside th... ... uptake ...sis ... BPA, which is actively transported by the L-a... ...em into cells (*12*) and which ... (*13–18*). Another ... ...very of ... number ... ...e tumor cells. Th... ...ds of this paper. The proposed ... take place at the BNCT facility (*19*) of ...h Flux Reactor (HFR) in Petten (The Netherlands) ing the available, well-collimated epithermal neutron The aim of the study is therefore to demon... homogeneous thermal neutron flux distr... ...livered to the liver using ... ...utron ... ...ds thermal neu-... possibility to treat liver cancers

MATERIALS AND METHO...

The Liver

...iver is the largest internal organ in the human body and ... spongy, wedge-shaped organ. According to the ...ght of a healthy male liver is around 1.5 that of ... ...kg. The maximum dimensi... in the body, are ... ...ed vertically, ... or right surface, up to 17... 12.5 cm. A liver with metastases ... However, the evolving calculatio... ...gest that ... ...ze with a spheroid-... ...e molded into a spheroidal shape, ... placed in a plastic bag, as is usually ... ...ib may clarify this approach; a female liver o... ...roid-shaped mold with a volume of 1.6 lite...

The pictures were t... General and ... the Universi... (G... ...n and prior to the discard... ...herefore, under German law, exempt fr... ...of the welfare of human subjects.

Medical Requirements

The University Hospital Essen is one of the mai... both diseased and living donor liver trans... ...o-

[3] Europhysi... Nuclear Physics and Tech-nologies. September 5–9, ...

rating and participating in the pr
HFR Petten, follo

The fi ...amined outside the body and the fi ...tained are critical issues. In our ...be outside the operating ...defined as 6 h. C... ...rt for organs, ...n be transported from the v... ... the ...n room at the HFR within 1 h. The time ... ...radiation facility and irradiation procedure, no m... ...be acceptable. After explantation, during transport and ir... ...er must be maintained constantly at a controlled temperature ...ver is a flexible organ; however, it should not suffer from ...chanical injury.

Radiation c...

In BNCT, the absorbed dose in ... ...eral dose components. S... ...beam, others ge... ...by nuclear reactions. The four do... ...e evaluated are the boron dose (D_B), th... ...n doses (D_p and D_n), and the γ-ray dose (D_γ) ... different dose components and to take into consid- ...ent biological effectiveness, the term total biologically ... D_w, has been proposed.[5] Pinelli *et al.* estimated the lim- ...e liver to be D_w = 15 Gy (*23*) when applying the we... ...ting from *in vitro* and *in vivo* experiment... ...and skin (*24–26*). Apart from th... ...anted liver irradiat... ...ure of ...s pr... ...ess follows the propo... ...en as an approximation. The limiting ... ...established through appropriate animal experiments.

It has to be stressed that only the ... to the tumor. All other dose components are no... duce an absorbed dose in the h... the limiting dose ...

Succe... ...ors: the minimization of the non- spe... ...boron uptake in healthy ...stases. T... ...the uptake and ...probably vary betwee... ...d for ...ase; this is currently being studied.

Goals and Limits in this Computational Study

...l of this study is to evaluate and compare the fluence in ...t reported in Pavia. Nevertheless, the total weighted do... ...to that reported in Pavia using the estimates describe... ...Pinelli *et al.* (*4*) report a D_w of 8.6 ± 0.5 Gy in the ... ...ion of 8 ppm and a D_w of 62 ± 2 Gy in the tu... Since the metastases are spread throughout th... flux distribution should be as ...

Rotat...

...n a thermal column, as in the Pavia setup, the opti- ...tor the liver is in its natural form when placed on a flat ...hermal column allows for the organ to be placed in effectively ...' of thermal neutrons. The thermal neutron flux will be ... the surface and will decay rather strongly into t... ...n the surface, the thermal neutron fl...

...nt status o... ...IAEA-TECDOC- ... ...2003): ^{10}B-uptake in different tu- mours using ... ...RPA. Study coordinator: W. Sauerwein.

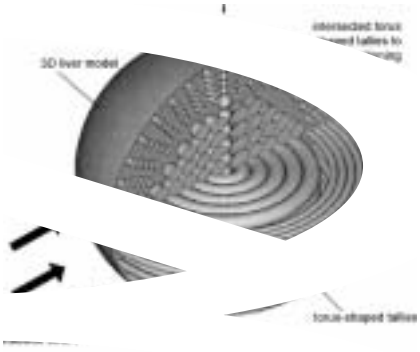

FIG. 2. Isometric view of th... torus-shaped tallies to s... ...al t... whole liver o...

...ace) value. An initial design considered fitting t... ...imaginary cylindrical container with a diameter of 25 cm ...eight of 8 cm. In this way, the thermal neutrons, coming f... sides, will deliver a homogeneously distributed dose in the ...

When dealing with an epithermal neutron beam, e... completely re-evaluated. With respect to the R... energy spectrum consists mainly of ...ergies mainly between 1... ...around 30 keV ..., has a very small divergence ...mm collimators of diameters 8, 12 and 15 ...ration of the epithermal neutrons has a maximum... ...half this max- imum value at 0.5 cm and 6.5 cm. Acc... ...ding the cylindrical approach as mentioned above, it c... most effective part of the neutron fluence, i.e. betwee... cm, can be used if the liver is inserted into a spheroid-sha... ...nd then rotated around the polar axis. In this way, when t... ...is moved slightly nearer to the surface by the scatter... ...ner material, the thermal fluence will be spr... ...er of the spheroid, the thermal fl... its lowe... ...distributed over a sm... when rotating.

When using one of the co... designed for BNCT, such as BNC... ...Plan (*29*), it is not possible ... ...calculate the ...was therefore necessary to ...e Monte Carlo code MCNP (*30*). To calculate ...liver, torus-shaped volumes were programmed ... ...ies in MCNP), there- by simulating the rotation (see ...

As illustrated in Fig. 2, ...orus is positioned s... ...cal a... of the ... ...the thermal flux ... ...ect more accurately, tori with si... ...ll at the vertical axis are spheres. ...g tori, only one calculation is needed in which the be... the liver from one direction. MCNP adds all the track l... particles inside the torus volume and gives, when dividi... of the torus, the flux. This averaging of the calculated

...J. T. West III, SABRINA: An I... ...Geom- etry-Modeling Progra... ...Laboratory Re-

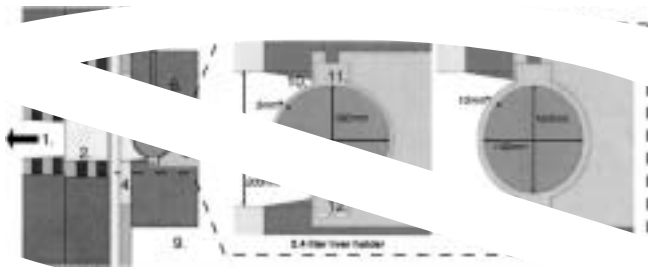

f the final setup: Right (surrounded by dashed lines)

possible ... 3. Wall
containing boron ... Graphite
reflect... cube surrounding holder. 9. BNCT ...
...MA holder for rotation and connecting the two halves (surrounded by ...
...ge 11 but also centered on Teflon cone.

...ent simulation of the flux distribution for the rotating
, a consequence, the flux becomes a time-averaged flux
ng liver.
flux is uniform in the whole torus after
...es to make the flux uniform

Liver Irra...

The design concept fo... does not require any changes to the ... ment. The neutron source spectrum and sour... to be adapted. The liver set... to install and re... ...ust be economical with regard to ...mponents. To keep the liver co... ...ion of the organ will ...es a precise ... This feature ...n such a way that it does ... ...as evolved from surrounding the live... r, moderator and coolant) toward a surroun... he same characteristics. It appears that the solid surroun... negligible difference in yield. However, it is easier to ...parison with something that must be watertight. After ...ulations with different materials and configurations ... ...ng we arrived at the final setup for irradiating a volu... ...1.6 liters, respectively, as shown in Fig. 3. The deriv... ...mmes are given in the next section.

Figure 3 is a collection of three geometrical ... left, a cross section of the lay... and the wall of ... ...facility for the liver is given ...inator, the beam diameter is 16 cm, ...es at the edges of the beam.
...ped container holding the liver is placed in a PMMA ...ith sides of 26 cm. The PMMA cube acts as a neutron ...pecially for the top and bottom of the spheroid. For back the cube is surrounded by pure graphite blocks (1.6 ...ntrance a graphite cone.
...heroid-shaped container for holding ... ...nsists of two equal par... ...e liver ...dvantages of ... ...shaped easily, is ...vated by the irradiation, and is ...vation of the liver within the moving device. A ... ...duction of γ rays due to the (n,γ) reaction from hy...

can be ... ...of the thermal neutrons in a ra... ...ne scattering cross section of the same hyd... ...ne same effect as the skin and cranium, which mo... ...thermal neutrons in the BNCT treatment of brain tumors. In designs for the 2.4-liter container, the wall of the PMMA cont... the thickest (5 mm) at the equator and decreased to 2 mm to... and bottom of the spheroid. Although the neutron flux ... be tuned even better in this way, for engineer... constant PMMA thickness.
...together with a ... into the container, the container ...h liquid (water or more conservation ... air gaps that would influence the irradiation field.
In this computational study, the liver co... ...be modeled human are taken from ICRU Report 46 ... volume inside the container is modeled as liver tissue, wi... rable with water and the conservation solution. During the tra... ...tions, a conservatively chosen 15 ppm of ^{10}B is distributed ... ...the liver. From the brain studies, it is known that the ... ...depth in the brain will be 4% higher wh... is ... ...d homogeneously (*33*). Therefo... servatively ... ...ncentration in healthy ... is lower than 15 ppm, ...her in this study.

... ...two optimal setups have been considered the... ...the upper limits. The lower limit is an i... ...of 1.6 liters; it is not e... ... with the ... conservation ... ...at are smaller than this vo... ...an irradiation volume capacity of 2.4 ...strained by the existing beam characteristics.

Thermal Neutron Flux Distribution

In BNCT, three of the four ma... ...are based on thermal neutr... ...al neutron ...ng parameter.

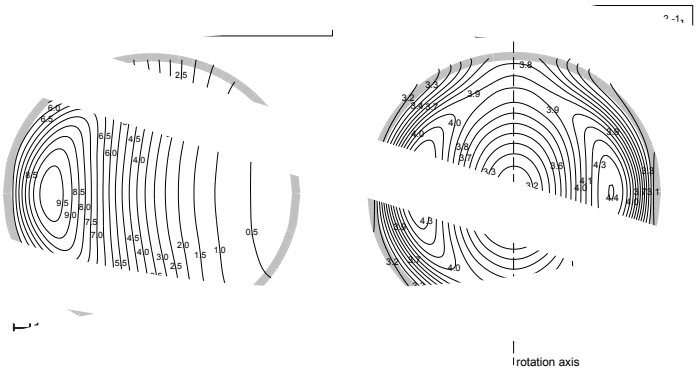

.. Panel a: Thermal neutron flux inside the 2.4-liter container when irradi
.mal neutron flux with the container rotating.

shows thermal neutron flux distribution f
4-liter volume: an equatorial r
ius of 8.0 cm. Ther
ener
proportion-
ally s
is given as back-
ground to u
tistical uncertainties in
the MCNP results pre
Figure 4a gives the thermal neutr
cross section along the be
tionary. The ne
the left; hence
it is n
ighest flux values at the
th
the liver. In Fig.
ver containe
his ro-
e flux distribution produc
. Note that the gradient of the ther
n the left panel gives a disturbed view wh
th the right panel due to a different step size

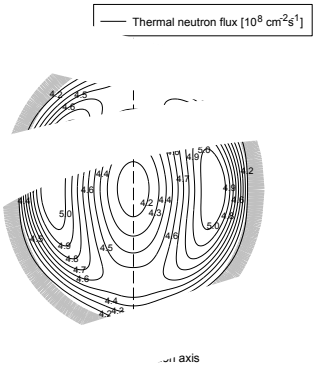

FIG. 5. Thermal neutr

nes. Clearly, from Fig. 4b, the thermal
ux is around 4.4×10^8 cm^{-2} s^{-1} at 3 cm from th
face. Similar results can be seen in Fig. 5, where
mal neutron flux contours are plotted for the
container. In this design, the loss of ve
for an more homogeneous
thermal neutron
at the center of the liver. Increas-
ages can be accom-
plished by more PMMA,
low down
more epithermal neutrons. To compe
f
thermal neutrons at the center, the equato
decreased. The optimal dimensions turn out to be
erial radius of 7.0 cm and polar radius of 8.0 c
rectly related to the size of the beam. In fa
6-liter spheroid is rotated whe
pared
tainer. Of course, th
absolutely no u
ed live
4 and 5 are 2D represen
essary to give information
on flux
e containers. Note
from the center describes a bigger
ser to the center. Figure
6 shows the therma
tograms for
both containers.
In 7% of th
el c
mal
$\times 3.3 \times 10^8$ cm^{-2} s
e 1.6-liter container, apart fro
al, all thermal neutron flux intervals ar
ess equal in filling the volume. The smaller wi
spectrum for the small container shows the g
geneity. Note that the lowest thermal neu
in the 2.4-liter container looks quite
own
as an iso-contour, as in F
center), but
ume (1.1%). For what

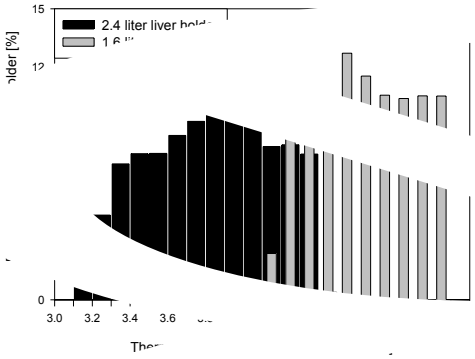

FIG. 6 ...ume histograms of the two liver containers.

...gives 5% to 15% higher thermal neutron ... ...ion within the liver. Although the surrounding ... scattering and buildup of thermal neutrons, ... the hydrogen and it therefore results in the ... photons. Near the center of both containers, aro... total photon dose is due to photons produce... ...he top and bottom of the containers, t... ...bsolute values, the photon ... at the bot... ...tainers is two ... total photon dose ... the minimum and maximu...

A single MCNP calculation ... ...mes to keep track of the parti... rotating liver. A s... ...and easy... terials h... ...s presented here for t... ...volumes: 1.6-liter and 2.4-liter

...hese experiments and mathematical evaluations ... been strongly stimulated by the pioneering work of Pinelli and co-workers from Pavia (Italy). It ... doubt a success to achieve 4-year surv... fering from multiple liver ... pro- ... ...y. It is regrettable ... ...s and the physical basis as well ... ...been published in detail. Most of the infor... ...ticle regarding the Pavia case has been taken ... ceedings (*4, 23, 34, 35*) and is based on o... sentations[3,8] and personal communications.[2]

Regarding the neutronics, the published work from ... ...] is based on a thermal column. Two other ... ...ve investigated the possibility of ... tracor... All of this work is diff... compare with t... ...are, which ... compared with a Finnis... ish work emphasizes the adv... ...mal neutrons in ... ..., and it ends

...on Capture Therapy, October 11–

...rth, the lowest thermal neutron fluxes are in ...volume fractions of the liver, which, it ...reases the probability that the...

Irradia...

A summary of t... ...is given in Table 1. As well as the maxim... neutron fluxes, the irradiation time ... ence of 4×10^{12} cm^{-2} ... reach the d... ...of 15 Gy are also given. To c... ...weighting factors ... ...ation (δ_F ... ...thy liver ... Pavia case have bee... ...sight into the composition of the ...s, Table 2 gives an overview of the major ... ...mponents. The applied ^{10}B concentrations for ...or tissue are the ones reported for the first pe...

Influence of t...

Small variations in the ther... certain positions within the liver ... the position of the ...

TABLE 1
...haracteristics of the Thermal Neutron Flux and Irradiation ... ...er Containers

		2.4-liter container
...utron flux (cm^{-2} s^{-1})		
	4.7×10^8	3.8×10^8
	4.1×10^8 (12% below average)	3.1×10^8 (20% below
	5.1×10^8 (9% above average)	4.5×10^8 (17% ab...
...n		
To deliv...	4×10^{12} cm^{-2}	142
To deliver D_w of ...		120

[illegible] Healthy and Tumor Tissue [illegible]

	Total biologically weighted dose rate		Physical dose rates			
	(Gy/h) (47 ppm ^{10}B)	Healthy	$\dot{D}_B$ (Gy/h) ^{10}B)	$\dot{D}_n$ (Gy/h)	$\dot{D}_p$ (Gy/h)	$\dot{D}_\gamma$ (Gy/h)
1.6 liters						
Minimum	23.7	5.2			0.3	2.2
Maximum	29.0	6.5	1.1			3.3
Average	26.5	6.0	1.0	0.[illegible]		2.8
		4.8	0.7	0.1		
Maxim[illegible]						2.9
Average						2.4

[illegible] as to what the influence of the irradiation [illegible]e, which is one of the objectives of the analy[illegible]ed in this paper.

[illegible]er holders, the desired thermal neutr[illegible] [illegible]m^{-2} ± 20% can be reach[illegible] [illegible] respect to th[illegible] [illegible] to the liv[illegible] [illegible]cued. This is a very cri[illegible] [illegible]gestion made by Pinelli *et al.* in 2001 (2[illegible] [illegible] maximum in a small volume. In 2002, [illegible] treated in Pavia received a total [illegible] ± 0.5 Gy (*4*) but did [illegible] received th[illegible] [illegible] presented here probably lead[illegible] [illegible]ion of all dose com[illegible]e liver, [illegible] [illegible]dvantage [illegible]o the tolerance dos[illegible] [illegible]nder the conditions used to irradi[illegible] [illegible]nimal experiments will be necessary to est[illegible] [illegible]e dose to a healthy explanted liver after BPA [illegible]ost suitable model would appear to be the [illegible] [illegible]rgans are of similar size to those of human[illegible]

Possible [illegible] [illegible]l fluence include a further reduction of the [illegible] highest thermal flux value in the liver [illegible] γ rays would requ[illegible] doubtful [illegible] [illegible]e to decrease the existing [illegible] [illegible] further without affecting the epi[illegible] [illegible] spectrum and flux. Decreasing the maxi[illegible] [illegible]al neutron flux at the thermal peak is impossible [illegible]s thermal peak is inherent to the use of an epith[illegible] [illegible]eam. Although it is feasible to shift the [illegible] [illegible] slightly, the procedure is limit[illegible] [illegible]n the fluxes at the [illegible] [illegible]center

[illegible] [illegible]chieved its objective and has lea[illegible] [illegible]hose encouraging the next step in the projec[illegible] a program of [illegible] [illegible]nts to valida[illegible] cul[illegible] [illegible]n of boron-10 throughout the irrad[illegible] [illegible]ast also be evaluated in detail to better deter[illegible] [illegible]ue dose delivered to the healthy tissue. A first st[illegible] been undertaken by the clinical trial EORTC 11[illegible] which investigates the uptake of BPA in [illegible] liver metastases.

In conclusion, th[illegible] [illegible] an extra[illegible] [illegible] the epithermal neutron [illegible] [illegible] be closely met. With the ther[illegible] [illegible] and ^{10}B con[illegible]centrations allow a safe and [illegible] [illegible]racorporal treatment of liver cancer by BNC[illegible] BNCT facility in Petten is feasible from the tec[illegible] of view.

ACKNOWLEDGMENTS

This work [illegible] [illegible]ly by the Europ[illegible] sion, contract no QLK[illegible]

Received: July 8, 2005; acce[illegible]

REFERENCES

1. A. Jemal, R. C. Tiwari, [illegible] [illegible]s E. Ward, E. J. Feuer and M. J. Th[illegible] [illegible] 8–29 (2004).

2. J. S[illegible] [illegible]ell-Hofmann and F. [illegible] [illegible]gular resection for colorectal sec[illegible] [illegible]9 (1991).

[illegible]. J. Bentrem, R. P. DeMatteo and L. H. Blumgart, Surg[illegible] for metastatic disease to the liver. *Annu. Rev. Med.* [illegible] (2005).

4. T. Pinelli, A. Zonta, S. Altieri, S. Barni, A. B[illegible] Bruschi, P. Chiari, C. Ferrari and C. Z[illegible] [illegible]ue first idea to the application to th[illegible] *and Development Neutron* [illegible], K. Moss and A. [illegible] Editore, Bologna, 2002.

5. E. Wilkinson, An out-of-body experience. *Lancet Oncol.* **4**, 64 (2003).

6. L. Roveda, U. Prati, J. Bakeine, F. Trotta, P. Marotta, P. Valsecchi, A. Zonta, R. Nano, A. Facoetti and P. Pedroni, How to study boron biodistribution in liver metastases from colorectal cancer. *J. Chemother.* **16**, 15–18 (2004).

7. R. Nano, S. Barni, P. Chiari, T. Pinelli, F. Fossati, S. Altieri, C. Zonta, U. Prati, L. Roveda and A. Zonta, Efficacy of boron neutron capture therapy on liver metastases of colon adenocarcinoma: optical and ultrastructural study in the rat. *Oncol. Rep.* **11**, 149–153 (2004).

8. P. Kotiluoto and I. Auterinen, MCNP study for epithermal neutron irradiation of an isolated liver at the Finnish BNCT facility. *Appl. Radiat. Isot.* **61**, 781–785 (2004).

9. M. Suzuki, Y. Sakurai, S. Masunaga, Y. Kinashi, K. Nagata and K. Ono, Dosimetric study of boron neutron capture therapy with borocaptate sodium (BSH)/lipiodol emulsion (BSH/lipiodol-BNCT) for treatment of multiple liver tumors. *Int. J. Radiat. Oncol. Biol. Phys.* **58**, 892–896 (2004).

10. H. Koivunoro, D. L. Bleuel, U. Nastasi, T. P. Lou, J. Reijonen and K. N. Leung, BNCT dose distribution in liver with epithermal D-D and D-T fusion-based neutron beams. *Appl. Radiat. Isot.* **61**, 853–859 (2004).

11. W. Sauerwein, Principles and history of neutron capture therapy. *Strahlenther. Onkol.* **169**, 1–6 (1993).

12. A. Wittig, W. Sauerwein and J. Coderre, Mechanisms of transport of p-borono-phenylalanine through the cell membranein vitro. *Radiat. Res.* **153**, 173–180 (2000).

13. W. Sauerwein and A. Zurlo, The EORTC Boron Neutron Capture Therapy (BNCT) Group: Achievements and future projects. *Eur. J. Cancer* **38**, S31–S34 (2002).

14. S. Obayashi, I. Kato, K. Ono, S. Masunaga, M. Suzuki, K. Nagata, Y. Sakurai and Y. Yura, Delivery of (10)boron to oral squamous cell carcinoma using boronophenylalanine and borocaptate sodium for boron neutron capture therapy. *Oral Oncol.* **40**, 474–482 (2004).

15. I. Kato, K. Ono, Y. Sakurai, M. Ohmae, A. Maruhashi, Y. Imahori, M. Kirihata, M. Nakazawa and Y. Yura, Effectiveness of BNCT for recurrent head and neck malignancies. *Appl. Radiat. Isot.* **61**, 1069–1073 (2004).

16. A. Z. Diaz, Assessment of the results from the phase I/II boron neutron capture therapy trials at the Brookhaven National Laboratory from a clinician's point of view. *J. Neurooncol.* **62**, 101–109 (2003).

17. H. Joensuu, L. Kankaanranta, T. Seppala, I. Auterinen, M. Kallio, M. Kulvik, J. Laakso, J. Vahatalo, M. Kortesniemi and S. Savolainen, Boron neutron capture therapy of brain tumors: Clinical trials at the Finnish facility using boronophenylalanine. *J. Neurooncol.* **62**, 123–134 (2003).

18. P. M. Busse, O. K. Harling, M. R. Palmer, W. S. Kiger, 3rd, J. Kaplan, I. Kaplan, C. F. Chuang, J. T. Goorley, K. J. Riley and R. G. Zamenhof, A critical examination of the results from the Harvard-MIT NCT program phase I clinical trial of neutron capture therapy for intracranial disease. *J. Neurooncol.* **62**, 111–121 (2003).

19. R. L. Moss, O. Aizawa, D. Beynon, R. Brugger, G. Constantine, O. Harling, H. B. Liu and P. Watkins, The requirements and development of neutron beams for neutron capture therapy of brain cancer. *J. Neurooncol.* **33**, 27–40 (1997).

20. H. Gray, *Anatomy of the Human Body*. Lea & Febiger, Philadelphia, 1918. [Thoroughly revised and re-edited by W. H. Lewis, New York, 2000; available online at http://www.bartleby.com/107]

21. M. Malago, G. Testa, A. Frilling, S. Nadalin, C. Valentin-Gamazo, A. Paul, H. Lang, U. Treichel and C. E. Broelsch, Cicinnati right living donor liver transplantation: An option for adult patients: Single institution experience with 74 patients. *Ann. Surg.* **238**, 853–862 (2003).

22. J. Rassow, W. Sauerwein, A. Wittig, E. Bourhis-Martin, K. Hideghéty and R. Moss, Advantage and limitations of weighting factors and weighted dose quantities and their units in boron neutron capture therapy. *Med. Phys.* **31**, 1128–1134 (2004).

23. T. Pinelli, S. Altieri, F. Fossati, A. Zonta, C. Ferrari, U. Prati, L. Roveda, S. Ngnitejeu Tata and D. M. Ferguson, Operative modalities and effects of BNCT on liver metastases of colon adenocarcinoma. In *Frontiers in Neutron Capture Therapy* (M. F. Hawthorne, K. Shelly and R. J. Wiersema, Eds.), pp. 1427–1440. Kluwer Academic, Plenum Publishers, New York, 2001.

24. J. A. Coderre, M. S. Makar, P. L. Micca, M. M. Nawrocky, H. B. Liu, D. D. Joel, D. N. Slatkin and H. I. Amols, Derivations of relative biological effectiveness for the high-LET radiations produced during boron neutron capture irradiation of the 9L rat gliosarcoma *in vitro* and *in vivo*. *Int. J. Radiat. Oncol. Biol. Phys.* **27**, 1121–1129 (1993).

25. G. M. Morris, J. A. Coderre, J. W. Hopewell, P. L. Micca, M. M. Nawrocky, H. B. Liu and A. Bywaters, Assessment of the response of the central nervous system to boron neutron capture therapy using a rat spinal cord model. *Radiother. Oncol.* **30**, 249–255 (1994).

26. H. Fukuda, J. Hiratsuka, C. Honda, T. Kobayashi, K. Yoshino, H. Karashima, J. Takahashi, Y. Abe, K. Kanda and M. Ichihashi, Boron neutron capture therapy of malignant melanoma using ^{10}B-paraboronophenylalanine with special reference to evaluation of radiation dose and damage to the normal skin. *Radiat. Res.* **138**, 435–442 (1994).

27. D. E. Wessol, R. S. Babcock, F. J. Wheeler, G. J. Harkin, L. L. Voss and M. W. Frandsen, *BNCT_Rtpe: BNCT Radiation Treatment Planning Environment User's Manual*, Version 2.2, 1997. [Available online at http:id.inel.gov/rtpe-manual/sec00.html]

28. D. E. Wessol, C. A. Wemple, F. J. Wheeler, M. T. Cohen, M. B. Rossmeier and J. J. Cogliati, *SERA: Simulation Environment for Radiotherapy Applications User's Manual*, version 1C0, 1999. [Available online at http:www.cs.montana.edu/~bnct/manual/sec00.html]

29. R. Zamenhof, E. Redmond, G. Solares, D. Katz, K. Riley, S. Kiger and O. Harling, Monte Carlo-based treatment planning for boron neutron capture therapy using custom-designed models automatically generated from CT data. *Int. J. Radiat. Oncol. Biol. Phys.* **35**, 383–397 (1996).

30. J. F. Briesmeister, Ed., *A General Monte Carlo N-Particle Code*, version 4C. Report LA-13079-M, Los Alamos National Laboratory, Los Alamos, NM, 2000.

31. K. A. Van Riper, New features in Sabrina. In *Radiation Protection for our National Priorities*, pp. 316–323. American Nuclear Society, La Grange Park, IL, 2000.

32. ICRU, *Photon, Electron, Proton and Neutron Interaction Data for Body Tissues.* Report 46, International Commission on Radiation Units and Measurements. Bethesda. MD, 1992.

33. S. J. Ye, Boron self-shielding effects on dose delivery of neutron capture therapy using epithermal beam and boronophenylalanine. *Med. Phys.* **26**, 2488–2493 (1999).

34. A. Zonta, U. Prati, L. Roveda, S. Zonta, C. Ferrari and C. Zonta, Clinical lessons from the first applications of BNCT on unresectable liver metastases. In *Europhysics Conference Abstracts* (A. Fontana, G Viesti and A. Zenoni, Eds.), pp. 97–98. European Physical Society, Pavia, 2005.

35. T. Pinelli, S. Altieri, F. Fossati, A. Zonta, D. Cossard, U. Prati, L. Roveda, G. Ricevuti and R. Nano, Development of a method to use boron neutron capture therapy for diffused tumours of liver (TA-ORMINA project). In *Cancer Neutron Capture Therapy* (Y. Mishima, Ed.), pp. 783–794. Plenum Press, New York, 1996.